Numerical Study of the Effect of Urbanization on the Climate of Desert Cities

by

Samy Kamal

A Dissertation Presented in Partial Fulfillment
of the Requirements for the Degree
Doctor of Philosophy

Approved September 2015 by the
Graduate Supervisory Committee:

Huei-Ping Huang,Co-Chair
James Anderson, Co-Chair
Marcus Herrmann
Ronald Calhoun
Soe Myint

ARIZONA STATE UNIVERSITY

December 2015

ABSTRACT

This study uses the Weather Research and Forecasting (WRF) model to simulate and predict the changes in local climate attributed to the urbanization for five desert cities. The simulations are performed in the fashion of climate downscaling, constrained by the surface boundary conditions generated from high resolution land-use maps. For each city, the land-use maps of 1985 and 2010 from Landsat satellite observation, and a projected land-use map for 2030, are used to represent the past, present, and future. An additional set of simulations for Las Vegas, the largest of the five cities, uses the NLCD 1992 and 2006 land-use maps and an idealized historical land-use map with no urban coverage for 1900.

The study finds that urbanization in Las Vegas produces a classic urban heat island (UHI) at night but a minor cooling during the day. A further analysis of the surface energy balance shows that the decrease in surface Albedo and increase effective emissivity play an important role in shaping the local climate change over urban areas. The emerging urban structures slow down the diurnal wind circulation over the city due to an increased effective surface roughness. This leads to a secondary modification of temperature due to the interaction between the mechanical and thermodynamic effects of urbanization.

The simulations for the five desert cities for 1985 and 2010 further confirm a common pattern of the climatic effect of urbanization with significant nighttime warming and moderate daytime cooling. This effect is confined to the urban area and is not sensitive to the size of the city or the detail of land cover in the surrounding areas. The pattern of nighttime warming and daytime cooling remains robust in the simulations for the future

climate of the five cities using the projected 2030 land-use maps. Inter-city differences among the five urban areas are discussed.

DEDICATION

To my best friends Sama Kamal, Dan Cunio, Noona and Corina Kamal. To everyone who, honestly, taught me anything from the slumps to Cairo to San Francisco.

ACKNOWLEDGMENTS

I would like to express my deepest gratitude to my adviser Dr. Huang for his continuous support and wise guidance during all the stages of the study and writing of this thesis. Without his honest mentoring this work wouldn't be possible.

Beside Dr. Huang I would like to thank the rest of my thesis committee: Dr. Anderson, Dr. Myint, Dr. Calhoun and Dr. Herrmann for their constant support and insightful comments. Special thanks to Dr. Myint for providing the Landsat land use maps used throughout the study. And Dr. Ceto for proving maps of future land use predictions. Thanks to my colleagues especially Dr. Sharma, for his help and advice.

This work is supported by NASA Grant NNX12AM88G and NSF Grant AGS-0934592. A seed fund from the Global Institute of Sustainability of Arizona State University supported the author in spring 2013.

TABLE OF CONTENTS

Page

CHAPTER Page

APPENDIX Page

LIST OF TABLES

LIST OF FIGURES

Figure Page

CHAPTER 1

INTRODUCTION

1.1 Motivation

This study will use climate downscaling to investigate the effects of urbanization on the local climate of multiple metropolitan areas around the world. Climate downscaling is the use of low resolution climate data, either from observations or from global climate model output, as the input for high resolution regional climate model simulation and prediction. We will use a comprehensive three dimensional atmospheric model to quantify the key effect of urbanization by numerical simulations. The Weather Research and Forecasting (WRF) model will be used for the principal simulations. The thermodynamic and mechanical effects of urbanization on climate will be extracted from a series of runs with different land surface boundary conditions.

The aridity of an area can be quantitatively classified using the Aridity Index (AI) defined as the ratio of precipitation to potential evapotranspiration. Semi-arid and arid areas have AI from 0.05-0.20 and 0.20-0.50 respectively, and desert from 0-0.05 (UNEP 1997). Globally, arid and semi-arid areas and desert cover about 32.4% of all land surface of the planet, and inhabited by more than 20% of the world's population. An accurate understanding of the factors effecting the local climate is especially needed for desert cities, as their populations depend on scarce water resources (Barnett and Pierce, 2008, Barnett et al., 2008).

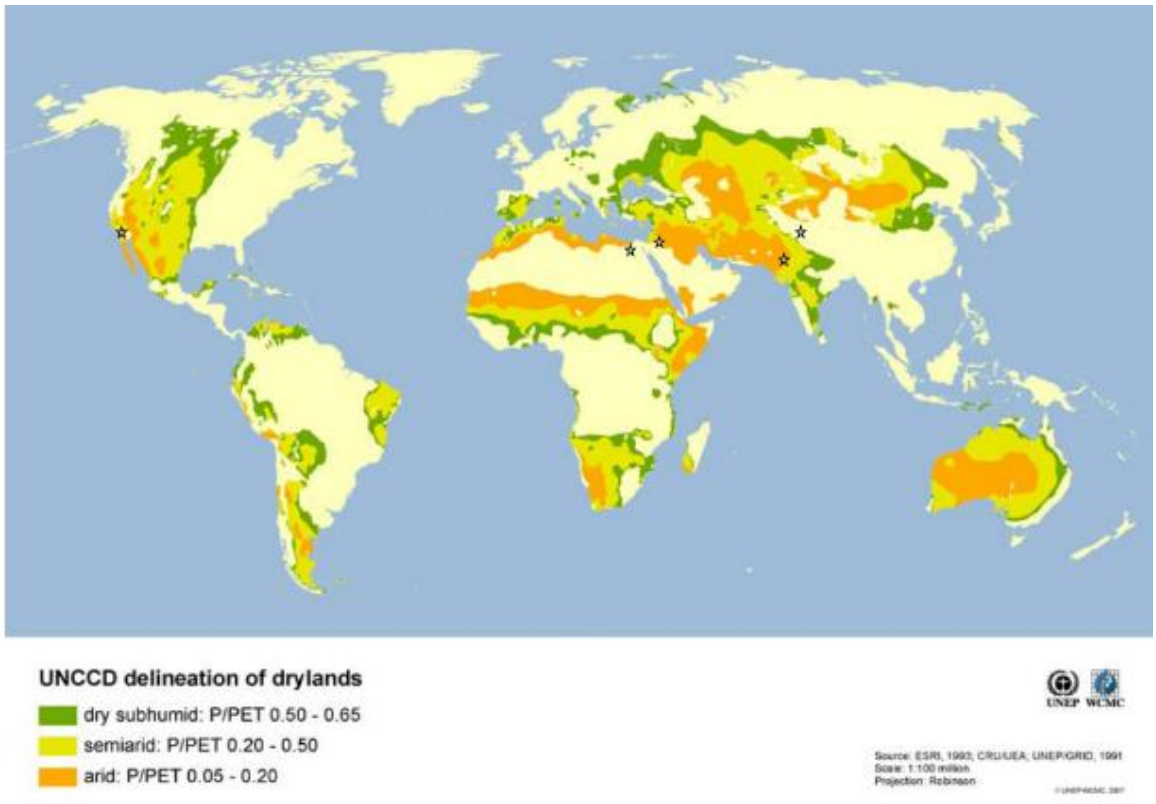

Figure 1. A world map showing the desert, arid and semi-arid areas. The stars show the locations of the 5 cities investigated in this study: Las Vegas, El Kharga (Egypt), Beer Sheva (Israel), Judhpur (India), and Hotan (China). (ESRI, 1993, UNEP/GRID 1991)

While the global climate is changing, land use shifts also play an important and less understood role in the change of local climates (National Research Council, 2005). It was shown that significant regional changes can affect the large scale circulation (Matsui and Pielke 2006). In the areas of the US with large farmland coverage, the average hot season temperature was shown to be 0.1 C less than urban areas (Diffenbaugh 2009). The same study also showed that using global models alone is not sufficient to predict the local surface weather.

The presence of urban areas can lead to significant local heating (Zhou et.al 2011 and Brazel et al. 2007) and even modifications of the path of thunderstorms (Changnon

2001). Land use changes can affect the climate through the modification of surface heat budget and temperature causing significant changes in the wind pattern and rainfall (Matsui and Pielke 2006). Land cover can also influence climate through biogeochemical processes (Pielke et al. 2002), which is beyond the scope of this study.

As an additional example of land use changes, Table 1 shows the evolution of coverage of different land surface types over the US in the last 3 decades. While cropland area decreased from 1978 to 2007, reaching its lowest level since 1945, urban buildup has grown at twice the rate of population growth quadrupling from 1945 to 2007 (Nickerson, et al., 2011). Clearly, the increase in urban type of land in the past decades is substantial. Moreover, this trend is likely to continue. Therefore, it important to quantify future climate over the cities based on the projections of future urban expansions (see chapter 6).

Table 1. Summary of land use areas in US from 1982 to 2007 in million acres (U.S. Department of Agriculture, Natural Resources Conservation Service 2009).

Year	Cropland	Conservation	Pasture land	Range land	Grazed forest land	Ungrazed forest land	Rural land	Developed land	Water and federal areas
1982	419.5	0.0	130.9	417.9	66.0	337.3	47.2	71.0	447.7
1987	405.5	13.8	126.7	412.6	63.9	341.4	47.5	76.9	449.3
1992	381.4	34.1	125.0	408.9	63.2	342.1	48.1	83.9	450.9
1997	376.1	32.7	119.8	407.5	60.7	345.9	48.7	94.6	451.6
2002	367.1	32.0	117.8	408.2	56.5	350.8	48.9	104.0	452.4
2007	357.0	32.9	118.6	409.1	56.1	350.3	49.6	111.3	452.8

1.2 Climate downscaling

Figure 2 shows the typical resolution of the global climates models used in the four Intergovernmental Panel on Climate Change (IPCC) reports, from the first report

(FAR) in 1990 to the forth report (AR4) in 2007. With the typical horizontal resolution of about a 100 km, an area comparable in size with the State of Arizona will be covered by only a few grid points. Global models are useful for simulating the main features of large scale flow (Giorgi, 1990, Hurrell, 1995) but not regional features, both natural and man-made, with a scale less than 100 km.

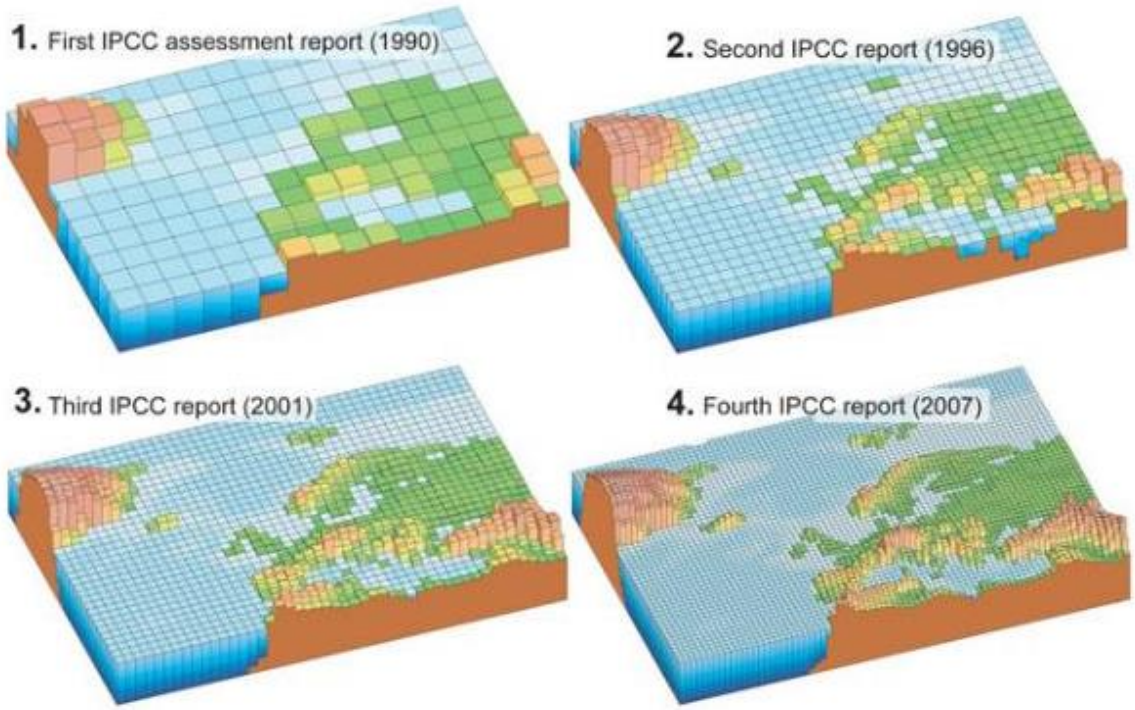

Figure 2. The grid system that covers Europe and North Atlantic as used global climate models in the four versions of IPCC assessment reports (IPCC 2007).

While regional models offer much higher resolution than global models, their computational domains cover only limited areas which require additional lateral boundary conditions. In the framework of climate downscaling, global model output or observational data is used as the boundary condition for the regional model which serves

to transfer the effect of the large scale flow to regional scales. Figure 3 shows the temperature distribution for California and Nevada at global and regional model resolutions. It shows that climate downscaling can be used to capture the fine details.

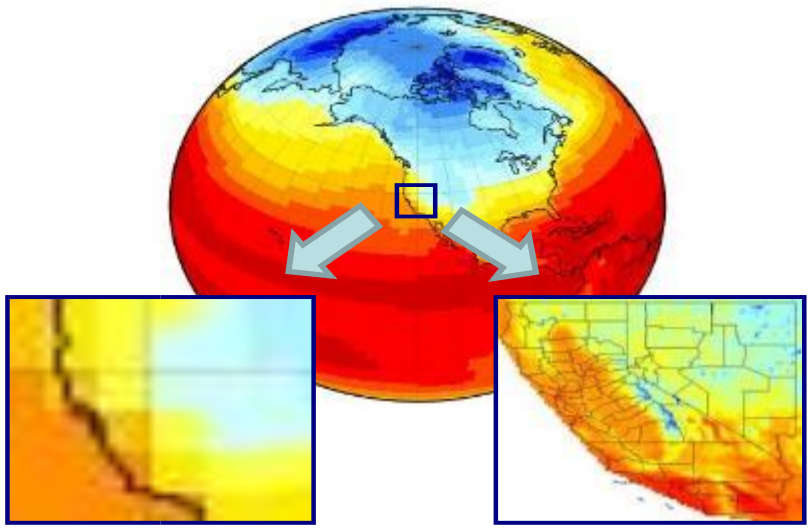

Figure 3. December 2000 temperature distribution for California from a global model (left, GFDL CM2.1) and a regional model (right) with resolution of about 12 km (Moser et al., 2009) Blue and red represent cold and hot temperatures.

1.3 Objective

As an important type of land use change, urbanization is known to induce substantial changes in local temperature. It has been elucidated in the classical paradigm of urban heat island (UHI)—emerging urban built structures facilitate an increased absorption of heat by surfaces during the day and release of it at night, resulting in a weakening of nighttime cooling (e.g., Oke 1982). While the effect of nighttime warming is qualitatively robust, the detailed changes in temperature and wind induced by urbanization can vary significantly from city to city.

For example, examining the multi-decadal trends over Baltimore and Phoenix metropolitan areas, Brazel et al. (2000) demonstrates a weak daytime warming for the former but weak daytime cooling for the latter as measured by the classic $T_u - T_r$ (urban temperature minus rural temperature). The weak daytime urban cooling relative to rural area in Phoenix is reproducible by numerical simulations (Georgescu et al. 2011). The contrast between Baltimore and Phoenix arises from the fact that, for the latter, the growth of urban structures is at the expense of arid lands instead of lands with high vegetation coverage (Brazel et al. 2000, 2007; Georgescu et al. 2011). Yet, this explanation might not apply to other cities, which also exhibit daytime cooling despite not being located in arid regions (e.g., Vancouver in Runnalls and Oke 2000; Indianapolis in Carnahan and Larson 1990).

These examples underscore the need for researchers to not only seek a universal mechanism for the influence of land cover on urban climate but also explore inter-city differences and attribute them to the detailed urban parameters of the individual cities. Detailed case studies for cities with unique landscape and history of urbanization adds to this important line of investigation. In this spirit, this study uses a three-dimensional atmospheric model to perform numerical simulations in order to quantify the impact of urbanization on the local climate of Las Vegas and four other cities.

While many studies have used climate downscaling to simulate regional climate (e.g., Caldwell et al., 2008, Heikkila et al,. 2010, Pan et al., 2011), relatively few have focused on arid and semi-arid regions. Moreover, the majority of previous studies used a horizontal resolution of 15-50 km, which is not sufficient for resolving urban landscape. With this background this study will:

(1) Use a regional model with 1-3 km horizontal resolution to explicitly resolve urban landscape in order to simulate the local climate change due to urbanization over arid and semi-arid areas.

In the few numerical studies that have considered the effect of land use changes on urban climate (Georgescu et al., 2008, 2009, Kusaka et al., 2012, Rozoff et al. 2002 for St. Louis, Meir et al. 2013 for New York City), the simulations were relatively short (e.g., 1 month) and the focus was always on a single city. The conclusions drawn from those studies might not be universal with respect to the size of the city and the composition of the land surface types. To make further contributions to this line of research, this study will

(2) Perform long simulations for multiple cities with different sizes and distributions of land surface type in order to determine the relevant physical processes which are universal as well as those which are not universal in producing local climate change. Previous studies have pointed to the possible role of the diurnal wind field in modifying the urban heat island (e.g., Morris et al. 2001; Takahashi et al. 2011; Lee et al. 2012). To substantially improve our understanding of the dynamical effects, this work will

(3) Analyze both dynamical and thermodynamic effects of urbanization on local climate from the extensive 3D numerical simulations with 3D output of temperature and wind field.

Few studies have systematically simulated future climate changes induced by urbanization due to a lack of reliable projections on the future extends of major urban areas. Nevertheless, progresses have recently been made to construct such projections

(Fragkias and Seto, 2007 and Seto, 2008). Taking advantages of the availability future land use scenarios provided by Dr. Karen Seto, this research will

(4) Use high resolution regional models to project future climate over multiple cities based on the projected scenarios of future urban expansion.

In addition to these four major objectives, this study will also validate the numerical simulations of local climate over urban area with in situ observations where they are available (e.g. Miller 2011).

CHAPTER 2

NUMERICAL MODEL

2.1 Governing Equations

The Weather Research and Forecasting (WRF) model is a non-hydrostatic numerical weather and climate prediction system. It is an open source model, a result of the cooperation between the National Center of Atmospheric Research (NCAR) and partners (Skamarock et al. 2008). As the main constituents of the atmosphere are gases and water in various physical forms, the main governing equations for the atmosphere are the fluid dynamics equations (for the gasses including water vapor) plus conservation of moisture. The core of the governing equations in WRF model are modified from Navier-Stokes equations in rotating coordinate, with ϑ denoting the vector of Earth's rotation:

$$\frac{\partial \vec{v}}{\partial t} + \frac{1}{\rho}\nabla p + \vec{v} \bullet \nabla \vec{v} - \nu \nabla^2 \vec{v} - 2\vartheta \times \vec{v} = 0 \qquad (1)$$

$$\frac{\partial \rho}{\partial t} + \nabla \bullet (\rho \vec{v}) = S \qquad (2)$$

$$\frac{\partial T}{\partial t} + \vec{v} \bullet \nabla T + k \nabla^2 T = F_T \qquad (3)$$

$$\frac{\partial q}{\partial t} + \vec{v} \bullet \nabla q = F_q , \qquad (4)$$

where Eq.(1)-(3) are the momentum, continuity, and thermodynamic energy equations and Eq.(4) describes the conservation of water vapor concentration. The terms in the RHS are the sources and sinks for the respective quantities. In those equations, ρ is density, $\vec{v}$ is the 3D velocity vector, p is pressure, ν and k are the molecular viscosity coefficient and thermal diffusivity, T is temperature, and q is the specific humidity. With

seven variables and only six equations, an equation of state is needed to close the system. We will introduce its detail later.

In the original Navier-Stokes equations, the effects of molecular viscosity and thermal diffusivity are confined to very small spatial scales (~cm). Those terms are not explicitly included in the WRF model. Instead their effects are parameterized and added to the RHS of the momentum and thermodynamic equations as additional sources and sinks. Even with 1 km horizontal resolution many physical processes cannot be explicitly resolved by the numerical model. Among them, the most important are longwave and shortwave radiative heating, boundary layer turbulence processes, cumulus convection, cloud microphysics, and land surface processes. The last one includes both natural processes and processes related to urbanization which will be further discussed in section 2.3.

The WRF model uses terrain-following vertical coordinate, which for a dry atmosphere is defined as

$$\eta = \left(p_h - p_{ht}\right)/\mu, \qquad (5)$$

where p_h and p_{ht} are the hydrostatic pressure at the model level and at the top of the model, $\mu = \left(p_{hs} - p_{ht}\right)$, where p_{hs} is the hydrostatic pressure at the surface. Figure 4 illustrates the geometry of the coordinate system. The value of η changes from 1 at the surface to 0 at the top of the model. The variable, $\mu(x, y)$, represents the mass per unit area within a column in the computational domain at the location (x, y). In the WRF model the total mass of the atmosphere is contributed by dry air and moisture. To accommodate the effect of moisture the η given in Eq.(5) is recast as

$\eta = (p_{dh} - p_{dht})/\mu_d$ where p_{dh} and p_{dht} are the hydrostatic pressure of the dry atmosphere at the model level and at the top of the model, and $\mu_d = (p_{dhs} - p_{dht})$, where p_{hs} is the hydrostatic pressure of the dry atmosphere at the surface.

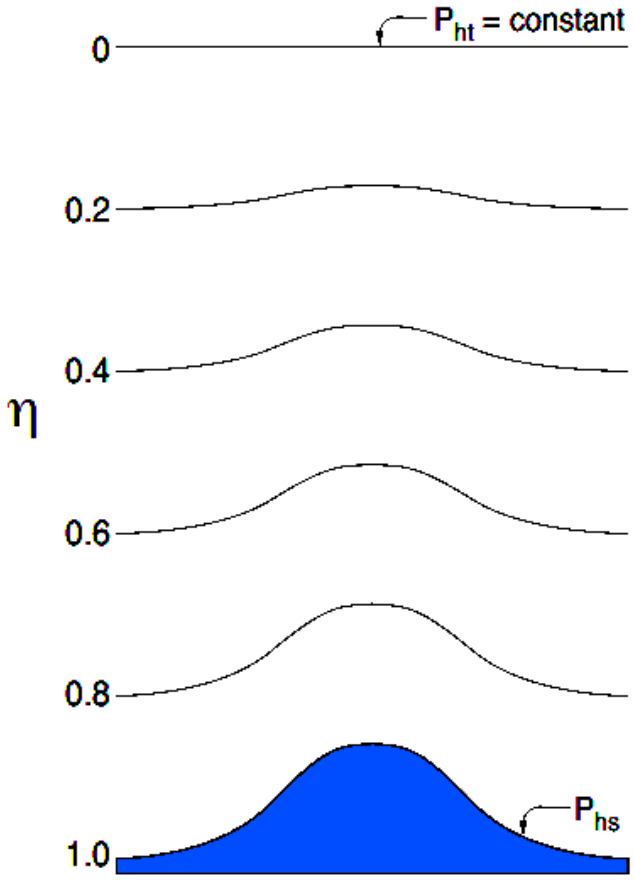

.

Figure 4. WRF terrain following vertical coordinate η (Skamarock et al., 2008),

To more conveniently represent the thermodynamics of a stratified atmosphere, in the model the temperature T is replaced by potential temperature, defined by $\theta = T\,(p/p_0)^{-R/Cp}$, Where p_0 is a reference pressure and R and C_p are the ideal gas constant and the heat capacity of the atmosphere. Moreover, the major prognostic variables are further

transformed to their counterparts with mass weighting: $\vec{V} = \mu_d \vec{v} = (U, V, W)$, $\Omega = \mu_d \eta^{\bullet}$, and $\Theta = \mu_d \theta$. The governing equations then become

$$\partial_t U + (\nabla \bullet \vec{V}u) + \mu_d \alpha \partial_x p + (\alpha / \alpha_d)\partial_\eta p \partial_x \phi = F_U \tag{6}$$

$$\partial_t V + (\nabla \bullet \vec{V}v) + \mu_d \alpha \partial_y p + (\alpha / \alpha_d)\partial_\eta p \partial_y \phi = F_V \tag{7}$$

$$\partial_t W + (\nabla \bullet \vec{V}\omega) - g((\alpha / \alpha_d)\partial_\eta p - \mu_d) = F_W \tag{8}$$

$$\partial_t \Theta + (\nabla \bullet \vec{V}\theta) = F_\Theta \tag{9}$$

$$\partial_t \mu_d + (\nabla \bullet \vec{V}) = 0 \tag{10}$$

$$\partial_t \phi + \mu_d^{-1}[(\vec{V} \bullet \nabla \phi) - gW] = 0 \tag{11}$$

$$\partial_\eta \phi = -\alpha \mu_d \tag{12}$$

$$\partial_t Q_m + (\nabla \bullet \vec{V}q_m) = F_{Q_m} \tag{13}$$

The ϕ and α in Eq. (12) are the geopotential ($\phi = gz$) and the inverse of density. The equation of state, $p = p_0 (R_d \theta / p_0 \alpha_d)^{\gamma}$, is also needed to close the system of equations. In these equations, the subscript "d" indicates dry air, and "m" indicated moisture. A thermodynamic variable without a subscript indicates the total of the quantity. Since other phases of water also exist in the atmosphere, the total inverse density is given as $\alpha = \alpha_d (1 + q_v + q_c + q_r + q_i + ...)^{-1}$, where q is the mixing ratio (mass per unit mass of dry air) and the subscripts denote various forms of water such as water vapor, liquid water in cloud and rain, and solid water in ice crystals in clouds.

The model automatically generate a curvilinear coordinate system for a domain specified by the user. It supports multiple schemes of map projection, under which the horizontal

grids will not be uniform. The model directly absorbs the non-uniform map factors into the governing equations by using the simple relation

$(m_x, m_y) = (\Delta x, \Delta y)/(\text{distance on earth})$, where the "distance on earth" is the physical distance between two grid points on earth surface. With this transformation, all the prognostic variables are further modified, e.g.

$U = \mu_d u / m_y$, $V = \mu_d v / m_x$, $W = \mu_d w / m_y$, and $\Omega = \mu_d \dot{\eta} / m_y$, and the corresponding governing equations are also modified. For example the east-west component of the momentum equation becomes

$$\partial_t U + m_x \left[\partial_x (Uu) + \partial_y (Vu)\right] + \partial_\eta (\Omega u) + \mu_d \alpha \partial_x p + (\alpha / \alpha_d)\partial_\eta p \partial_x \phi = F_U \quad . \qquad (14)$$

The rest of the equations are transformed in a similar manner.

2.2 Grid and Discretization

For spatial discretization the model uses Arakawa C-grid which is staggered in both horizontal and vertical directions, as shown in Figure 5. Users have the option of using 2nd- to 6th-order numerical schemes for advection. For time integration, the model uses the third order Runge-Kutta (RK3) scheme.

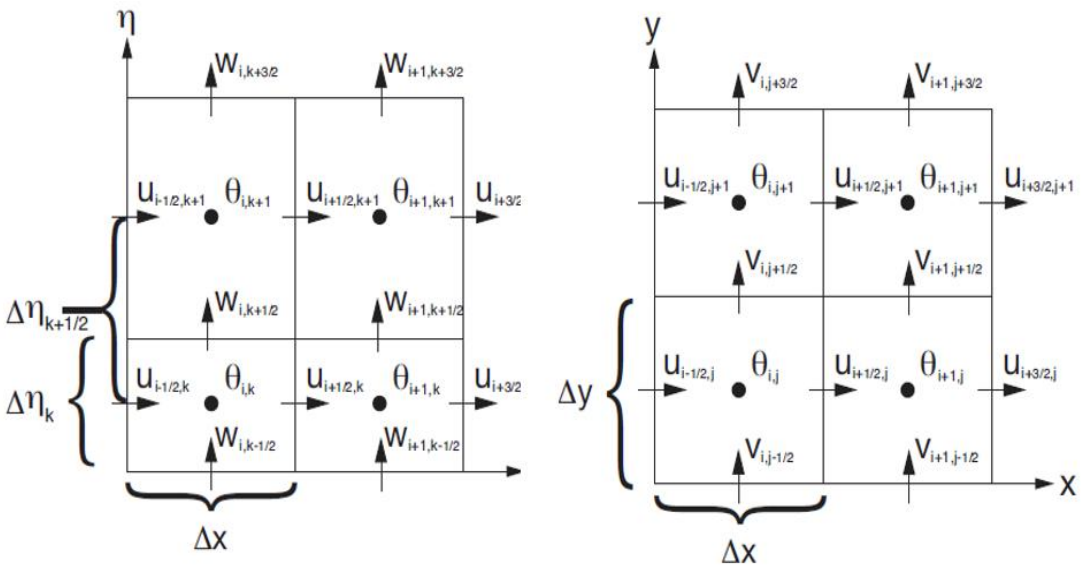

Figure 5. The horizontal (right) and vertical (left) grid configurations in WRF (Skamarock et al., 2008),

The model uses a time split scheme (Wicker and Skamarock 2002) which allows the use of a smaller acoustic time step to resolve the fast propagating sound waves, which exist in the non-hydrostatic model due to compressibility in the vertical direction. Figure 6 shows the flow chart of the time split integration scheme used for WRF. Note that the forcing terms do not need to be calculated at every time step. The efficiency of the scheme lies in the fact that the global time step for RK3 is much larger than the acoustic time step.

The model allows the use of multiple layers of nesting with different resolutions. Each nested region is entirely contained within a single coarser (parent) gird and uses the value of the variables at the interface from the parent domain as the lateral boundary conditions. Figure 7 shows an example of one layer nesting with a 3:1 ratio of the grid

size of the parent and the nested domains. Using multiple nesting, one is allowed to use a high resolution (e.g., 1-3km) for the innermost domain to resolve urban landscape while maintaining a coarse resolution for the outer most domain (e.g., 25-50 km) where the boundary conditions from global model output or observations are applied. In WRF, the lateral boundary conditions imposed at the outermost domain are allowed to be time-varying, which will be needed for our simulations (details in chapter 3).The surface boundary conditions are constructed from land use maps which the model will automatically interpolate onto the computational domain and grid. For our simulations we choose to set the top of the model to a constant pressure of 50 mbar.

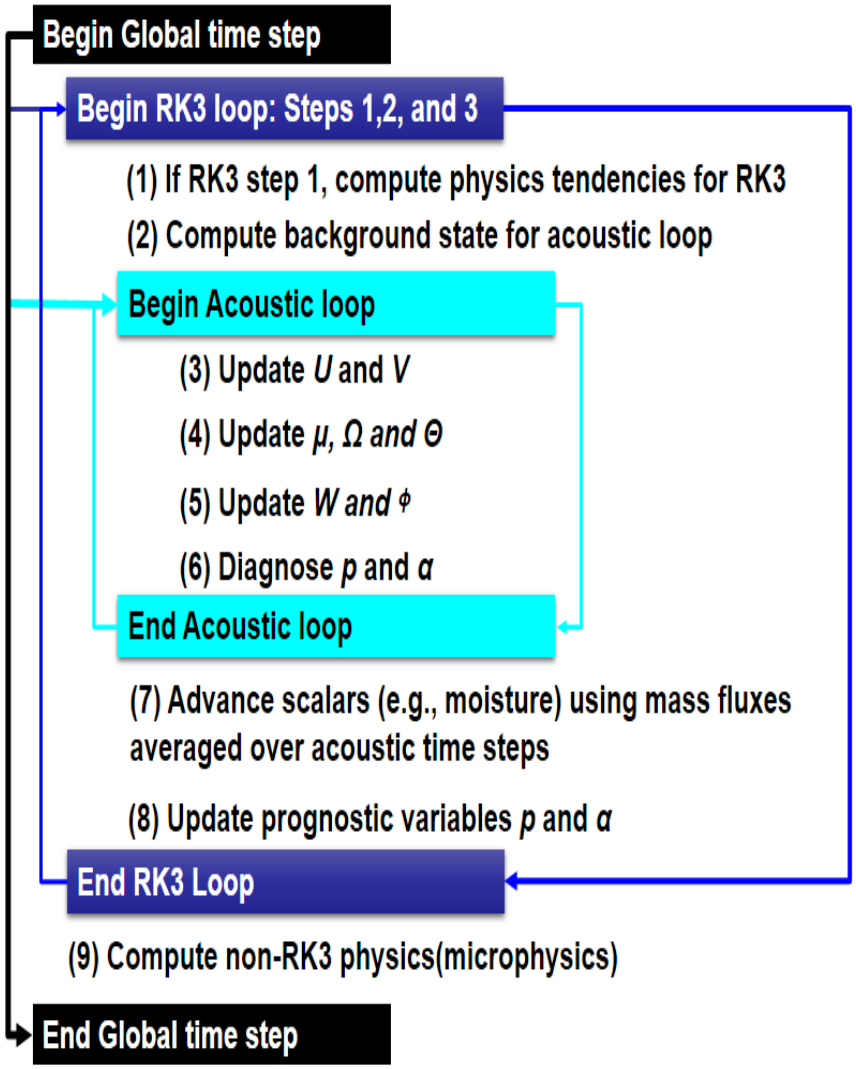

Figure 6. Flow chart of the time split scheme used for WRF (Skamarock et al. 2008)

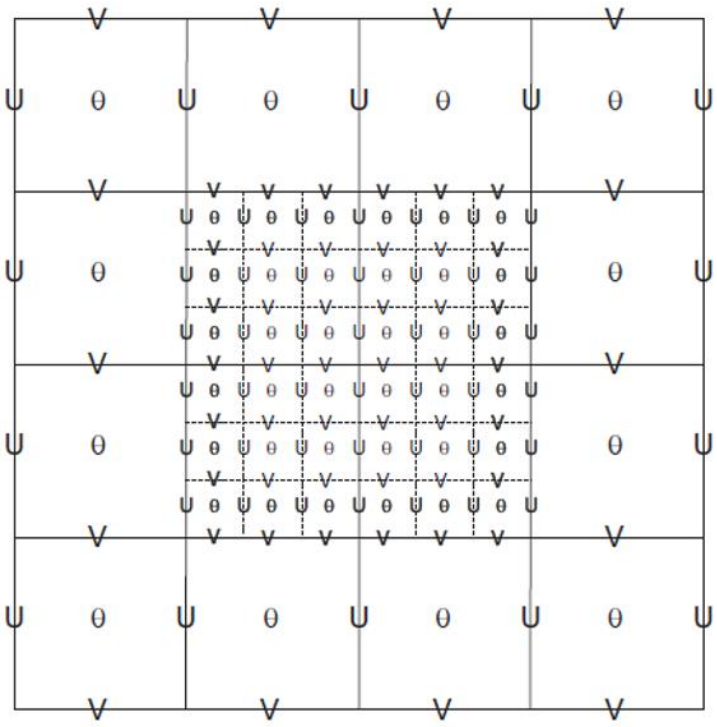

Figure 7. Staggered grid for a part of the parent domain and an imbedded nest domain with a 3:1 grid size ration. The bold typeface variables along the interface between the coarse and fine grid define the locations where the lateral boundaries for the nest are in effect WRF (Skamarock et al., 2008).

2.3 Land Surface Model and Urban Canopy Model

Figure 8 shows the processes that involve the interactions between the atmosphere and surface. Such processes are included in the land surface model embedded in WRF. It includes the exchange of momentum, energy (e.g. radiation, sensible and latent heat), and moisture between the surface and the atmospheric boundary layer. A change in the land surface type would affect the surface energy balance through the modification of the surface albedo and emissivity, exchange coefficients of moisture, and surface roughness.

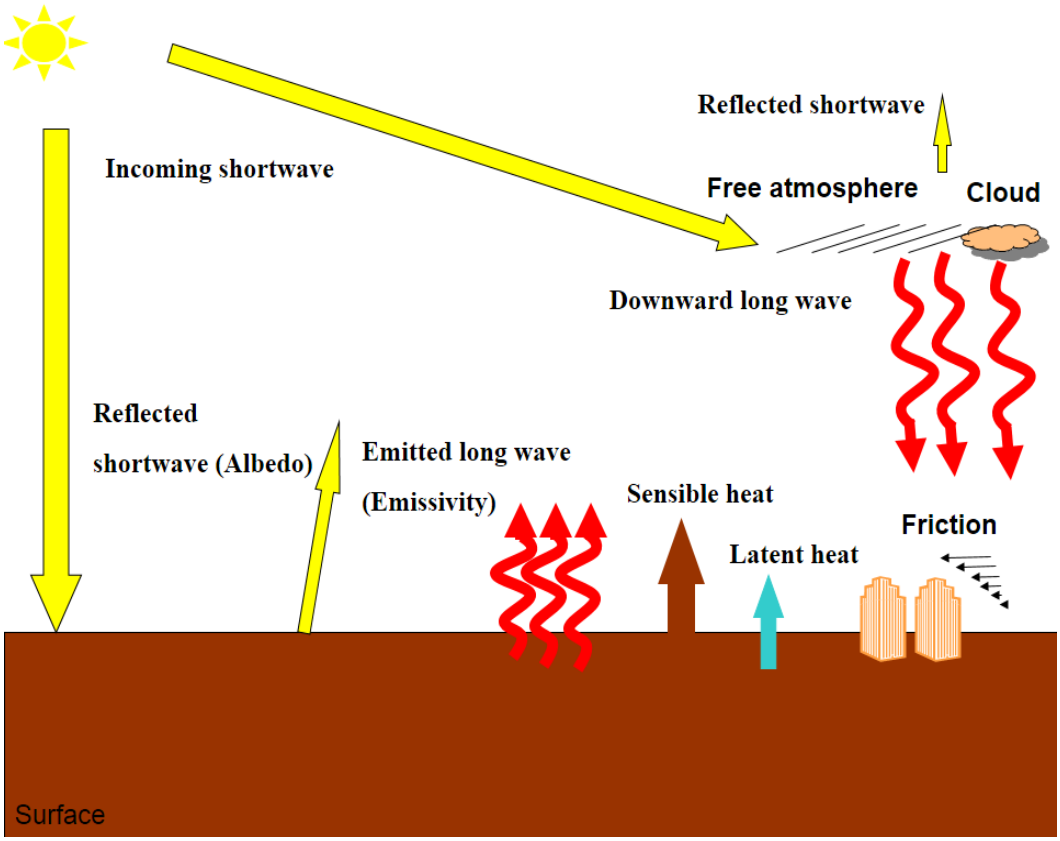

Figure 8. Processes included in land surface and radiation models.

To better capture the physics of urban climate we choose to activate the option in WRF to run a single layer Urban Canopy Model (UCM). The model was developed by Kusaka et al. (2001) and Kusaka and Kimura (2004) and takes into account the shadow effect, skyline effect, and street canyon effect. Figure 9 shows a schematic diagram of the urban canopy model. It allows the walls, roofs and street canyon, to have a different temperature.

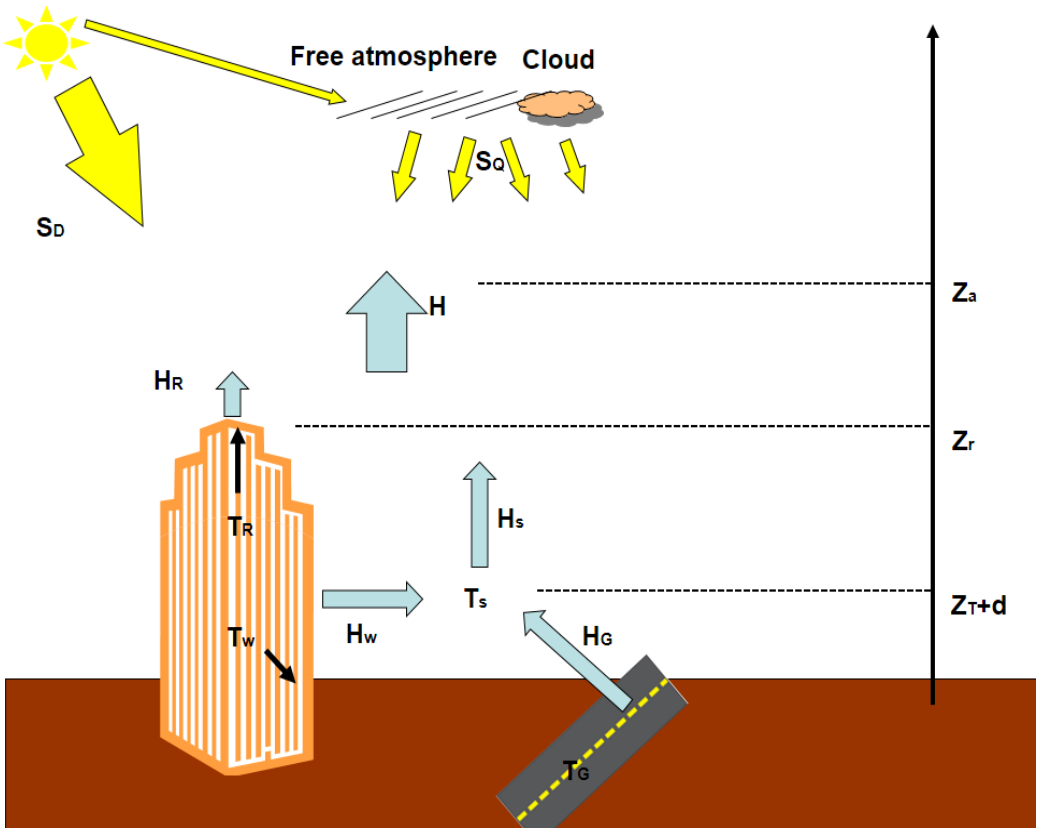

Figure 9. Schematic diagram of the single layer urban canopy model. Za: height of the lowest model level; Ta: air temperature at Za; H: aggregated sensible heat flux; Zr: building height; ZT: roughness length for heat; d: zero displacement height. TR, TW, and TG are surface temperature of roof, wall, and road, respectively; and HR, Ha, Hw, and HG are sensible heat fluxes from the roof, canyon, wall, and road, respectively. SD and SQ are direct and diffused solar radiation (Kusaka et al., 2001).

Figure 10 shows how it is implemented in the WRF model. It incorporates a set of user defined urban parameters, WRF generated flow state variables, and heat fluxes to generate urban state variables. The urban parameters are unique to each city and include, to name a few, building height, roughness length above canyon for momentum, building coverage ratio, urban fraction, and heat capacity of the roof, road and walls, thermal connectivity of roof. The urban state variables include, to name a few, urban roof skin temperature, urban road skin temperature, urban canopy wind speed, urban heat and radiation fluxes. For Las Vegas, we use the default value of those variables, for example

building height, urban fraction and heat capacity of roof were chosen to be 7.5 m, 0.9, and $1.0*10^6$ J/m^{3}K respectively.

Through the exchange coefficients, building walls exchange radiation and sensible heat with the street and air, allowing for indirect absorption of radiation. The urban canopy model is coupled to the land surface model through the parameter "urban fraction" which quantifies the urban sub-grid scale heterogeneity. For example, the grid scale sensible heat flux is calculated as follows,

$$H = A_{Natural} H_{LSM} + A_{Urban} H_{UCM}, \quad (15)$$

where H is the grid scale sensible heat flux from the surface to lowest model level, $A_{Natural}$ is the fraction of natural surface such as water, grassland and crop, A_{Urban} is the fraction of the urban buildup, H_{LSM} is the sensible heat flux from the land surface model, and H_{UCM} is the sensible heat flux from the urban canopy model. Latent heat flux and long wave fluxes are calculated in a similar way. A formula similar to Eq. (15) is used to calculate the infrared radiation, σT^4, for surface skin temperature.

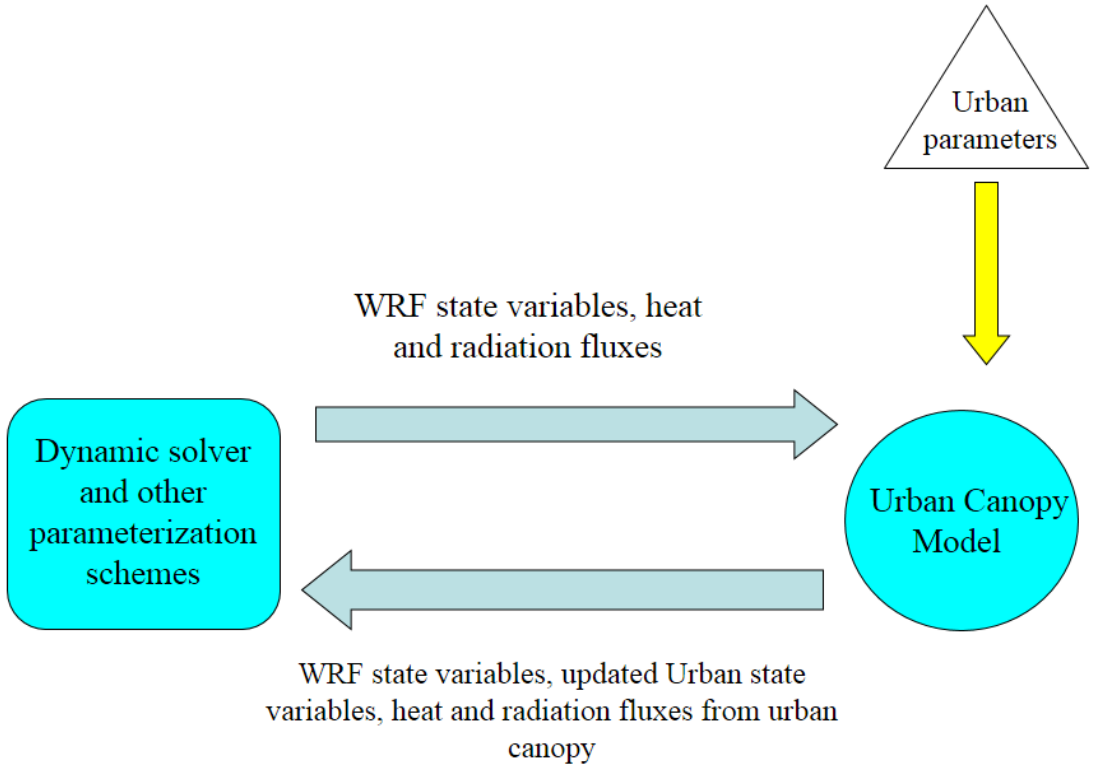

Figure 10. Flow chart of the interaction of UCM with WRF.

CHAPTER 3

DATA SETS FOR BOUNDARY CONDITIONS.

For each simulation, two types of land use maps are used to construct the surface boundary conditions. Away from the city, WRF's default USGS land use map is used. In the close vicinity of the cities one of three land use maps are used. The first is the National Land Cover Database (NLCD) produced by the Multi-Resolution Land Characteristics Consortium (MRLC). The data set (hereafter called NLCD) has a 30 meter resolution which covers the entire United States for 2006 and 1992 and is used only for Las Vegas. The details and results for these runs are presented in chapter 4.

For 2006, NLCD2006 has 16 land use categories and is based primarily on the unsupervised classification of the Landsat Enhanced Thematic Mapper+ (Fry et al., 2011).

For 1992, NLCD1992 has 21 land use categories and is based on Landsat Enhanced Thematic Mapper plus other sources like topography, census, and agricultural statistics, soil characteristics, and other types of land cover and wetland maps (Vogelmann et al., 2001), see appendix.

The second source of data is Landsat Thematic Mapper data (hereafter called Landsat data) with a 30 meter resolution over the selected cities for 1985, and 2010. For each of the aforementioned years, at least one cloud free image is used for each city of our interest. The maps are produced and tailored to our numerical experiment by Dr. Soe Myint. More details about these maps are presented in chapter 5.

The third source is a collection of projection maps of urban expansion provided to us Dr. Karen Seto, Projection maps are produced by using a physical urban growth model that requires few, but widely available, spatially explicit data, see chapter 7 for details

The resolution of the satellite land use maps is about 30 m while the resolution of WRF's computational domain is from 1 to 3 km. Which means that every grid point in the computational domain will have 30~ 100 satellite image pixels. While the classification of land cover in WRF includes 24 categories, the NLCD2006 and NLCD1992 data have 16 and 21 categories, respectively. The cross references listed in Table 9 were adopted to convert the NLCD categories to their corresponding WRF categories. The categories not listed in Table 9 together account for less than 1% of the land coverage over the greater Las Vegas area. For simplicity, they are all converted to the dominant background land category of shrubland. The resolution of the NLCD data is much higher (at 30 m) compared to the 3 km resolution for the innermost domain of WRF in the simulations. To map the NLCD data onto WRF grid, a "democracy" scheme is used for counting the numbers of the NLCD pixels in each WRF grid box and picking the most dominant land type to overtake the WRF grid box.

For each city at least three land use maps are used. Two of the maps represent two stages of urbanization in the past separated by at least 15 years and the third represent predicted future stages of urbanization. Such a separation in time will allow for a sharper contrast in the urban landscape used in the boundary conditions for WRF, which will in turn allow us to deduce local climate change from the simulations with a higher level of statistical significance. To investigate the extreme case of land use change a new land

surface map for Las Vegas will be constructed by truing all urban use grid points to the background (shrub-land). This will be nominally called the 1900 Las Vegas.

For initial and lateral boundary conditions, the NCEP observation based data (NCEP 2000) were used. The data has resolution of 1^o by 1^o and include several variables, to name a few, air temperature, albedo, humidity, hydrostatic pressure, and velocity. The boundary conditions are applied to outer most domain and updated every 6 hours.

CHAPTER 4

THE INFRUENCE OF URBANIZATION ON THE CLIMATE OF LAS VEGAS

This study uses a three-dimensional atmospheric model to perform numerical simulations in order to quantify the impact of urbanization on the local climate of Las Vegas. The choice of Las Vegas as the study area is motivated by three considerations. First, as one of the most important desert cities in the U.S. in terms of population and land area, the effect of urbanization on the local climate of Las Vegas has not been studied extensively when compared to cities such as Phoenix. A detailed study and comparison of the results with existing studies for Phoenix (Surveys of recent studies for Phoenix can be found in Brazel et al. 2000, 2007; Georgescu et al. 2009; Myint et al., 2013; Zheng et al., 2014) and other large desert cities will help affirm the common features of the effect of urbanization for all those cities. For example, a recent observational study by Miller (2011) hints that the aforementioned daytime cooling also exists in Las Vegas.

Secondly, despite their similarity in population and size, Las Vegas differs from Phoenix in that the former has seen almost no agricultural development through its history. For Las Vegas, urbanization is simply the process of replacing shrubland with urban structures. The dominance of only two land surface classes makes it more straightforward to interpret the results of numerical experiments for the city.
Thirdly, Las Vegas is surrounded by dramatic topography, which helps sustain a diurnal cycle of strong and coherent low-level wind over the city. This makes Las Vegas an ideal location to study the mechanical effect of urbanization on the wind field which

complements most of previous studies that focused on temperature. Since previous studies have pointed to the possible role of the diurnal wind field in modifying the urban heat island (e.g., Morris et al. 2001; Takahashi et al. 2011; Lee et al. 2012), the numerical experiments also serves to explore how the thermodynamic and mechanical effects interact to shape the climate change induced by urbanization.

The numerical simulations in this work use the approach of dynamical downscaling (e.g., Leung et al. 2003; Mearns et al. 2012). A regional atmospheric model is driven by imposed, but time-varying, lateral boundary conditions constructed from large-scale observations. Multiple layers of nesting are adopted to allow a high resolution for the innermost model domain that encompasses Las Vegas. Each set of numerical experiments are carried out by keeping all boundary conditions the same except changing the land surface boundary condition within the metropolitan area. In this manner, the difference in the climate between two simulations can be solely attributed to the influence of land use changes by urbanization. This complements observational studies in which it is more difficult to isolate the effects of land use changes on local climate.

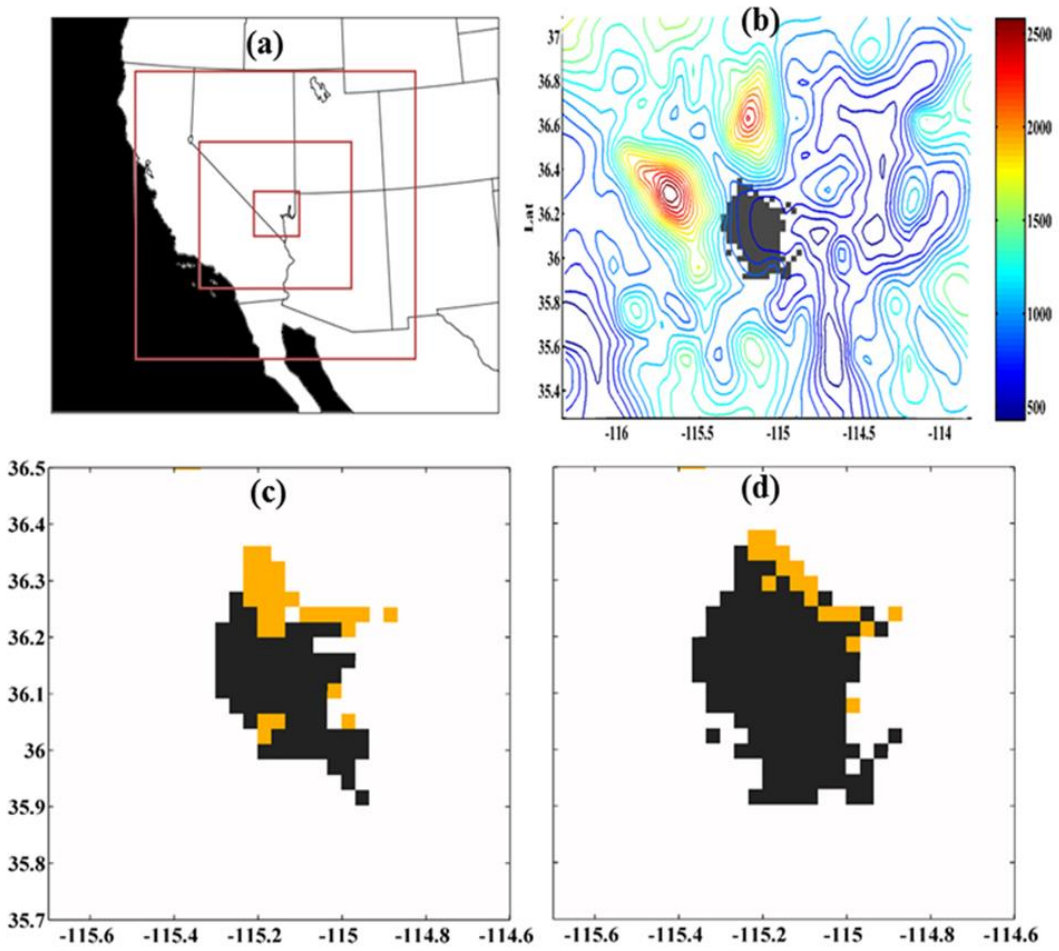

Figure 11. (a) The computational domains and nesting for WRF model used in this study. (b) The topographic map (contours of elevation in feet) for the innermost model domain. The 2006 urban extent of Las Vegas is indicated in black shading. (c) and (d) show the land use map over Las Vegas metropolitan area for 1992 and 2006, respectively, as used in the numerical simulations. Black, brown, and white grid boxes are those covered by urban land, barren surface with sparse vegetation, and background shrub land. The data for (c) and (d) are constructed from the NLCD1992 and NLCD2006 datasets. Longitude and latitude are marked at the margins of (a)-(c).

4.1 Experimental Design

For the main simulations, Noah Land Surface parameterization scheme is used. The scheme has four layers of soil and uses unified NCEP/NCAR/AFWA scheme with soil temperature and moisture, fractional snow cover and frozen soil physics (Chen and Dudhia 2001). A single layer urban canopy model is used. The canopy model was

developed by Kusaka et al. (2001) and Kusaka and Kimura (2004) and modified by Chen et al., (2006). To test the sensitivity of the model, another run is completed with simple land surface model based on MM5 5-layer soil temperature model with the urban canopy model turned off. Shown in Figure 11(a) three levels of nesting will be used decreasing in resolution from 3 km around the city to about 48 km in the outer most domain which covers most of the southwest US.

To only account for land use changes in the city, grid points away from the city (outside of the box) were left at WRF's default land use state. In the close vicinity of the city (inside the box) NLCD1992 and NLCD 2006 data was downscaled and used. To deduce the maximum impact of urbanization, a third set of land use data was constructed in which the whole city was removed and all the grid points with urban buildup were reverted to the background state of shrubland. This third case corresponds to an ideal 1900 before the city existed.

To quantify the changes in climate of the city, three domains were defined.

Domain 1: represents the urban buildup of Las Vegas as of 1992.

Domain 2: represents the additional urban buildup from 1992 to 2006.

Domain 3 (2006 Las Vegas): represents the city with 2006 boundaries. All domains are used in comparison with the 1900 map where no grid points were urbanized. Figure 12 shows the 4 land use maps considered for the run and the domains.

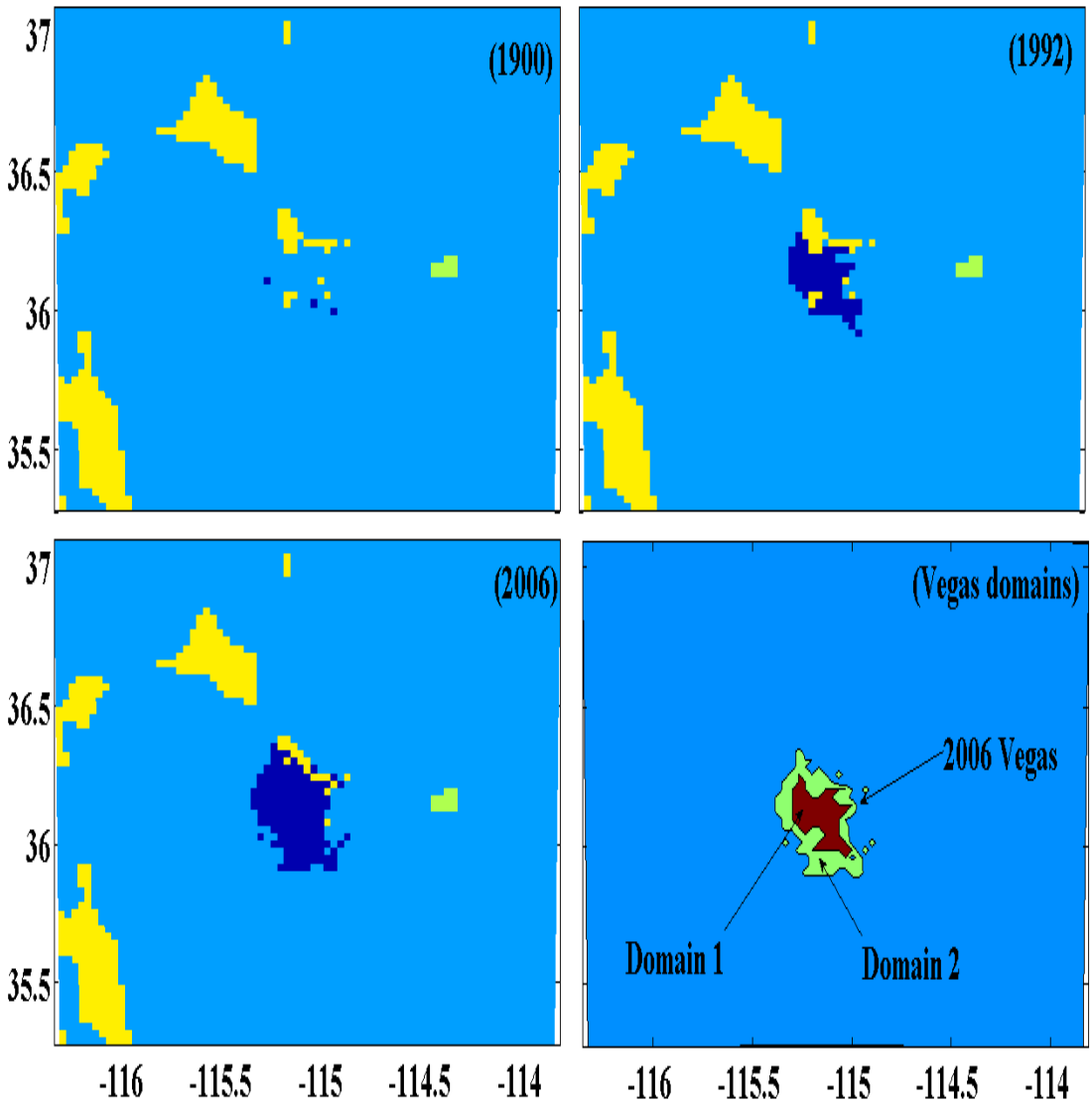

Figure 12. The land use maps of Las Vegas used in the actual runs. Light yellow represents water, dark yellow represents mountains, light blue represents shrubland, and the dark blue represents urban buildup. On the top left is the map for 1900, top right is for 1992, and bottom left is for 2006. In the bottom right corner is schematic representation of the 3 domains used.

The main simulation consisted of 6 runs and each lasted for 3 months. The lateral boundary conditions for the outer most domain were taken for the summer (05/03/2006 to 08/03/2006) and winter (10/03/2005 to 02/03/2006). The surface boundary conditions were taken for 2006, 1992, and 1900. Sensitivity test runs were completed for summer and winter using the 2006 lateral boundary conditions but with the urban

parameterization scheme turned off. Table 2 summarizes all the runs: six main runs for three land use maps and two seasons, as well as two sensitivity runs for 2006.

Table 2**.** Summary of all the runs

Run type	Lateral B.C	Surface B.C	UCM	Duration (days)
main run 1	summer 2006	Las Vegas 2006	On	123
main run 2	summer 2006	Las Vegas 1992	On	123
main run 3	summer 2006	Las Vegas 1900	On	123
main run 4	winter 2006	Las Vegas 2006	On	123
main run 5	winter 2006	Las Vegas 1992	On	123
main run 6	winter 2006	Las Vegas 1900	On	123
sensitivity test 1	summer 2006	Las Vegas 2006	Off	123
sensitivity test 2	winter 2006	Las Vegas 2006	Off	123

4.2 Model Validation

To validate the model simulation, the 2 m air temperature in the winter and summer runs for 2006 were first compared with the archived (by National Climate Data Center) observations from the meteorological station at McCarran Airport in Las Vegas. The station, at 36°05' N 115°09' W, is chosen because it is located near the center of the urban core of the city. The station's temperature measurements are not precisely timed so the raw observations were interpolated to model output times (hourly). Since the station

does not perfectly coincide with a grid point of the model, the average over all grid points within a 0.06° radius of the station is taken as the model result for comparison.

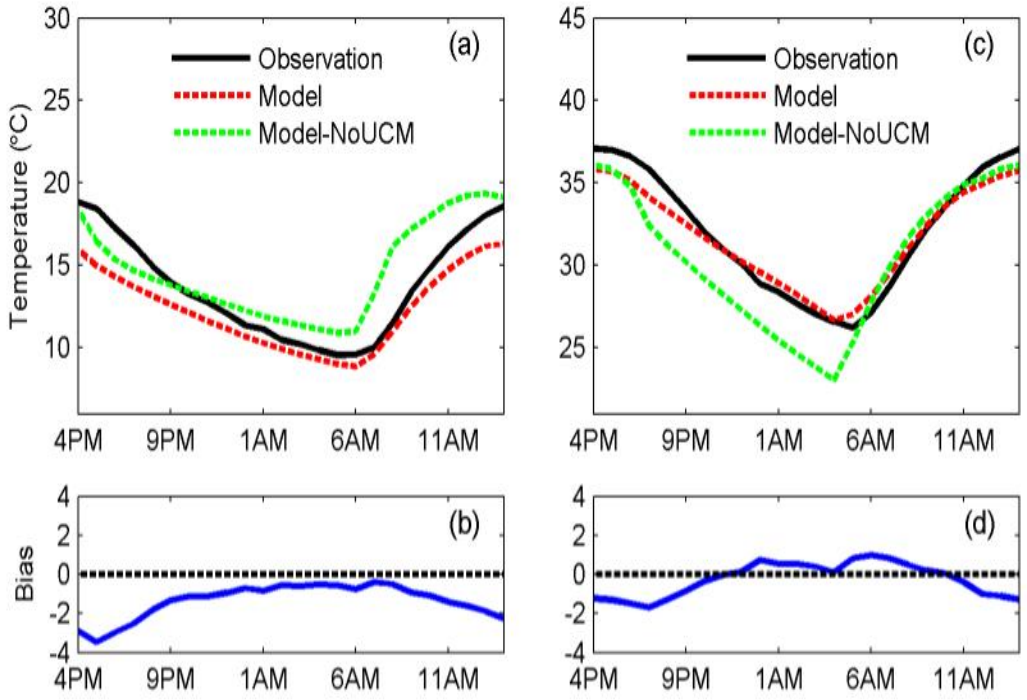

Figure 13. (a) A comparison of the diurnal cycle of 2m air temperature from the observation at McCarran Airport of Las Vegas (black) and the WRF simulations with (red) and without (green) an activated urban canopy model. All three are the average over the Winter 2006 (October 2005-January 2006). The time of the day is indicated at bottom margin. (b) The model bias, defined as the run with UCM minus observation from panel (a). (c) and (d) are the same as (a) and (b) but for Summer 2006 (May-August 2006).

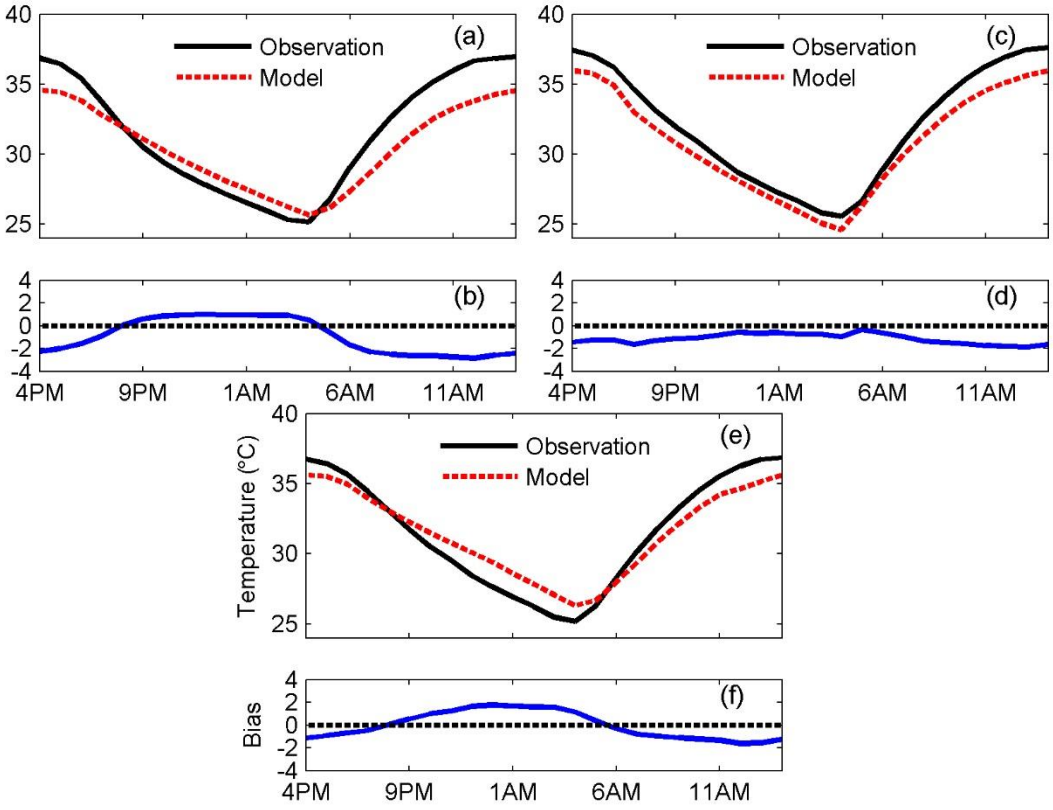

Figure 14. Similar to Fig. 13 but for the comparison of the simulation with UCM (red) to observation (black) for Summer 2006 at Henderson Executive Airport (3a and 3b), Nellis Airforce Base (3c and 3d), and North Las Vegas Airport (3e and 3f). The bias, defined as model minus observation, is shown in blue for each station.

Figure 13a show the hourly surface air temperature, averaged over winter (October 2005-January 2006) from the observation and two sets of WRF simulations with and without activating the urban canopy model. Figure 13b is the bias (model minus observation) deduced from Fig. 13a and using the run with urban canopy model turned on. (The bias for the run without UCM is larger and is not shown.) Figures 13c and 2d are the counterparts of Figs 13a and 2b but for summer (May 2006-August 2006). For both seasons, the run without the UCM produces a greater bias. Specifically, it produces a diurnal cycle of temperature with excessive cooling after sunset or excessive heating

after sunrise. Given the closer match of the WRF+UCM simulation to observation, the UCM is kept on in all major simulations and its default setting (which is adopted to produce the results in Fig. 13) is retained.

Figure 14 shows additional model validation for Summer 2006 using the surface air temperature from three more stations: Henderson Executive Airport (35°58' N 115°08' W) as shown in Figs 14a and 3b, Nellis Airforce Base (36°15' N 115°02' W) in Figs. 14c and 3d, and North Las Vegas Airport (36°12' N 115°11' W) in Figs. 3e and 3f. They are located at, respectively, the south, northeast, and northwest edges of the city. Only the run with UCM is shown. From Figs. 13 and 14, the model shows a cold bias during the day and a less pronounced warm bias in late night and early morning. Nevertheless, with the UCM, the simulations capture the essential structure of the diurnal cycle of temperature.

We did not emphasize the validation for vertical structure because sounding sites are very sparse in Las Vegas region. (To our knowledge, there is only one long-term sounding site within the Las Vegas region. It might not be fair to use it to validate the model simulation.) We considered using the North American Regional Reanalysis data for upper air, but none of the grid points in NARR are located within the Las Vegas urban area. Another reason that we did not emphasize the vertical structure is that, in our simulation, the direct thermal response to urban land-use change has a very shallow structure. It is largely confined to the lower boundary layer.

While some biases remain in the model, further cancellation of the biases is expected by taking the difference between two runs, which differ only in the surface boundary conditions, to extract the urban effect.

4.3 Las Vegas Area Climatology

Figure 15 and 16 show the climatology of Las Vegas for summer and winter respectively. By visual inspection, the city appears noticeably hotter than the surrounding desert at 9 PM and 3 AM for both summer and winter, making the city a night hot island. The mountains to northeast of the city are always cooler due to the increase of altitude. The wind direction between the two mountains changes to and from the city depending on the time of the day. The city lies in a relatively strong, time dependent wind field with wind velocity around the city in the order of few meters per second.

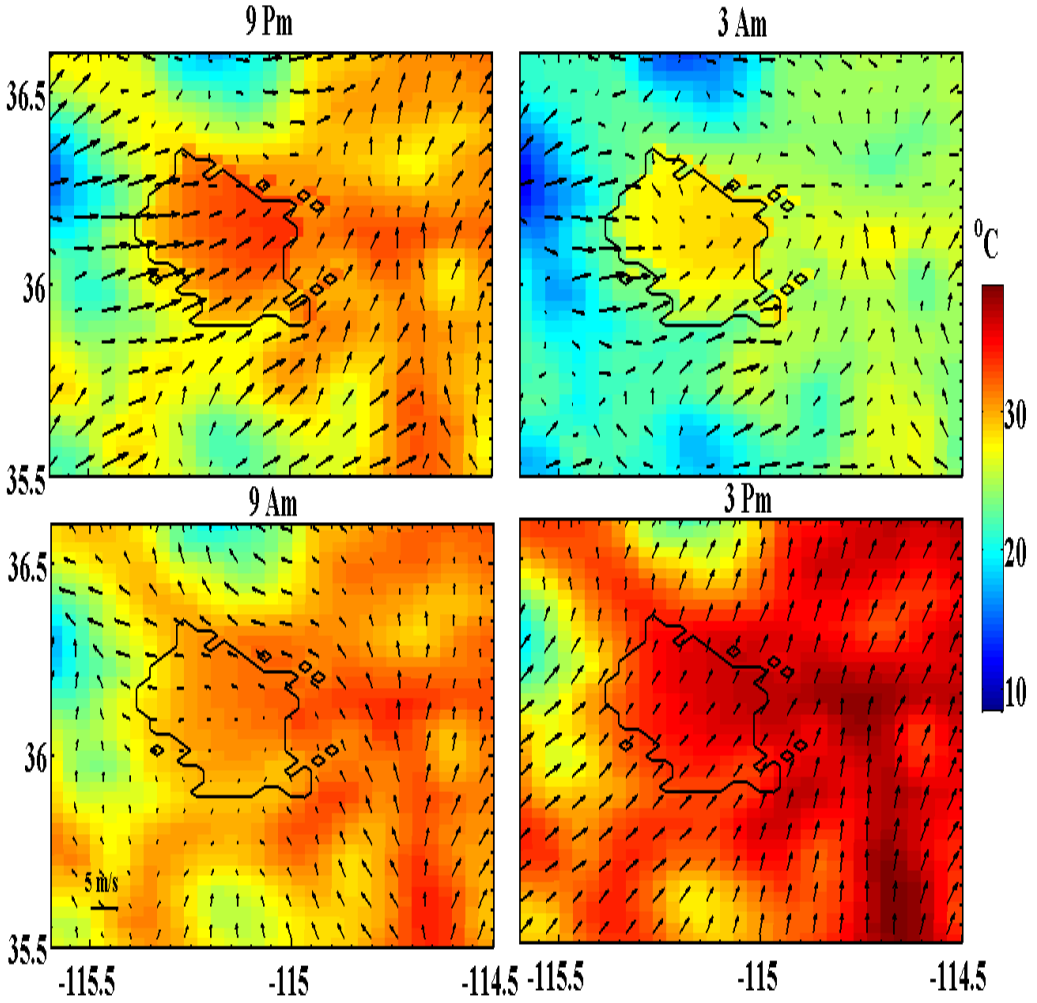

Figure 15. Climatology of the summer. The vectors represent the 10 meter level horizontal wind scaled to the same scale (left bottom graph). The color map shows the 2 m temperature in degree C. The black contour shows the extent of the urban buildup of the city for 2006.

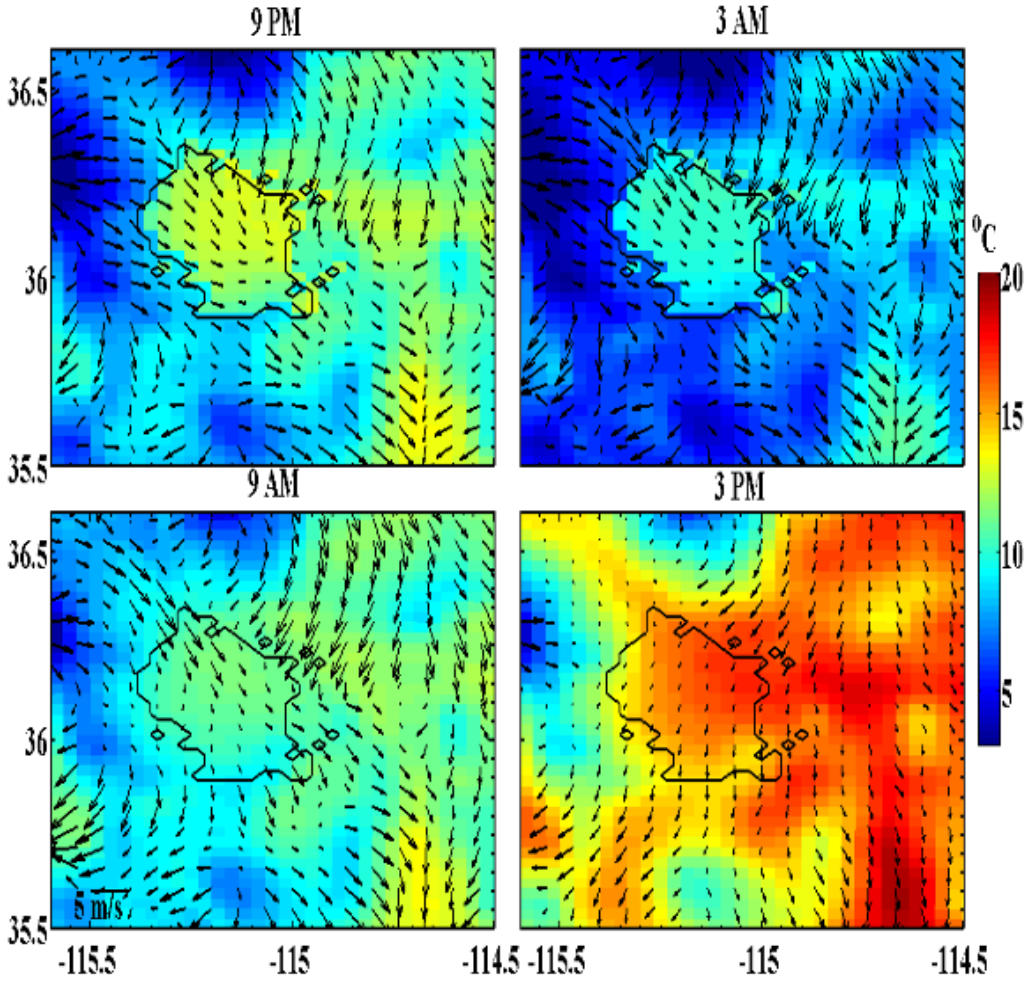

Figure 16. Climatology of the winter averages at 9AM and 3PM local time. The vectors represent the 10 meter level horizontal wind scaled to the same scale (left bottom graph). The color map shows the 2 m temperature in degree C. The black contour shows the extent of the urban buildup of the city for 2006.

4.4 Effects of Urbanization on Surface Air Temperature

Figure 17 shows the domain and season averaged difference in the 2 meter temperature for domains D1 and D2 for the summer and winter seasons. No significant

change in temperature was observed for the old part of the city (D1, blue and green curves). However, the new extension of the city (D2 black and red) witnessed night time heating and a slight day time cooling during both the summer and winter. The city witnessed maximum difference in temperature of about 2.7 degrees at 6 AM during the summer, and 2.4 degrees at 7 AM during the winter.

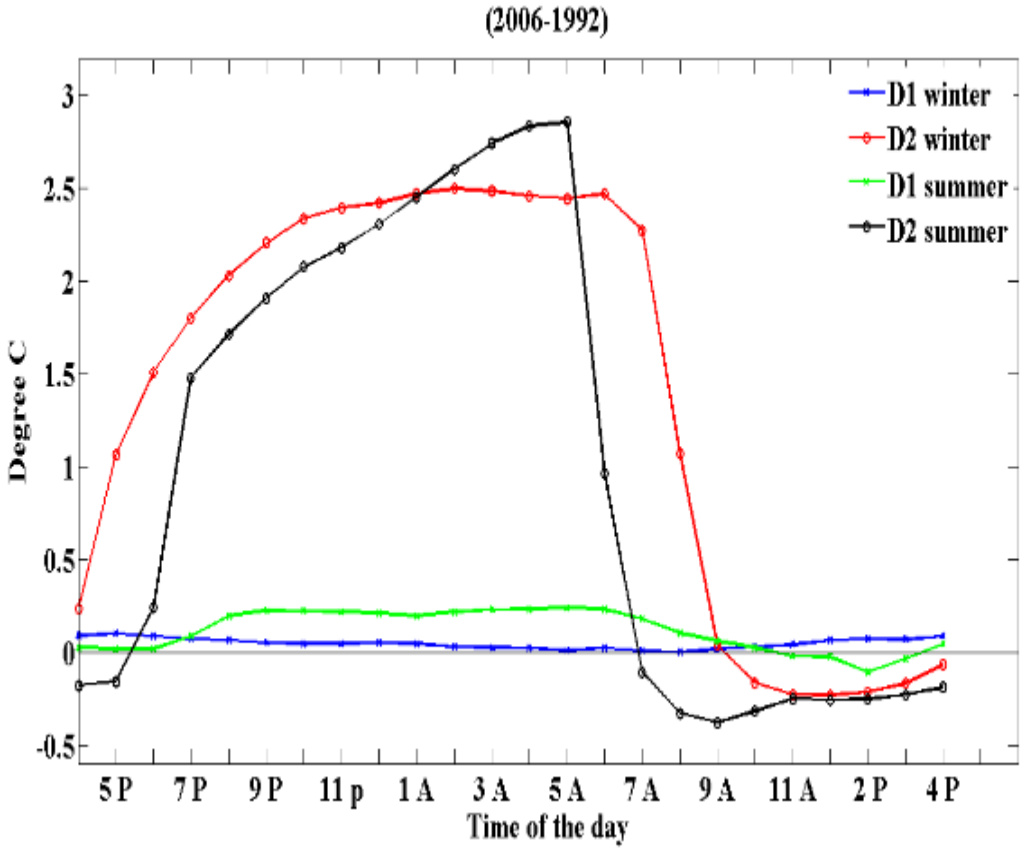

Figure 17. Diurnally averaged, domain averaged, season averaged difference between 2006 and 1992 in 2m temperature avenged over domains 1 and 2 for winter and summer.

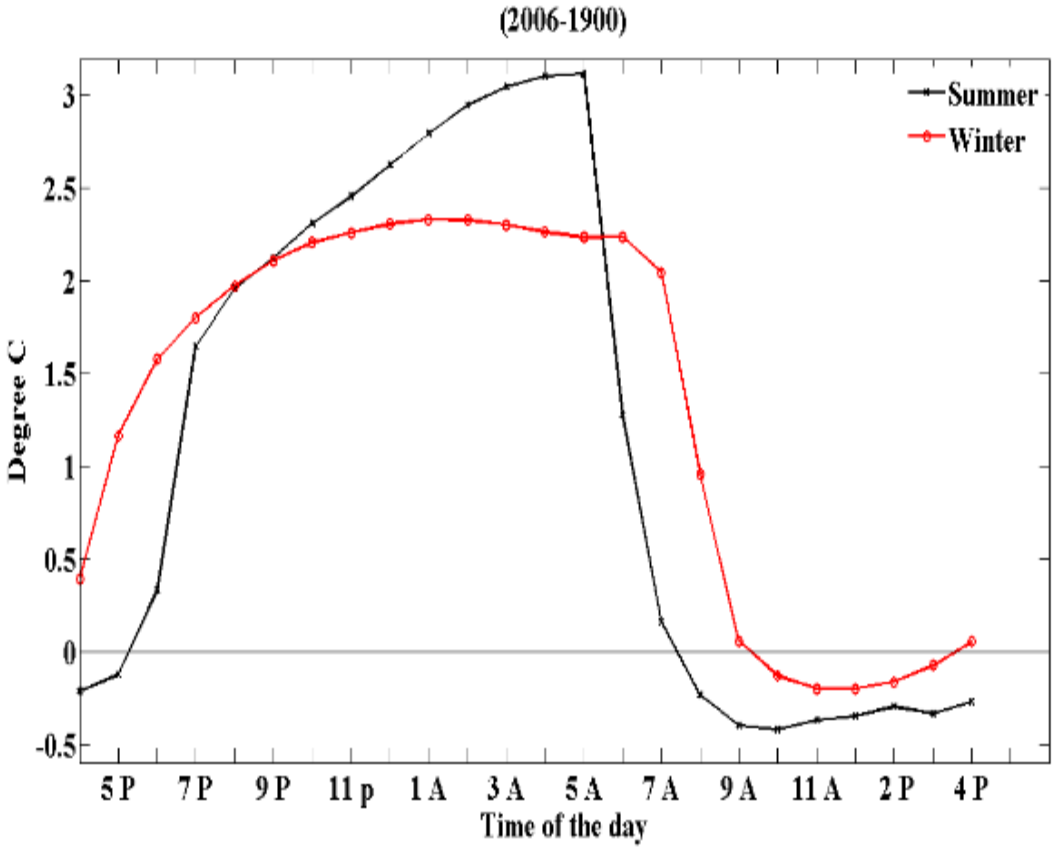

Figure 18. Diurnally averaged, domain averaged, season averaged difference between 2006 and 1900 in 2m temperature averaged over Las Vegas for winter and summer

Figure 18 shows the domain and season averaged difference (2006 run -1900 run) in 2 meter temperature for both seasons. It shows that during the summer night, the city witnesses a 3.1 degree maximum heating at 5 AM and 0.4 degree maximum cooling at 11 am. During the winter night, the city witnesses a 2 degree maximum heating at 7 AM and 0.2 degree maximum cooling at 12 AM. The heating of the city is more pronounced during the summer but the distribution is broader for winter.

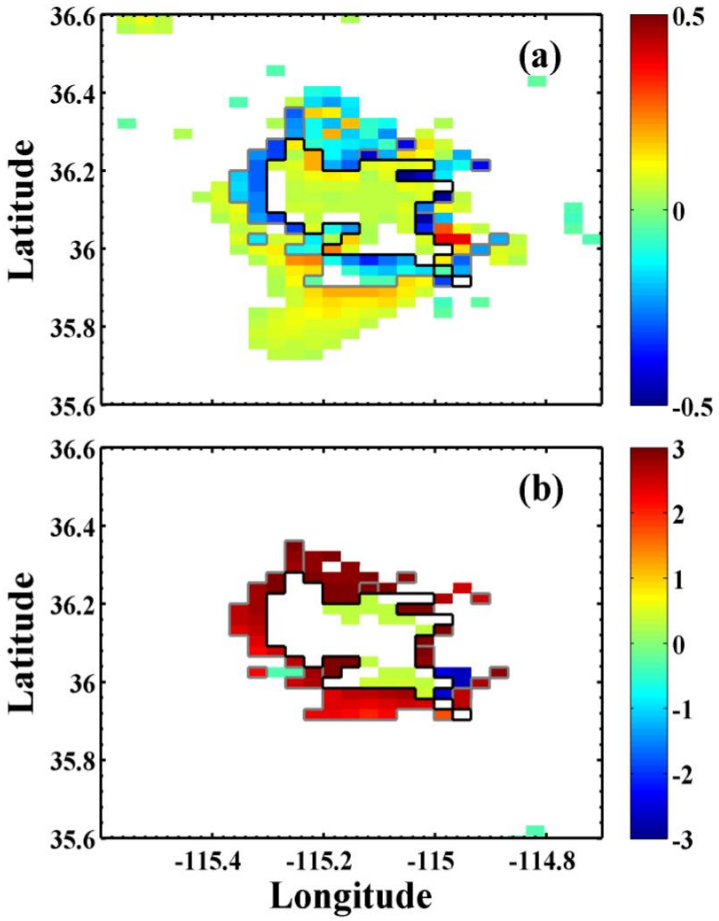

Figure 19. The "2006 minus 1992" difference in the 2 m temperature averaged over winter (October-January) from the "2006" and "1992" simulations. (a) At 1 PM. (b) At 3 AM. A smaller color range (shown at right) is used for panel (a) due to the weaker daytime cooling compared to the strong nighttime warming in (b). To focus on areas with more significant changes in temperature, in (a) the areas with less than 0.04 °C change in temperature are masked in white. In (b), the threshold is 0.5 °C. The black border outlines the 2006 urban extent of Las Vegas.

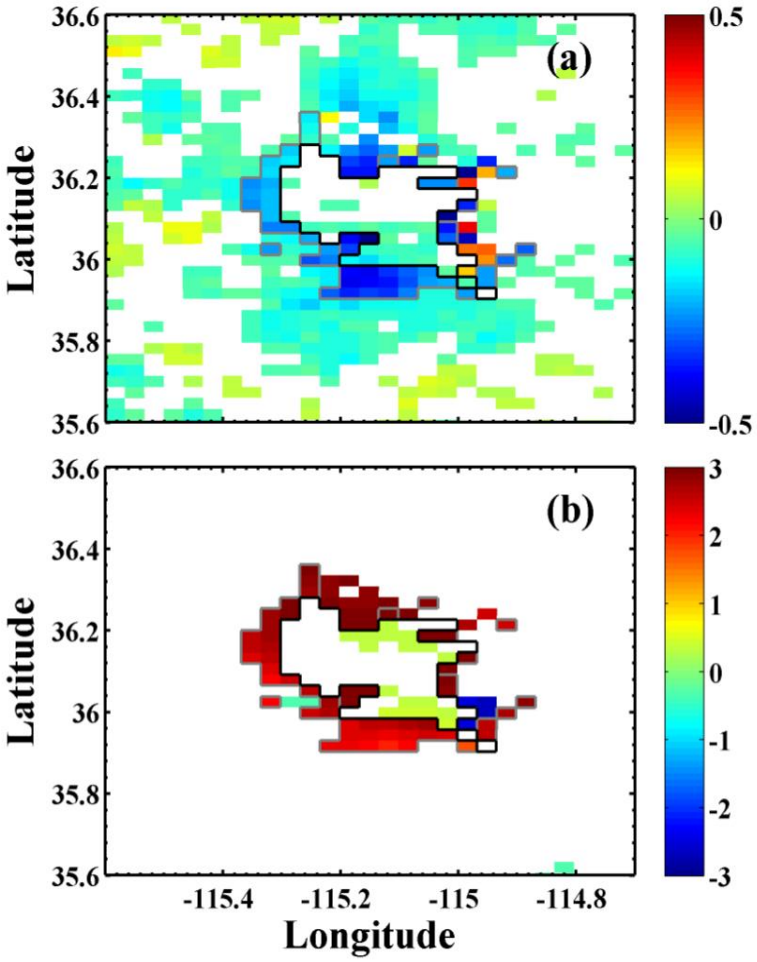

Figure 20. Same as Figure 19 but for summer but for summer (May-August). (a) and (b) are the difference maps at 1 PM and 3 AM.

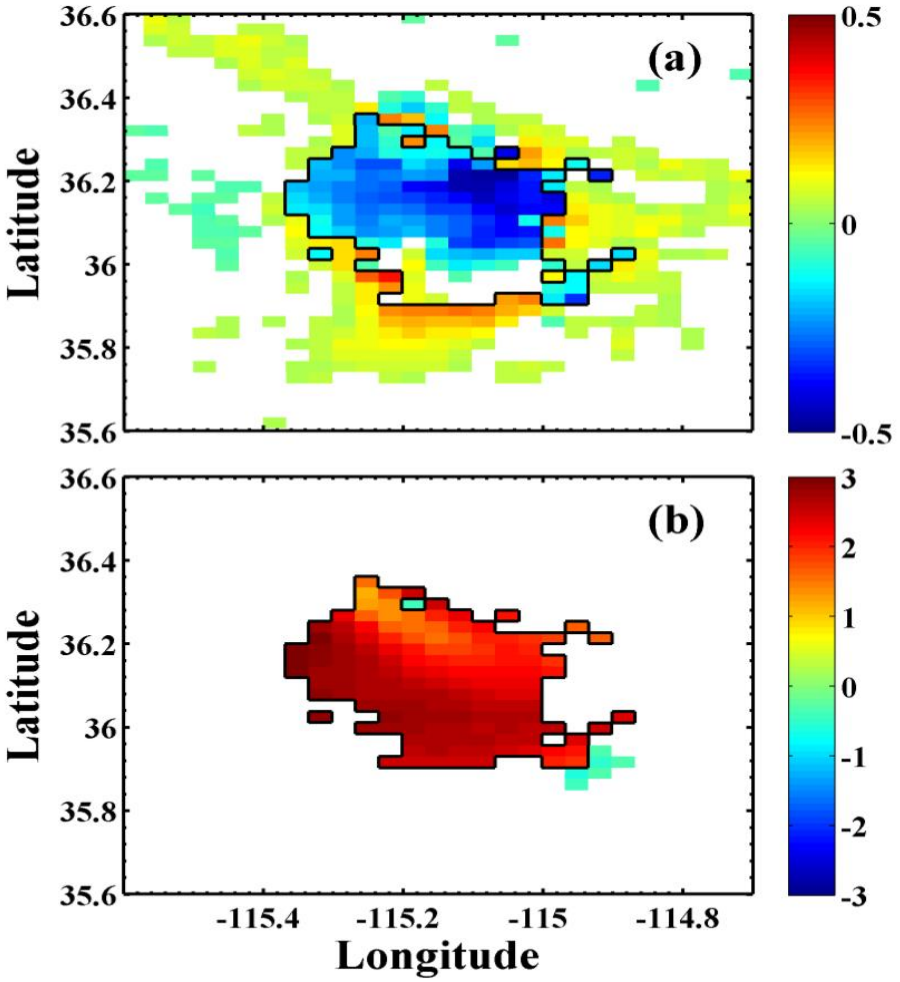

Figure 21. The "2006 minus 1992" difference in the 2 m temperature averaged over winter (October-January) from the "2006" and "1992" simulations. (a) At 1 PM. (b) At 3 AM. A smaller color range (shown at right) is used for panel (a) due to the weaker daytime cooling compared to the strong nighttime warming in (b). To focus on areas with more significant changes in temperature, in (a) the areas with less than 0.04 °C change in temperature are masked in white. In (b), the threshold is 0.5 °C. The black border outlines the 2006 urban extent of Las Vegas.

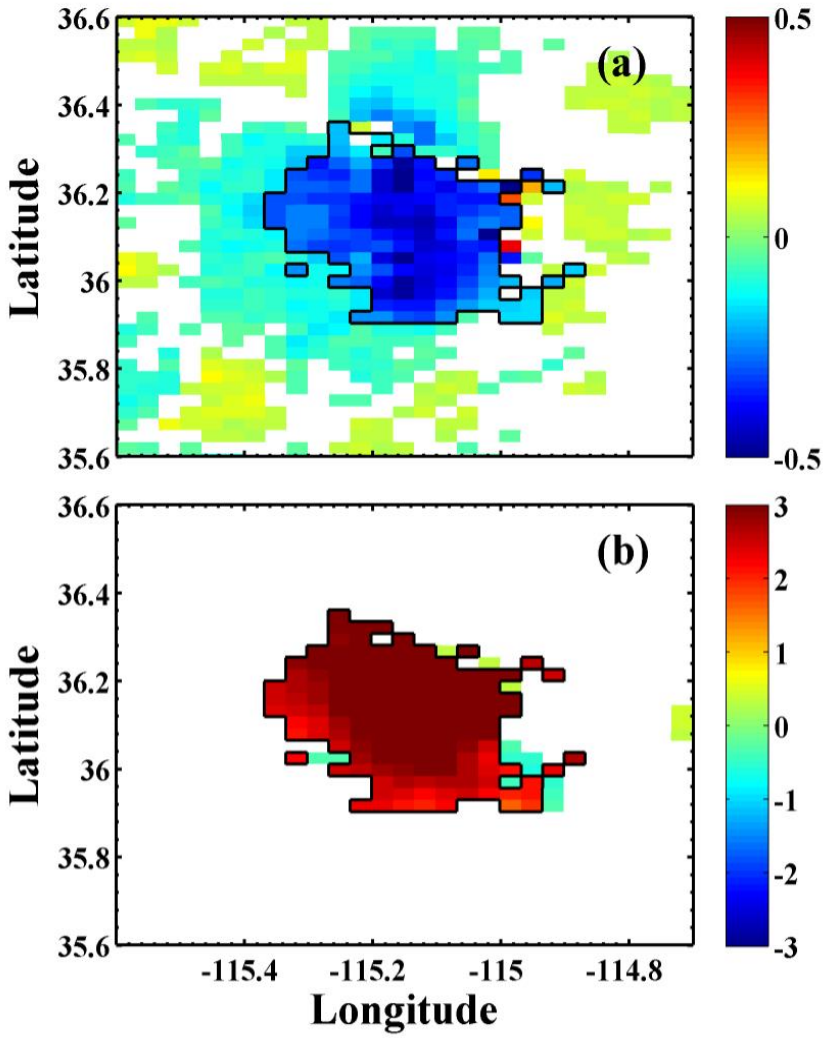

Figure 22. Same as Figure 21 but for the average over summer (May-August). (a) and (b) are the difference maps at 1 PM and 3 AM.

Figures 19 and 20 shows a color map of the difference in 2m temperature between 2006 and 1992 averaged for two particular times (one for day and one for night) for each of summer and winter. Black contour represents the borders of the domains of the city, old domain (Domain 1) and new extension (Domain 2). Figures 21 and 22 shows a color map of the difference in 2m temperature between 2006 and 1900 the black

contour represents the 2006 Las Vegas domain. Strong temperature difference is only observed for the grid points that were changed from shrubland (desert) to urban buildup. For grid points that changed from shrubland to urban, day time cooling of a fraction of a degree and night time warming of about 2~3 degrees were witnessed.

To understand the mechanism with which urbanization of the desert around the city affects climate, various terms of equation (9) will be evaluated.

$$\partial_t \Theta + \left(\nabla \bullet \vec{V}\theta\right) = F_\Theta \qquad (9)$$

The right hand side of equation (9) is the forcing term. It is calculated by the radiative, Planetary Boundary Layer (PBL), surface, and cumulus parameterization schemes. Only processes that happen at or near the surface will be affected by the change in land use. In the next section, the contribution of each of the terms on the Right Hand Side (RHS) will be investigated.

4.5 Surface Energy Budget

The changes in local climate induced by urbanization are closely related to the changes in the physical properties of the surface (e.g., Oke 1982), which alter the energy budget at the surface. Figure 23 summarizes the changes, calculated from the "2006 minus "1900" difference, for winter and summer in the major terms in the surface energy balance – net longwave and shortwave radiation, sensible heat flux, and latent heat flux (all defined as positive upward) averaged over the 2006 extent of the urban area (the black area in Figure 12d). The counterpart of Figure 23 for the "2006 minus 1992" difference (as averaged over the area where urbanization took place between 1992 and 2006) is very similar to Figure 22 and is not shown.

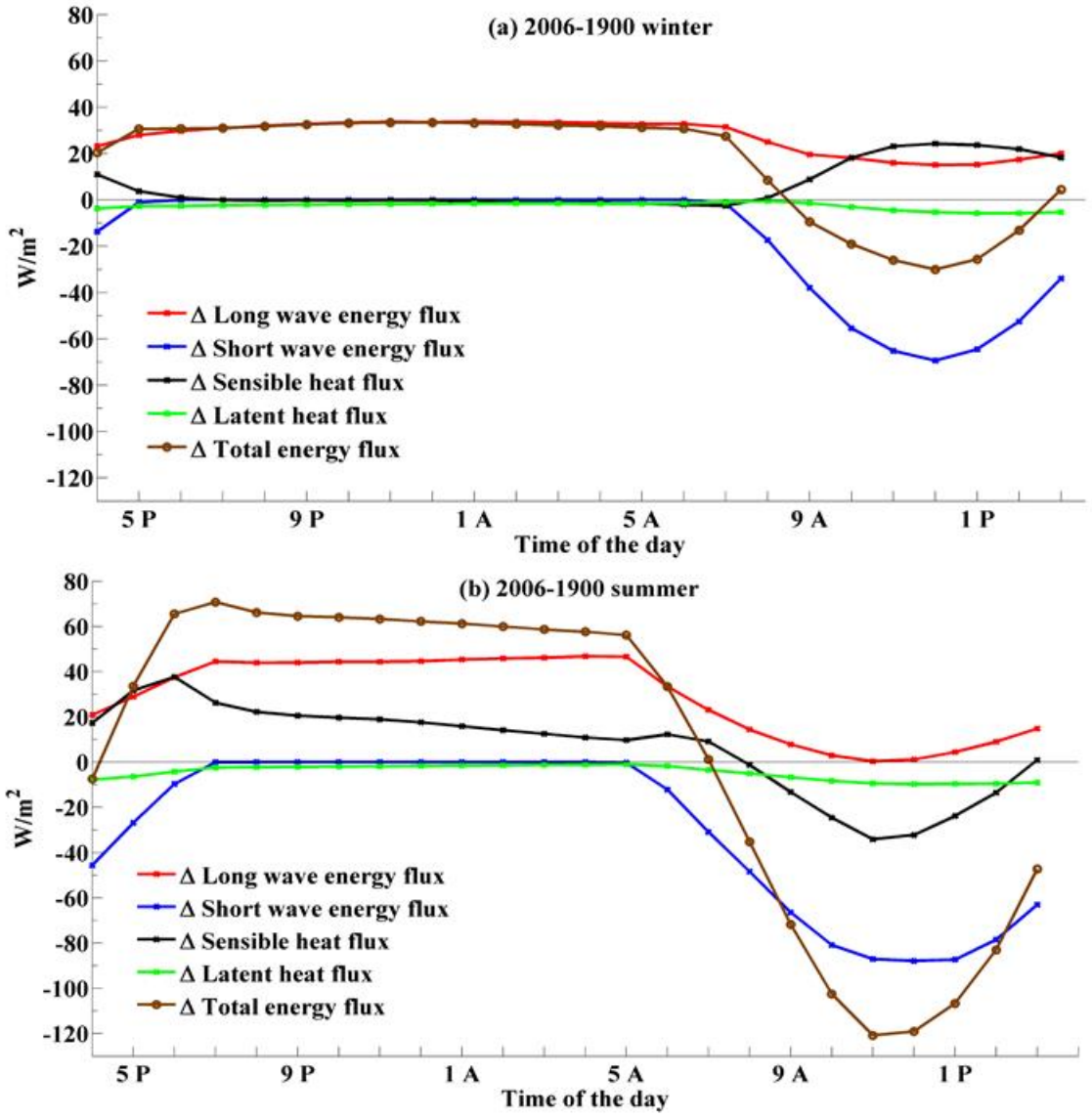

Figure 23. The "2006 minus 1900" difference in the major terms of surface heat or energy flux, defined as positive upward. Shown are the diurnal cycles of each flux averaged over the season and over the 2006 urban extent of Las Vegas. The net upward longwave and shortwave radiation are in red and blue, and sensible and latent heat fluxes are in black and green, and the sum of the four is in brown. (a) Winter (October-January), (b) Summer (May-August).

For both winter and summer, the change in latent heat flux is minor given that in the model the surface is generally dry either pre- or post-urbanization. This is distinctive from the situation with non-desert cities where a conversion from grass or agricultural land to urban structures can substantially reduce surface evaporation. It is worth noting that Miller (2011) showed evidence of an upward trend in dewpoint temperature over Las Vegas in the post-1970s era. That our model did not simulate this trend could be interpreted in several ways: First, while urbanization generally leads to increased irrigation for a desert city, this effect is not yet properly represented in the model. Secondly, with the 3-km horizontal resolution, the sub-kilometer details in urban landscape (e.g., the contrast between park and pavement) are not resolved by the model. Thirdly, in the observation, part of the trend could be due to other influences (e.g., large-scale climate change) unrelated to urbanization. Since we have designed the numerical experiment to isolate the effect of land-use changes (by replacing only the surface boundary conditions but keeping the lateral boundary conditions the same), the large-scale influence is also not included in the simulations.

In both seasons, during the day, urbanization leads to a decrease in the net upward shortwave radiation which is due to the decrease in surface albedo from 0.26 for shrubland to 0.17 for urban land. The excessive absorption of solar radiation is redistributed as an overall increase of the upward longwave radiation through the whole day but particularly at night. Note that the weaker but still positive increase in the upward longwave radiation during the day does not contradict the fact that temperature decreases slightly in daytime, because emissivity increases from 0.88 for shrubland to close to 0.98 for urban land. (The value of 0.98 is as provided by the output of the model and is

understood as the effective emissivity, taking into account the increased area for emission given the existence of buildings and other urban structures. Without the geometric effect of urban structures as parameterized in the urban canopy model in WRF, merely turning shrubland to a flat concrete slab would not lead to such a significant increase in emissivity.)

Note that the intensity (of emitted power per unit area) of longwave radiation can be written as $R = \varepsilon \sigma T^4$ where ε and σ are emissivity and Stefan-Boltzmann constant and T is temperature in °K. If (ε, T) are the pre-urbanization values which are changed to ($\varepsilon + \Delta\varepsilon$, $T+\Delta T$) after urbanization, the ratio of the post-urbanization radiation intensity, $R+\Delta R$, to its pre-urbanization counterpart is

$$\frac{R+\Delta R}{R} = \frac{(\varepsilon+\Delta\varepsilon)(T+\Delta T)^4}{\varepsilon T^4} \approx \left(1+\frac{\Delta\varepsilon}{\varepsilon}\right)\left(1+\frac{4\,\Delta T}{T}\right). \qquad (16)$$

(The approximation in Eq. (16) is based on $|\Delta T / T| << 1$.) Thus, as long as $\Delta\varepsilon/\varepsilon > -4\,\Delta T/T$ (note that ΔT is negative for cooling) the effect of an increase in emissivity overwhelms that of a decrease in temperature, leading to an increase in the upward longwave radiation. This is indeed the case for the simulation of Las Vegas in which $\Delta\varepsilon/\varepsilon$ is close to 10% while the $-4\,\Delta T/T$ associated with the daytime cooling is less than 1 %.

The changes in the sensible heat flux exhibit a more complicated seasonal and diurnal dependence. In winter, the change is very small at night. This is not unexpected since atmospheric boundary layer is very stable in the cold winter night and would likely remain stable even with some warming induced by urbanization. An increase in the sensible heat flux is found in daytime in winter. Since the surface actually cools slightly during the day, this is likely related to more complicated dynamical processes in the boundary layer which would require a separate study. In summer, the boundary layer is

closer to neutral or unstable such that the change in sensible heat flux appears to have a more direct relation to the change in surface temperature. The sensible heat flux increases during the night when surface temperature increases, and decreases during the day when the surface cools slightly. The changes in the total upward energy flux (sum of all flux terms discussed above) are also shown in Fig. 23. For both seasons, an increase of the total flux at night and a decrease during the day is found. This diurnal contrast is more pronounced in summer.

Table 3. Maximum absolute values and mean values of the change in the downward

	Summer max(abs)	Summer mean	Winter max(abs)	Winter mean
Δ Long wave down(W/m^2)	2.469	1.149	0.844	0.426
Δ Short wave down(W/m^2)	4.9186	-0.3046	0.8791	-0.0335

Table 3 shows the maximum absolute value and the daily mean value of the change in the downward long and short wave fluxes from 1900 to 2006 case. Changes in the downward fluxes are small compared to the radiation fluxes, suggesting that the changes in surface energy budget are not due to changes in the amount of cloud cover. Instead, it is due to a change in surface properties such as reflectivity and emissivity. In turn, reflectivity and emissivity change the short and long wave fluxes emitted from the surface.

4.6 Dynamic Effects of Urbanization (Wind Advection)

The effect of urbanization on the local atmospheric velocity has so far received less attention than the effect on temperature. Using the WRF simulations, analysis of the changes in the 10 m wind induced by the land cover changes is performed. Since the topographically induced diurnal circulation over Las Vegas exhibits a particularly coherent pattern in the night and early morning (see Figs. 24 and 25), the study focuses on those times. Figure 24 shows the "2006 minus 1900" difference in the 10 m wind speed (as contours) and velocity (as arrows) at 9 PM and 3 AM, for winter and

Comparing those panels with the climatology in Figures. 14 and 15, results show that (i) The change in wind speed is almost uniformly negative, and (ii) The change in velocity is predominantly in the direction opposite to the direction of the climatological velocity vector. These two characteristics remain robust if the "2006 minus 1992" difference (in which the area of urbanization is much smaller), as shown in Fig. 26, is considered. They strongly indicate that the change in the near-surface wind is due to a simple mechanical effect of the retardation of the climatological wind by the emerging buildings and urban structures. This increase in surface friction can be quantified, for example, by the classical surface roughness scale u*, which is indeed significantly higher over the urban areas (not shown).

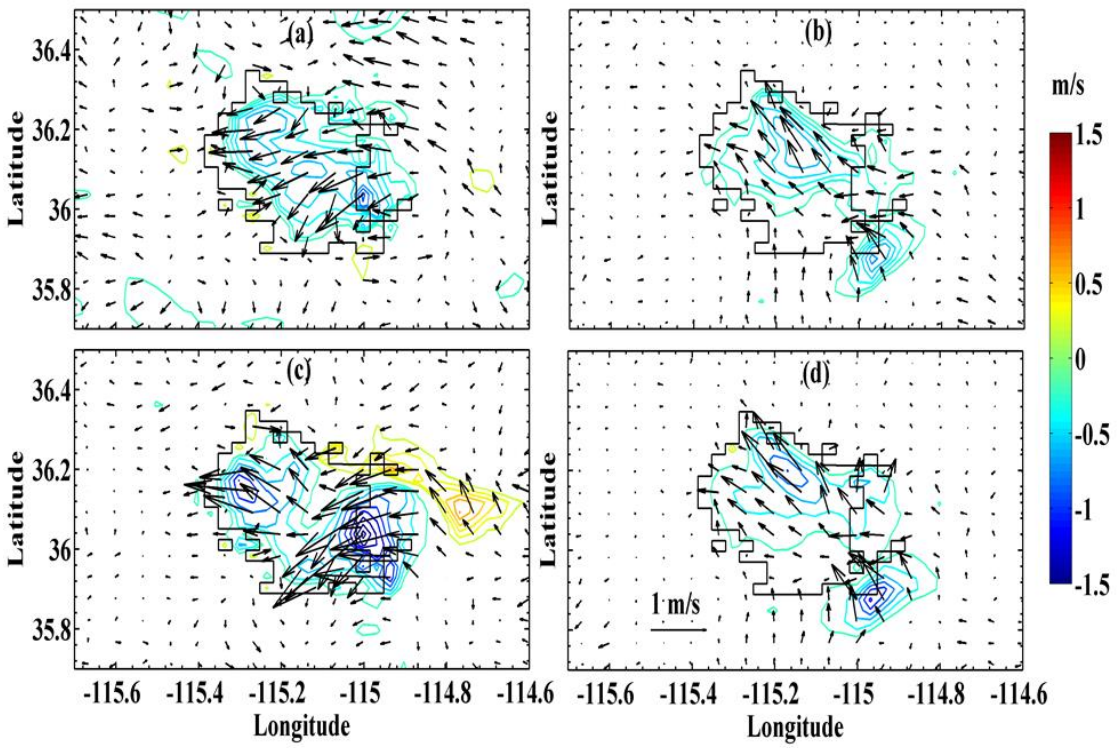

Figure 24. The "2006 minus 1900" difference in the wind speed (contours with color scale at right) and velocity (arrows with scale indicated in the lower left corner of panel (d)) averaged over the season. (a) 9 PM in summer. (b) 9 PM in winter, (c) 3 AM in summer, (d) 3 AM in winter. The contour interval for the change in wind speed is 0.2 m/s. The black border outlines the 2006 urban extent of Las Vegas. Longitude and latitude are indicated at the margins.

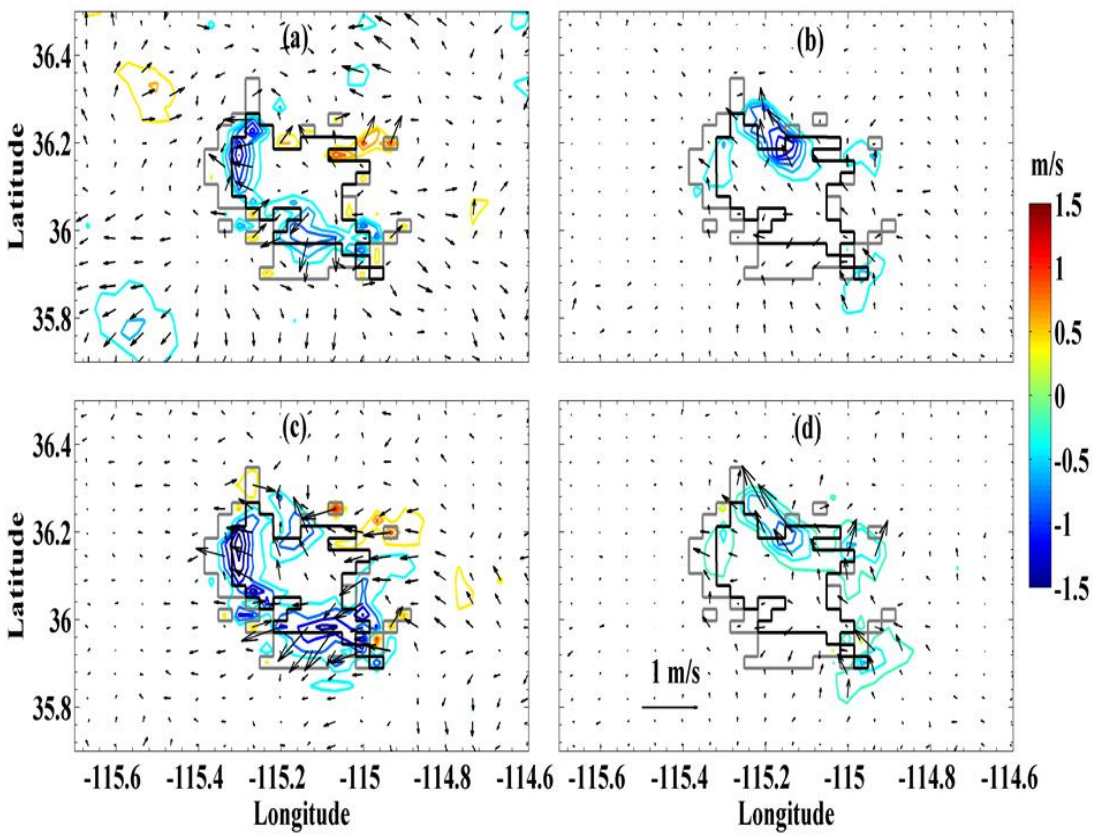

Figure 25. Same as Fig. 24 but for the "2006 minus 1992" difference in the wind speed and velocity. The formats of presentation are the same as Fig. 11, except that the gray border outlines the 2006 urban extent and black border outlines the 1992 urban extent of Las Vegas.

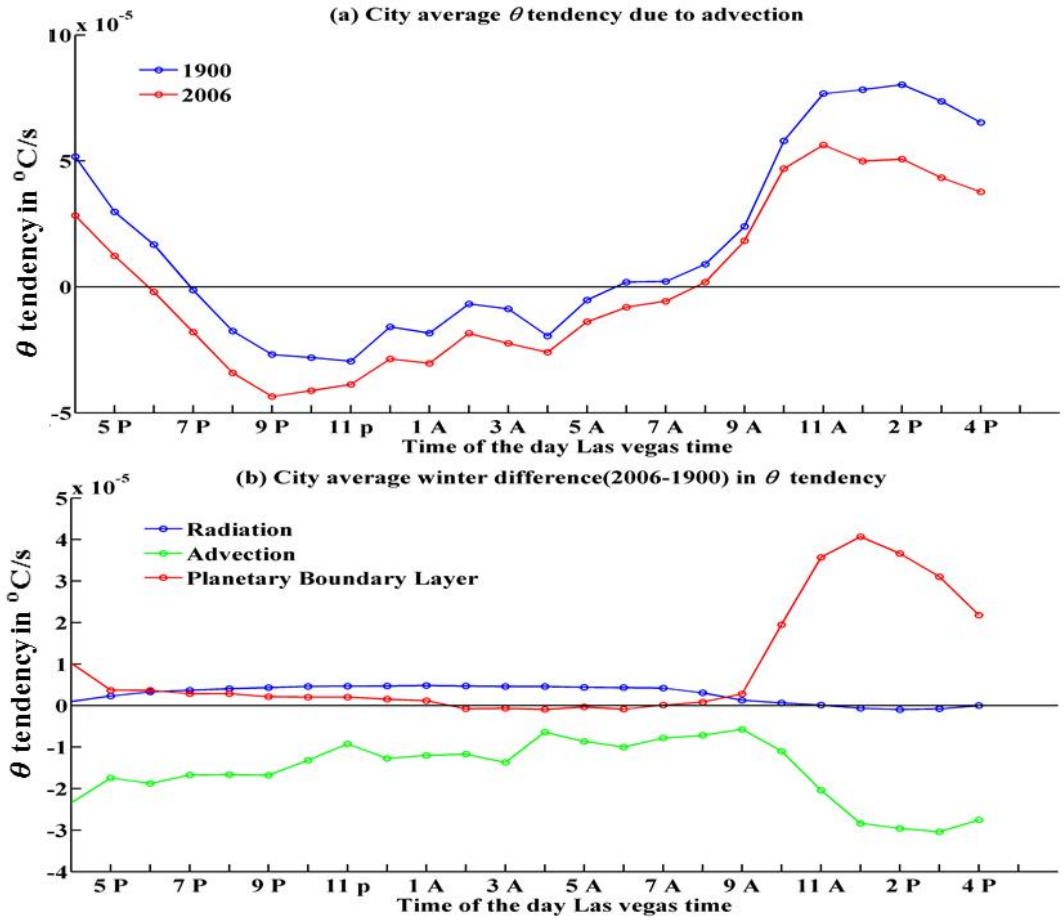

Figure 26. (a) The diurnal cycle of the θ-advection term averaged over the winter season (October-January) and over the 2006 urban extent of Las Vegas (see text for detail) from the 2006 (red) and 1900 (blue) runs. (b) The "2006 minus 1900" difference in the θ-advection term (green), convergence of the vertical potential temperature flux by boundary layer turbulence (red) and radiative forcing (blue), averaged in time and space in the same manner as (a). All calculations are performed at the pressure level with p = 900 hPa. The time of the day is indicated at bottom margin.

Given the overall reduction of the wind speed (but relatively minor changes in wind direction) induced by urbanization, one may further infer its impact on temperature itself. Previous studies suggest that local wind circulation generally provides ventilation to alleviate the urban heat island effect (e.g., Takahashi et al. 2011; Lee et al. 2012, 2014). The ventilation is accomplished by the advection of warmer air out of the city, or advection of cooler air into the city. If both the strength and direction of the wind remain

the same during urban expansion, the increased temperature gradient between the urban and rural areas combined with an unchanged velocity field would imply a strengthening of the temperature advection. If so, the ventilation effect increases with an increase of the urban heat island effect itself.

The situation with Las Vegas from the simulations is more complicated. In nighttime, while temperature of the city increases, the wind speed decreases due to urbanization. The two would have the opposite effects on the strength of temperature advection. During the day, the desert areas surrounding the city can have a higher temperature than the city itself. With the retardation of the wind, there could be a reduction of the advection of hotter air into the city, a cooling effect. Although these conjectures cannot be unequivocally affirmed within the framework of the WRF model simulations (given that in the model one cannot artificially hold either wind or temperature constant), a diagnostic analysis of the temperature advection term provides some useful insights.

As a convenient framework for the diagnostics, the right-hand-side (r.h.s.) terms of the potential temperature equation at a pressure level are considered:

$$\frac{\partial \theta}{\partial t} = -\boldsymbol{V} \bullet \nabla\theta - \frac{\partial}{\partial p}(\overline{\omega'\theta'}) + Q \ , \qquad (17)$$

where θ is potential temperature, p is pressure, ω ≡ dp/dt is the "vertical velocity" in p-coordinate, and Q is diabatic forcing. The choice of potential temperature stems from the considerations that (i) The governing equation for θ is simpler that for temperature; (ii) At a constant pressure level, the variation of θ is proportional to the variation of temperature.

Since WRF uses a terrain-following vertical coordinate, η, the relevant variables are converted from the η-levels to the level of p = 900 hPa by vertical interpolation. And since the physical height of 900hPa level is a variable in time and position the interpolation is done for every time step for every grid point For Las Vegas, 900 hPa corresponds to lower to middle boundary layer over the city. If at a location the 900 hPa level intersects with, or is too close to, the surface, the data there is excluded from the analysis and does not contribute to the domain average.

The first term in the r.h.s. is the 3-D advection of potential temperature by the resolved velocity from the WRF model. It represents the main effect of ventilation by the wind. For conciseness, the term is not split further into the contributions from the horizontal and "vertical" advection but the former generally dominates (not shown). The second term in the r.h.s. is the convergence of the vertical potential temperature flux by unresolved turbulence in the boundary layer. Its value is calculated by WRF with the boundary layer parameterization scheme. The diabatic forcing includes the latent heat release due to moist convection or cloud/fog formation (both are very rare occurrences at the lower-middle boundary layer under the very dry climate of Las Vegas) and the atmospheric absorption of longwave and shortwave radiation.

Figure 26(a) shows the diurnal cycle of the climatological value of the advection term (the 1st term in the r.h.s. of Eq. (16)), averaged over the 2006 urban extent of Las Vegas, from the 2006 and 1900 simulations for winter. (Winter was chosen as the wind pattern is less organized in summer.) At night, the advection of colder air through the northwest corridor into the city is reflected in the negative value of the θ-advection term. With urbanization, cooling by advection is found to become stronger. Since the wind

speed, $|\boldsymbol{V}|$, is decreased, this suggests that the increase in $|\nabla\theta|$ due to urban warming is significant enough to overcome the reduced wind speed such that the ventilation effect still increases with urbanization. The positive climatological value of the advection term during the day reflects the tendency for the warmer air in the surrounding desert areas to intrude into the city. Since during the day the temperature of the city changes only slightly by urbanization, the reduction of the wind speed by the mechanical effect should decrease this intrusion of warm air. This is indeed the case as shown in Fig. 26a (note that red line falls below blue line during daytime).

The "2006 minus 1900" difference (red line minus blue line in Fig 26a) in the θ-advection term in winter is shown as the green line in Fig. 26b. Also imposed are the "2006 minus 1900" differences in the convergence of turbulent potential temperature flux (2^{nd} term in the r.h.s. of Eq. (16)) and radiative heating (from the Q term in Eq. (16)). As explained before, the heating due to moist convection or formation of cloud/fog is small at 900 hPa and is not shown. The radiative heating term in Fig. 26b is small, which is understandable since urbanization is not expected to significantly change atmospheric absorption (by changing either atmospheric composition or cloudiness) of longwave/shortwave radiation.

The change in the turbulent heat flux convergence is small at night, likely because the boundary layer is very stable in winter night and remains undisturbed even with the surface warming by urbanization. During the day, the heating due to turbulent flux convergence increases with urbanization. This is consistent with the decrease in the positive temperature advection into the city in daytime as shown in Fig. 26a. Since the air in mid-boundary layer is cooler but the temperature at the surface changes only slightly

with urbanization, the static stability of the lower boundary layer decreases which favors more turbulent heat transfer upward. In this context, the changes in the 1st and 2nd terms in the r.h.s. of Eq. (17) partially cancel each other.

The preceding analysis suggests that the changes in the wind field by the mechanical effect of urbanization can have a secondary influence on the temperature of the city. This effect is noticeable for Las Vegas because there exists a strong and coherent diurnal circulation over its metropolitan area. The detail of the wind effect on temperature will vary from city to city and will be an interesting aspect for future studies on urban climate.

CHAPTER 5

NUMERICAL EXPERIMENTS FOR THE FIVE CITIES

In the past chapter we numerically investigated the effect of urbanization in the climate of Las Vegas. Our study of Las Vegas and other studies involving phoenix hint at a potentially common feature, namely, a weak daytime cooling (relative to the surrounding rural area) due to urbanization. While this feature is not unique to desert cities, e.g., daytime cooling was also found in Vancouver (Runnalls and Oke 2000) and Indianapolis (Carnahan and Larson 1990),

Kamal et al. (2015) suggest that there are mechanisms specific to desert cities that support the relative urban cooling. First, urban-type impervious surfaces generally have a higher albedo than the background surfaces of desert or shrubland. Secondly, the build-up of urban structures helps increase the shadow effect and the effective area for infrared emission as compared to a flat surface covered by the same material. While the signal of daytime cooling and nighttime heating is robust, it is not clear if it applies to other desert cities. In order to examine the universal features of urbanization on desert municipalities, we will perform numerical experiments involving 5 different cities using land use maps from two different eras, separated by rapid urban sprawl.

The five cities chosen are (1) Las Vegas, United States, (2) Beer Sheva, Israel, (3) Kharga, Egypt, (4) Hotan, China, and (5) Jodhpur, India. Figures 27 (a)-1(c) show the locations and the corresponding model domains for those cities.

5.1 Land-use Data Used for the Five Cities

For each city, two contrasting land-use maps are generated from Landsat satellite observations for 1985 and 2010, which represent the start and end of a period of rapid urban growth. The maps were produced and tailored to our numerical experiment by Dr. Soe Myint. Since Landsat observations have a much higher (30 m) resolution, a simple scheme of "choosing the majority" is adopted to weave multiple Landsat pixels into a grid box for WRF (Kamal et al. 2015).

Figure 29 summarizes the land-use maps on the WRF model grid for 1985 and 2010 for all five cities. Shown are the innermost model domains for the respective cities. The major land-use categories that appear in figure 28 are summarized in Table 4. For our purpose, the default land-use maps in WRF are used for the intermediate and outermost domains. Although all five cities are located in desert regions, the detailed composition of land cover and the scenario of land-use change differ from city to city.

For Kharga and Beer Sheva, urban land spreads from a concentrated small area in 1985 to multiple clusters in 2010. Hotan and Jodhpur are characterized by a large coverage of cropland, wetland, or mixed forest with the relatively small urban core (see inset for Hotan) embedded within it. This provides a contrast to Las Vegas which is surrounded mainly by shrubland. To incorporate the influence of the differing background land types, the innermost model domain is chosen to be significantly larger than the urban core itself.

Figure 29 summarizes land-use changes that occurred between 1985 and 2010 for the five cities. The most relevant categories of changes that involve urbanization (i.e., conversion of a non-urban type of land to urban land) are shown in red-hued colors. The

remaining categories are shown in blue-green hued colors. The major types of land-use changes that appear in Figure 29 are summarized in Table 5.

The five cities differ significantly in size: The urban area of Las Vegas has a linear dimension of 50 km, while Kharga is only a few km across. The five cities are located in different climate zones: Hotan and Beer Sheva have continental and Mediterranean climates, respectively and Jodhpur is influenced by Indian Monsoon in summer. Out of this wide range of background, we will determine the common features of the climatic effect of urbanization.

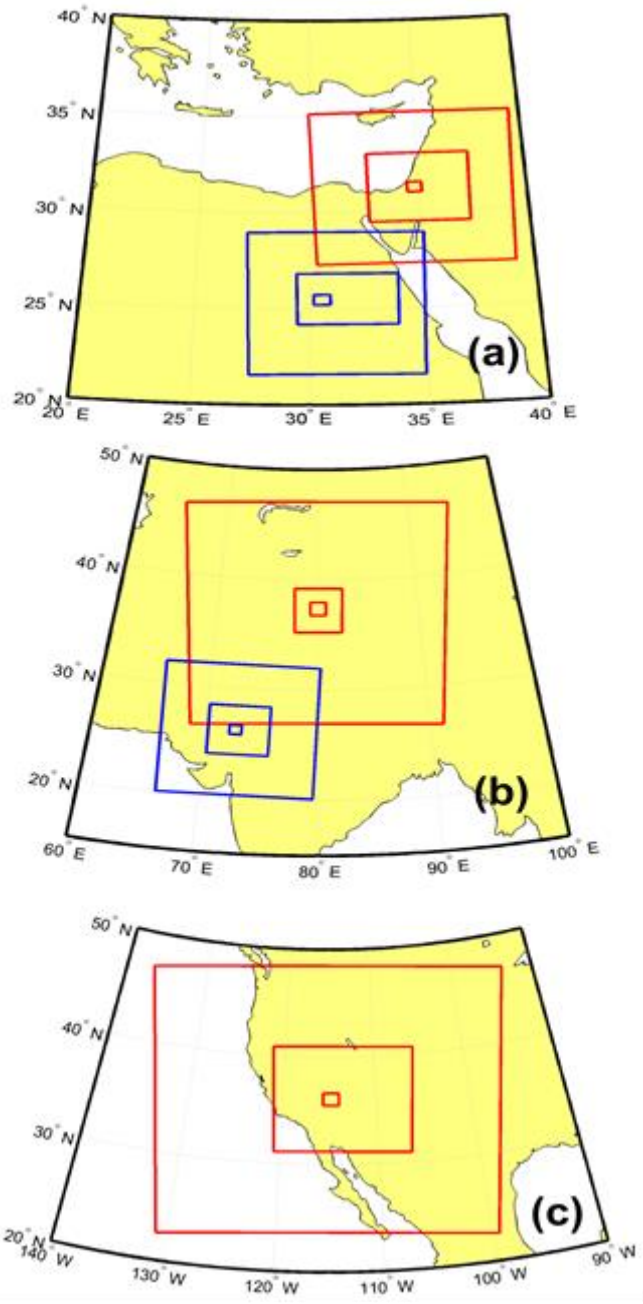

Figure 27. The locations and model domains for the five cities: (a) Beer Sheva, Israel (red) and Kharga, Egypt (blue). (b) Hotan, China (red) and Jodhpur, India (blue). (c) Las Vegas, USA. Three nested domains are used for each city. The urban area of each city is located within the innermost domain in each case. Land area is colored in brown.

5.2 Numerical Experiment Design for the Five Cities

To isolate the climatic effect of land-use changes, multiple sets of "twin experiments" are performed. Each pair of numerical simulations are carried out by keeping all boundary conditions the same except changing the land surface boundary condition within the innermost model domain (as shown in Fig. 27) that covers the urban area. In this manner, the difference in the climate between the two runs can be attributed to the influence of land use changes. The land-use maps for 1985 and 2010 are used to define the surface boundary conditions for the pair of runs. Otherwise, both runs are constrained in the fashion of climate downscaling by the same lateral boundary conditions. Specifically, four-time daily meteorological variables from NCEP global analysis for 2010 are imposed to the boundary of the outermost domain through the duration of each run.

Since the baseline climatology differs significantly between winter and summer, two sets of twin experiments are performed for each city. The winter run is from October-January (preceded by a short spin-up period) using the lateral boundary condition from October 2009-January 2010; summer run is from May-August and constrained by the lateral boundary condition from May 2010-August 2010. Together, 20 seasonal runs (4 for each city) with a total of 2460 days of output are produced for this part of the study.

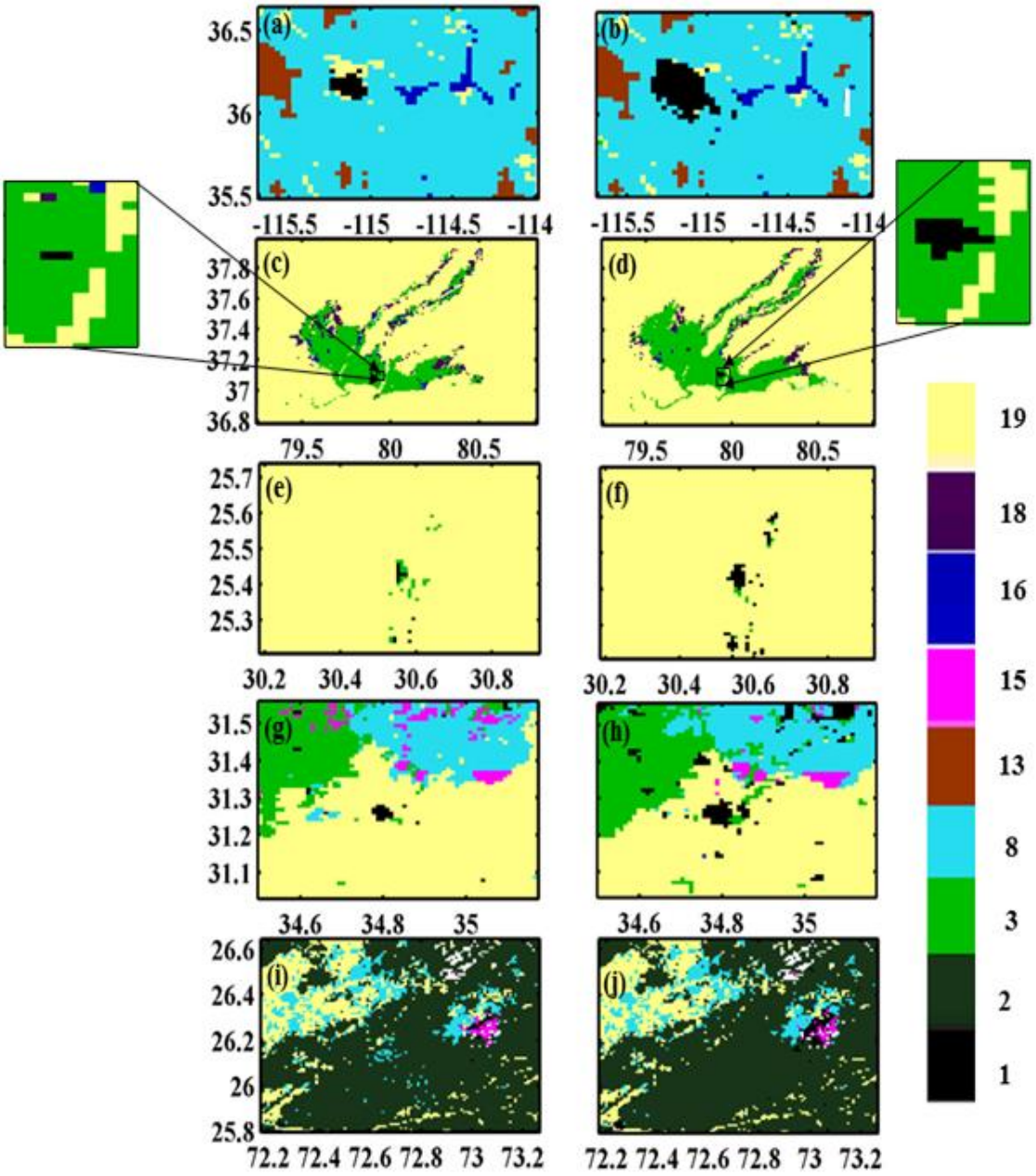

Figure 28. Land use maps for all five city, the left and right columns represent pre and post urbanization respectively. Each row represent a different city in the following order, Las Vegas, Hotan, El Kharga, Beer Sheva, and Jodhpur. The color bar shows the number of land use categories (using the USGS 24 land use types) Black represents urban buildup, Light green Irrigated Cropland and Pasture, dark green is Dry Cropland and Pasture, light blue Shrubland, dark blue is Waterbodies.

Table 4 Land use categories shown in Figure 28.

Land use category name	Number
Urban and Build-up Land	1
Dry Cropland and Pasture	2
Irrigated Cropland and Pasture	3
Shrubland	8
Evergreen Broadleaf	13
Mixed Forest	15
Water Bodies	16
Wooden Wetland	18
Barren or Sparely Vegetated	19

5.3 Surface Air Temperature Changes for the Five Cities

Figure 30 shows the changes in 2 m air temperature in nighttime induced by land-use changes as deduced from the difference of the "2010 run" minus "1985 run" from each pair of twin experiment. For brevity, shown are the difference maps at 2 AM local time which is representative of late night and early morning. The domains shown in Figure 30 are the same as their counterparts in Fig. 28, i.e., they are the innermost domains for the WRF model.

Nighttime warming akin to the classic UHI is found in all five cities over the grid points where urbanization occurred between 1985 and 2010. It is insensitive to the specific type of pre-urbanization land cover in 1985 from which the conversion to urban land occurred. For example, for Las Vegas a "ring" of elevated temperature is found to coincide with the new urban land converted primarily from the category of shrubland or

barren with sparse vegetation. For Jodhpur, urban land emerged mainly at the expense of dry cropland and pasture. The feature of nighttime warming is qualitatively similar for winter and summer. The influence of urbanization on the surface air temperature is relatively local; the nighttime warming does not spill significantly beyond the vicinity of the new urban area. The characteristic of nighttime warming is not sensitive to the specific type of land cover in the surrounding areas of the urban core.

Although the cases with conversions between two non-urban land types are not of our main interest, they do occur at many grid points in the surrounding areas away from the cities, especially Hotan. Unlike urban development, the non-urban types of land-use changes are not spatially concentrated but are characterized by a complicated juxtaposition of multiple types of conversions. For Hotan, the areas with agricultural development (conversion from barren or wooden wetland to irrigated cropland) generally exhibits a nighttime cooling.

Figure 31 shows the changes in 2 m air temperature at daytime. Shown are the temperature maps at 2 PM, except for Beer Sheva for which 11 AM is chosen because the temperature response peaks earlier in the day. In contrast to UHI at nighttime, all cities exhibit daytime cooling over the grid points where urban land emerges between 1985 and 2010. Like the nighttime response, this feature is insensitive to the pre-urbanization land type and the size of the city (see the summary in Figure 32). It is also found in both winter and summer.

For the land-use changes that do not involve urbanization, scattered daytime warming is found in Hotan outside the urban area especially in winter. This is associated

mainly with the conversion from a drier type (barren or sparsely vegetated) to a wetter type (wooden wetland or irrigated cropland) of land cover.

Over the non-urban areas in Beer Sheva and Jodhpur, some features of temperature changes shown in Figure 30 cannot be clearly identified with the local land-use changes in Figure 28. Those are meteorological noise due to the influence of regional circulation which overwhelms the climatic signal produced by land-use changes. For Jodhpur, the influence of Indian Monsoon in summer is hard to remove from the simulation for just one particular year. For Beer Sheva, with the proximity of the city to the Mediterranean Sea the urban effect is susceptive to the detail of land-sea breeze type of diurnal circulation. Since urbanization can also affect local circulation which in turn affects temperature (Kamal et al. 2015), a definitive quantification of the urban effect for these two cases would require using much longer simulations to potentially extract the signals in both temperature and wind. This is challenging due to the noisiness of wind field over urban areas (Kamal et al. 2015).

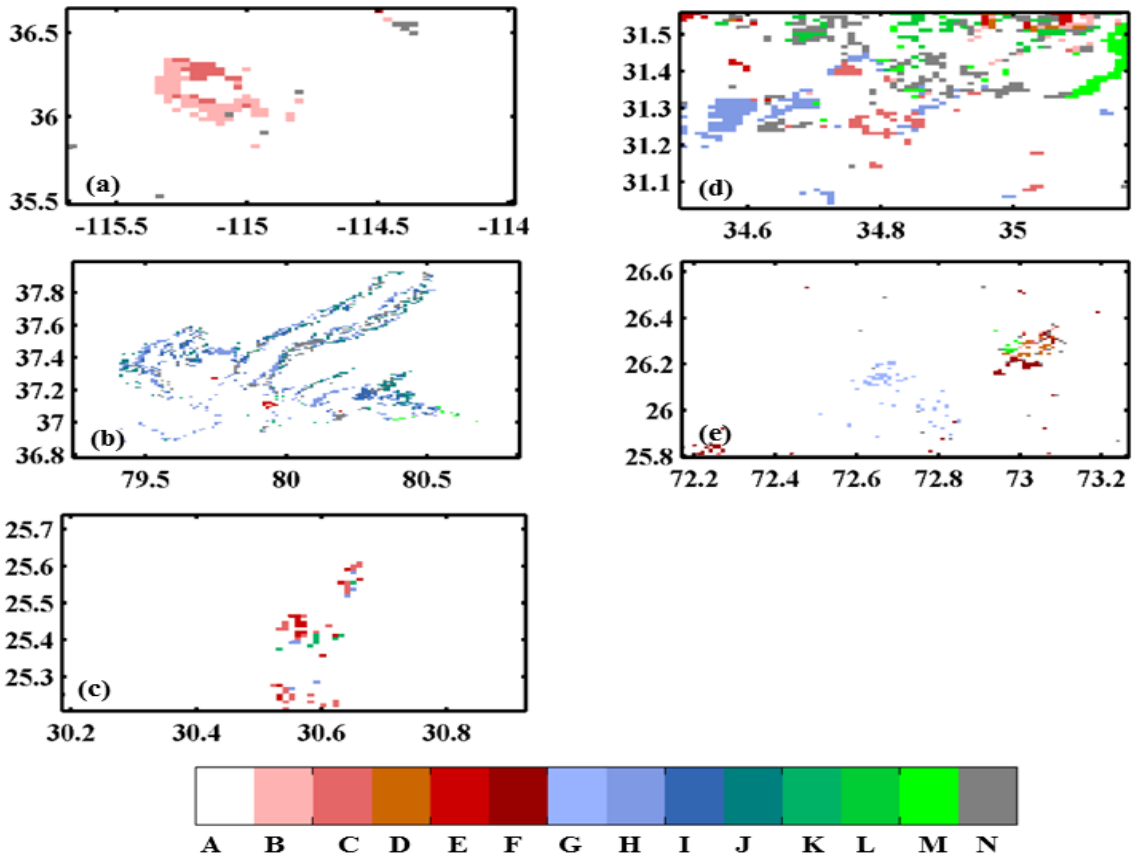

Figure 29. Summary of all relevant land-use changes.

Table 5. Main land use changes

Type of land-use change	LU index in 1985	LU index in 2010
A	No change occurred	
B	**8**	**1**
C	**19**	**1**
D	**15**	**1**
E	**3**	**1**
F	**2**	**1**
G	8	2
H	19	3
I	18	3
J	19	18
K	3	19
L	15	8
M	19	8
N	All other minor types of changes	

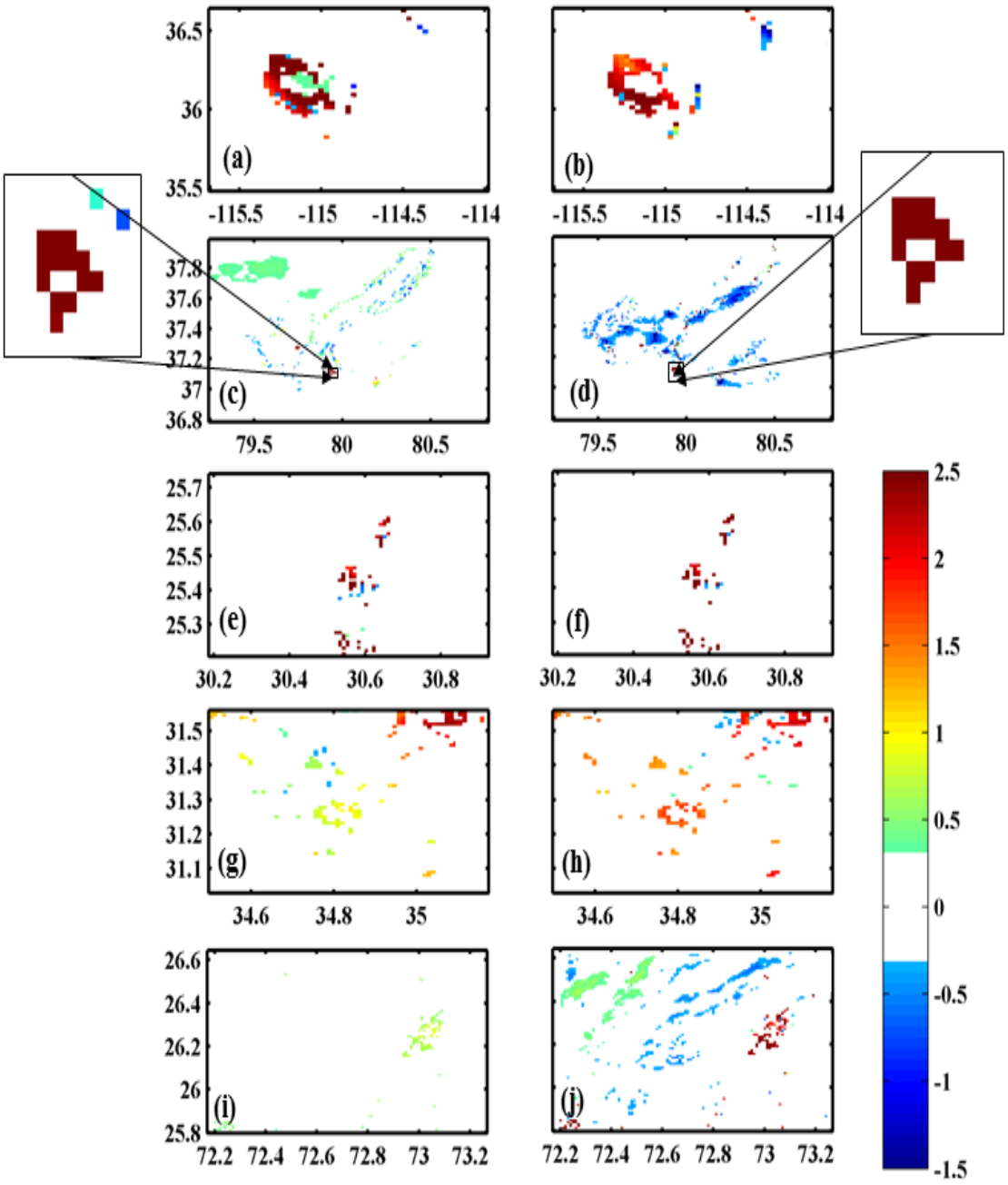

Figure 30. Color map representation of the change in 2 m temperature averaged at 2 AM local time of each of each of cities, for summer (left) and winter (right) for all five cities (Las Vegas, Hotan, El Kharga, Beer Sheva, and Jodhpur). To the side of row 2 shown a high resolution map of the actual urban extend of Hotan. To the right of the figure is the color map for the figure (red is hot and blue is cold).

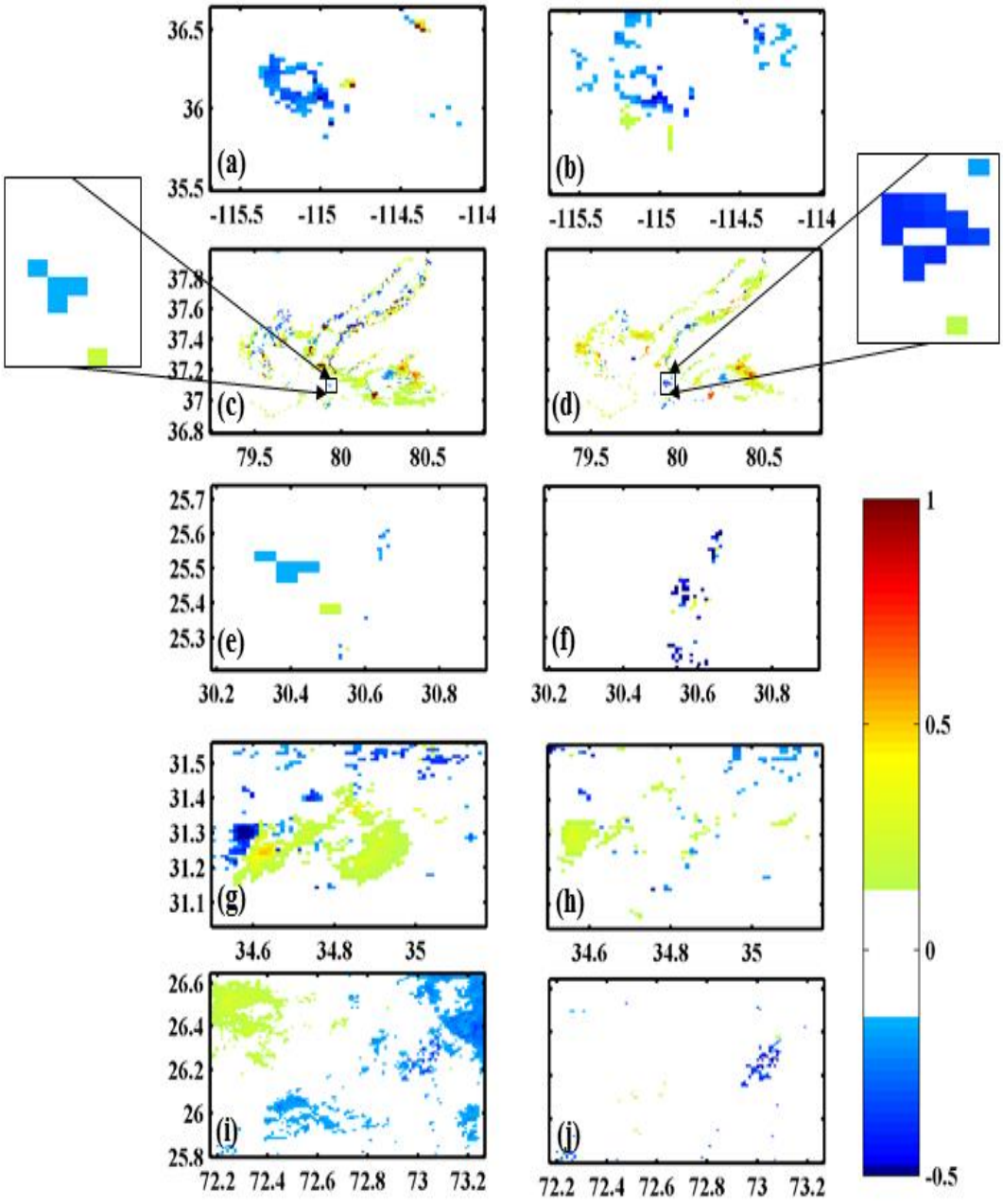

Figure 31. Same as Fig.29 but for day (2PM) for all the cities and (11 AM for Beer Sheva).

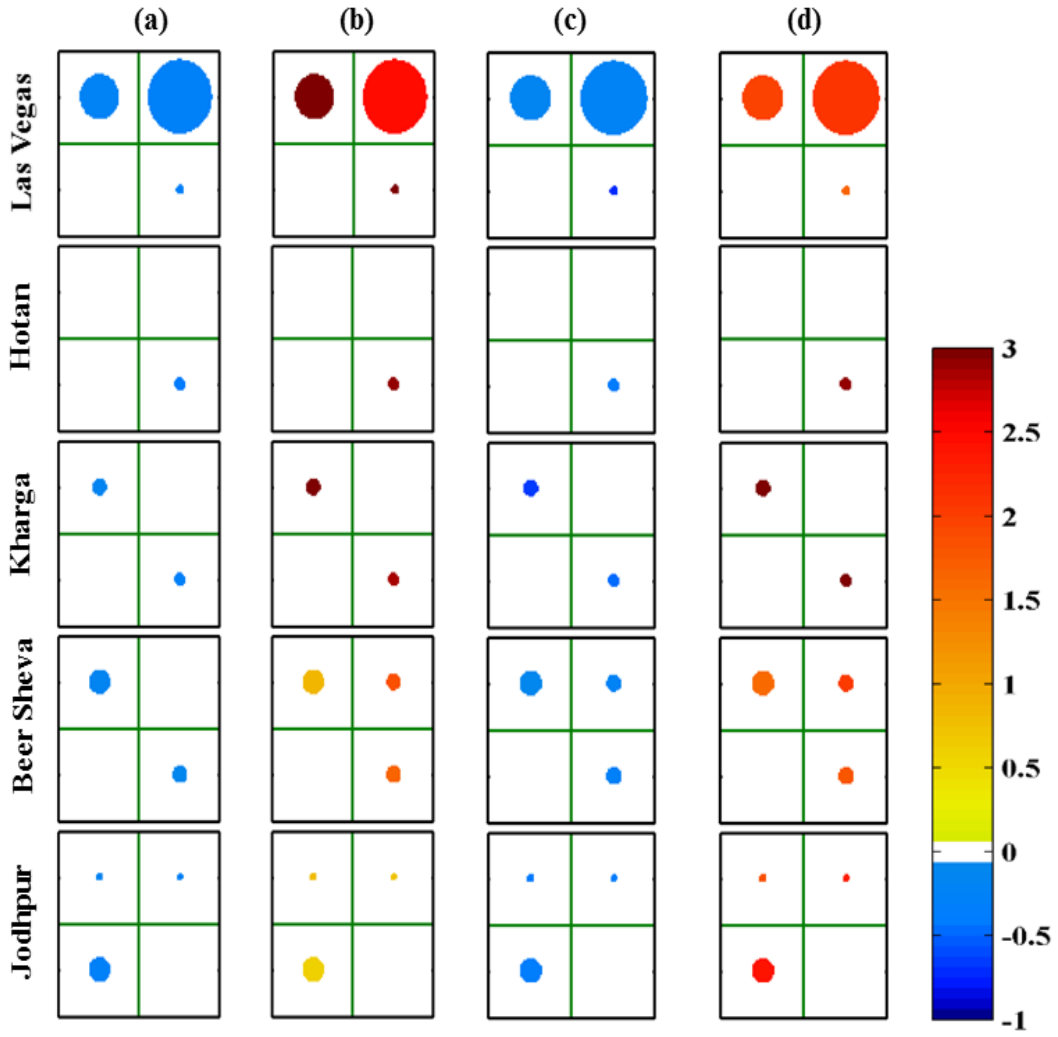

Figure 32. The color of each circle represents the temperature change due to a particular land use change and size of the circle is proportional to area of where such change happened, each raw represents a city, columns (a),(b),(c), and (d) represent summer day, summer night, winter day and winter night respectively. The four corners of each square represent the following transitions, starting from the top left and going clockwise: Barren or Sparely vegetated to Urban and Build-up land, Shrubland to Urban and Build-up, Dry Cropland and Pasture to Urban and Build-up Land, and From Dry Cropland to Urban and Build-up land.

CHAPTER 6

PREDICTIONS FOR FUTURE LAND USE PROJECTIONS

6.1 Numerical experiment design for future climate projections.

In the Last chapter we simulated the climate of five desert cities. We investigated the effect of the rapid urban development on their climate. In this part of the study we use the same frame to predict future climate changes of these cities using future projection maps.

While the prediction of global trends in population is valuable, it is not very useful to predict the local change in the climate of an area due to its predicted land use change. Furthermore most of the predicted desert urbanization is happening in poor or developing areas where data is scarce or incomplete, and where global averages don't accurately reflect the local changes.

Spatially explicit models predict land use change at the site or at a pixel level, but do not address the overall level challenge. There is a suit of spatially explicit models, that predict the probability of land-use change as a function of variables such as soil quality, accessibility and land prices (Chomitz and Gary 1996 Nelson and Hellaerstein, 1997; Pfaff, 1999, Nelson and Geoghegan, 2002, and Geophen et.al 2004). The URBANSIM model documents urban expansion without reference to farmland status. Despite this, the model has been used extensively to predict farmland loss from urban expansion. The model is expanded to incorporating the role of non-urban land use (i.e, agricultural use) in the urban growth process and using the historical satellite records to build models for future urban growth.

A new method is developed to use binary/non-binary urban maps generated by remote sensing analysis to create maps for the most probable locations and periods of future urban land-use changes (Fragkias and Seto 2007). The model was developed for data-sparse environments in developing areas. Withe fundamental assumption that that the land will be used such that the net return value land use change will be maximized. That is the likelihood that a parcel of agricultural land will be converted to urban increases as the return to the urban land exceeds the return to other non-urban land use

Few studies have systematically simulated future climate changes induced by urbanization due to a lack of reliable projections on the future extends of major urban areas. Nevertheless, progresses have recently been made to construct such projections (Fragkias and Seto, 2007 and Seto, 2008). Taking advantages of the availability future land use projection maps provided by Dr. Karen Seto, the maps will be downscaled to inner-most domain resolutions and used to construct surface boundary condition for the 5 cities (about 3 km for Las Vegas and 1 km for the rest). I will use 2010 lateral boundary conditions on the outer most domain, for summer (05-03-2010 to 09-03-2010) and winter (10-03-2009 to 02-03-2010). By fixing the lateral boundary conditions to 2010 one can compare the results with the 2010 run and isolate the effect of the land use change between 2010 and 2030.

Utilizing same the computational domains used in chapter 5 (shown in Figure 28). With a total of 10 runs corresponding to winter and summer for each of the cities.

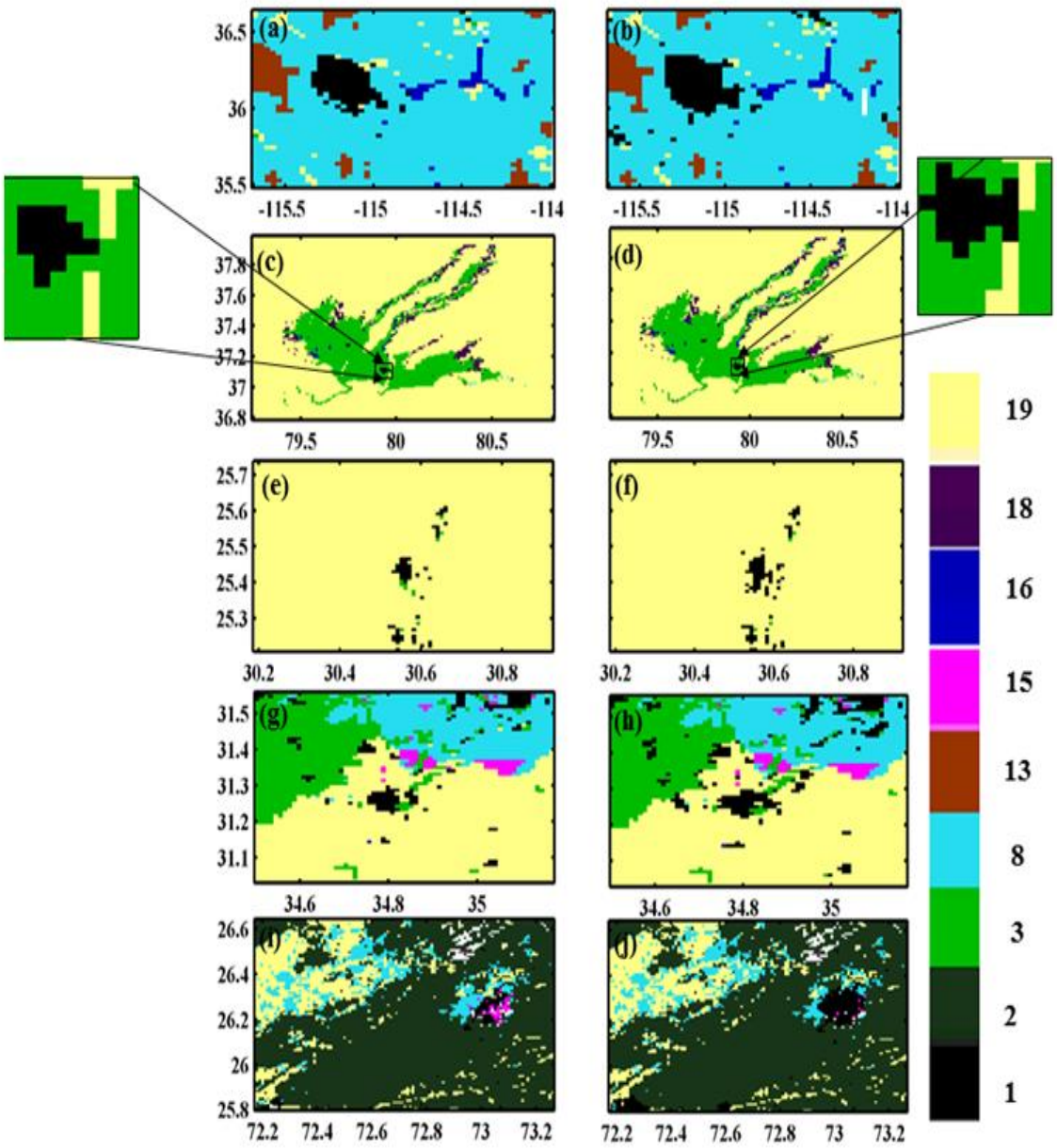

Figure 33. Land use maps of inner domain of each of the five cities. The first column represent the map for the 2010 and second column represent the map for future predictions (2030). Each row represent a different city in the following order, Las Vegas, Hotan, El Kharga, Beer Sheva, and Jodhpur. The color bar shows the number of land use categories (using the USGS 24 land use types) Black represents urban buildup, Light green Irrigated Cropland and Pasture, dark green is Dry Cropland and Pasture, light blue Shrubland, dark blue is Waterbodies.

Figure 33 summarizes the land use maps of the WRFs innermost domain (Figure 28) for both 2010 and 2030. Major land uses appearing in figure 33 are summarized in Table 6. Default WRF land use maps are using on the intermediate and outer most domain. While all the five cities are located in desert areas and all are expected witness urbanization, the detailed composition and location of the expected change is diverse. Figure 34 show the dominant land use changes for all five cities. Table 7 shows the predicted land use shifts for each city and the total area effected by each change. Las Vegas is expected to witness the largest shifts to urban build up, mainly from the surrounding shrubland. Hotan witnessed small and scattered development on the expense of irrigated cropland the second highest expected land use change happen in Jodhpur in which 100km2 are expected to turn from Shrubland, and Dry to urban build up. In Jodhpur 45 km2 are expected to transition from mixed forest to urban build up embedded in the surrounding the old urban core. With this contrast in size and location, the main climate signal is (the value of temperature change from non-urban to urban) is not very different, as we will see in the next chapter.

Table 6. Predicted land use changes for each of the five cities

City	Area(km^2)	From		To	
Las Vegas	369 108	8 19	Shrubland Barren	1 1	Urban build up
Jodhpur	57 54 45 38	8 2 15 19	Shrubland Dryland Mixed Forest Barren	1 1 1 1	Urban build up
Hotan	11 3	3 3	Irrigated Cropland Irrigated Cropland	1 19	Urban build up Barren
Beer Sheva	48 30 25	19 8 3	Barren Shrubland Irrigated Cropland	1 1 1	Urban build up
Kharga	22 7	19 3	Barren or Sparely Irrigated Cropland	1 1	Urban and Build up

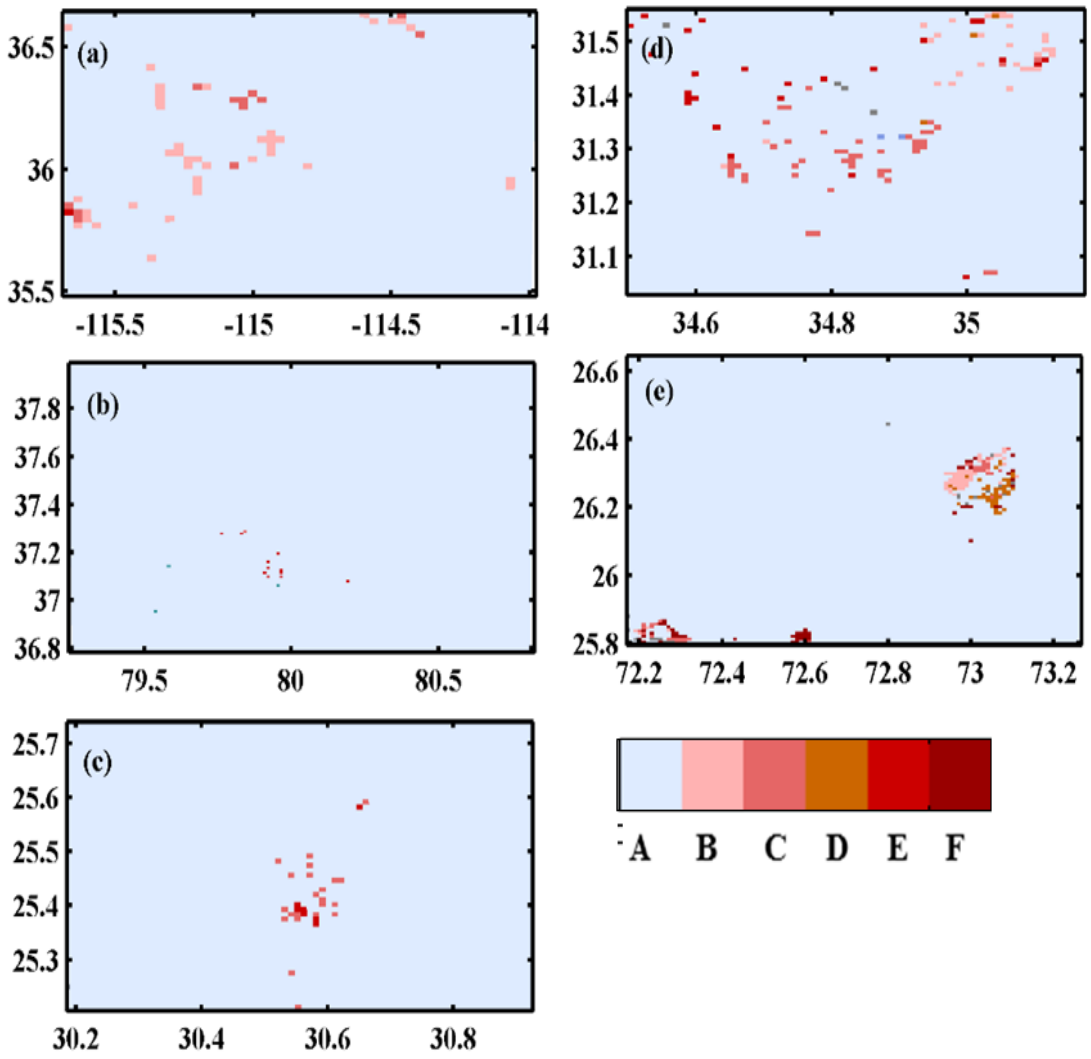

Figure 34. A summary of the major land use changes that are predicted for the five cities. (a) represents Las Vegas, (b) Hotan, (c) Kharga, (d) Beer Sheva, and (c) is for Jodhpur. The color scheme is descried in Table 7.

Table 7. Land use changes descried in Fig34.

Land use change	2010	2030
A	No change	No change
B	8	1
C	19	1
D	15	1
E	3	1
F	2	1

6.2 Predicted surface temperature changes for the five cities

Shown in Figure 35 are the temperature maps for summer at 2 PM, except for Beer Sheva for which 11 AM is chosen because the temperature response peaks earlier in the day. All cities are expected to exhibit daytime cooling over the grid points where urban land is projected. This feature is insensitive to the pre-urbanization land type and the size of the city (see the summary in Fig. 38). It is also found in both winter and summer.

It is insensitive to the specific type of pre-urbanization land cover in 2010 from which the conversion to urban land occurred. For example, for Las Vegas a "ring" of elevated temperature is found to coincide with the new urban land converted primarily from the category of shrubland or barren with sparse vegetation. For Jodhpur, urban land emerged mainly at the expense of dry cropland and pasture and mixed forest.

The feature of nighttime warming is qualitatively similar for winter and summer

Figures 36 Show the changes in 2 m temperature for nighttime summer induced by land-use changes from “2030” run minus “2010” run from each pair of twin experiments. For brevity shown are the difference maps at 2 AM representing late night and early morning. In contrast with the daytime cooling, nighttime warming analogous to the classic UHI is expected for all grid points projected to witness urbanization in all the five cities

While the main signal of daytime cooling and night time warming is qualitatively similar for all cities. The relative magnitude of heating and cooling reflect the inter-city diversity. The daytime cooling is most pronounced in Las Vegas and Jodhpur. And while the changes to urban build up in Las Vegas was mainly from shrubland and barren land, the changes for Jodhpur are more diverse, with large part of is on the cost of the mixed forced the around the old town’s center leading to more pronounced cooling.

Over non-urban areas in Beer Sheva and Jodhpur, some features of temperature changes shown in figure 35 and 36 cannot be clearly correlated with land-use change (shown in figures 33 and 34). Such features also existed in figures 29 and 30 and represent metrological noise caused by disturbances in the regional climate masking the climate signal produced by land-use changes. For Jodhpur the effect of Indian monsoon in the summer cannot be filtered by 8 months of simulation. Beer Sheva is in the close vicinity of the Mediterranean shore and urban induced temperature changes interacts with the land-sea type of diurnal circulation. As urbanization also effects local circulation which in turn effects urbanization (Kamal et al. 2015), much longer simulation is needed to extract signal in both wind and temperature.

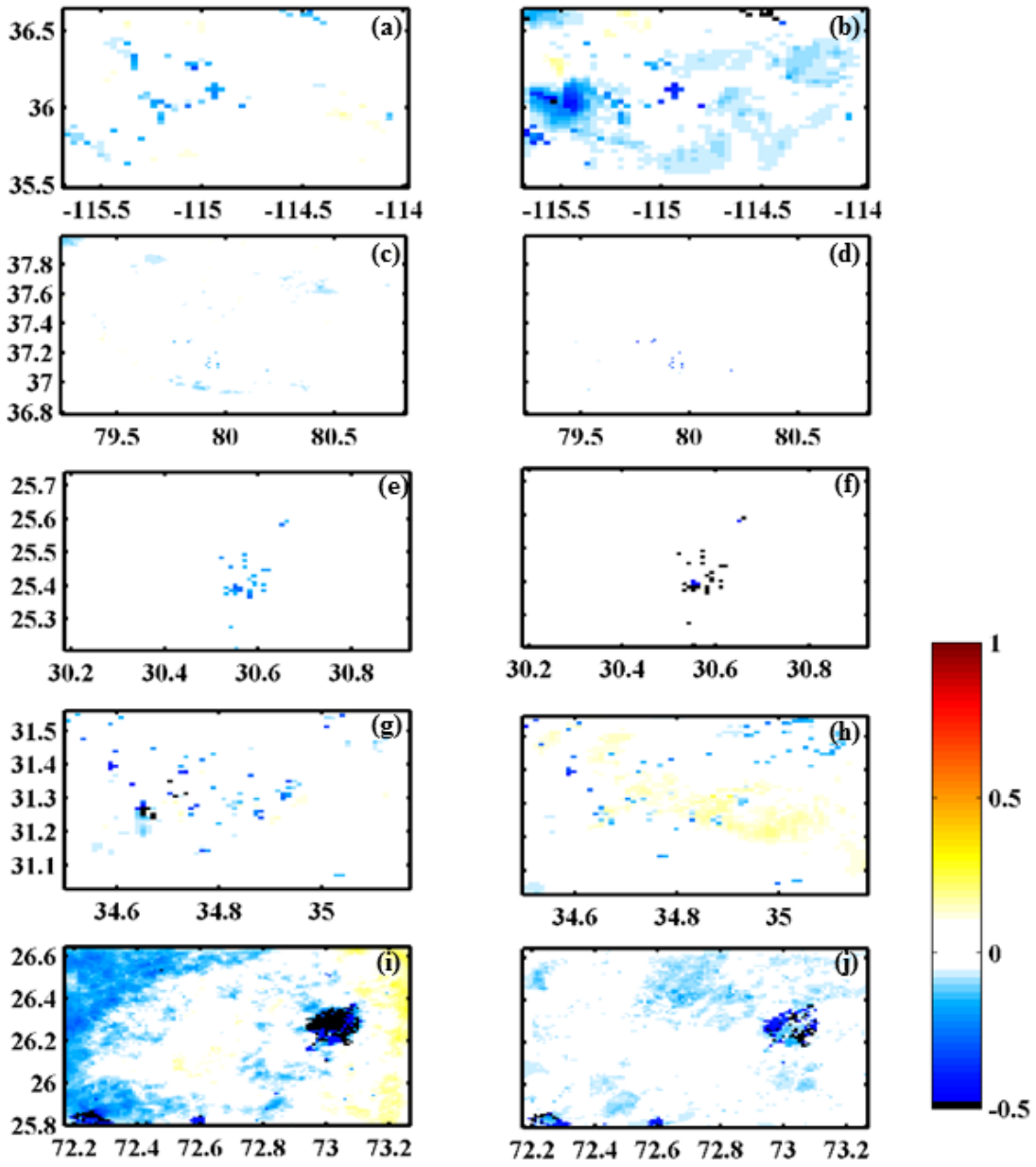

Figure 35. Summer and winter averaged map of the change in 2 m temperature between 2030 and 2010 for day (2 PM for all the cities and 11 AM for Beer Sheva). The cities are LasVegas, Hotan, Kharga, Beer Sheva, and Jodhpur.

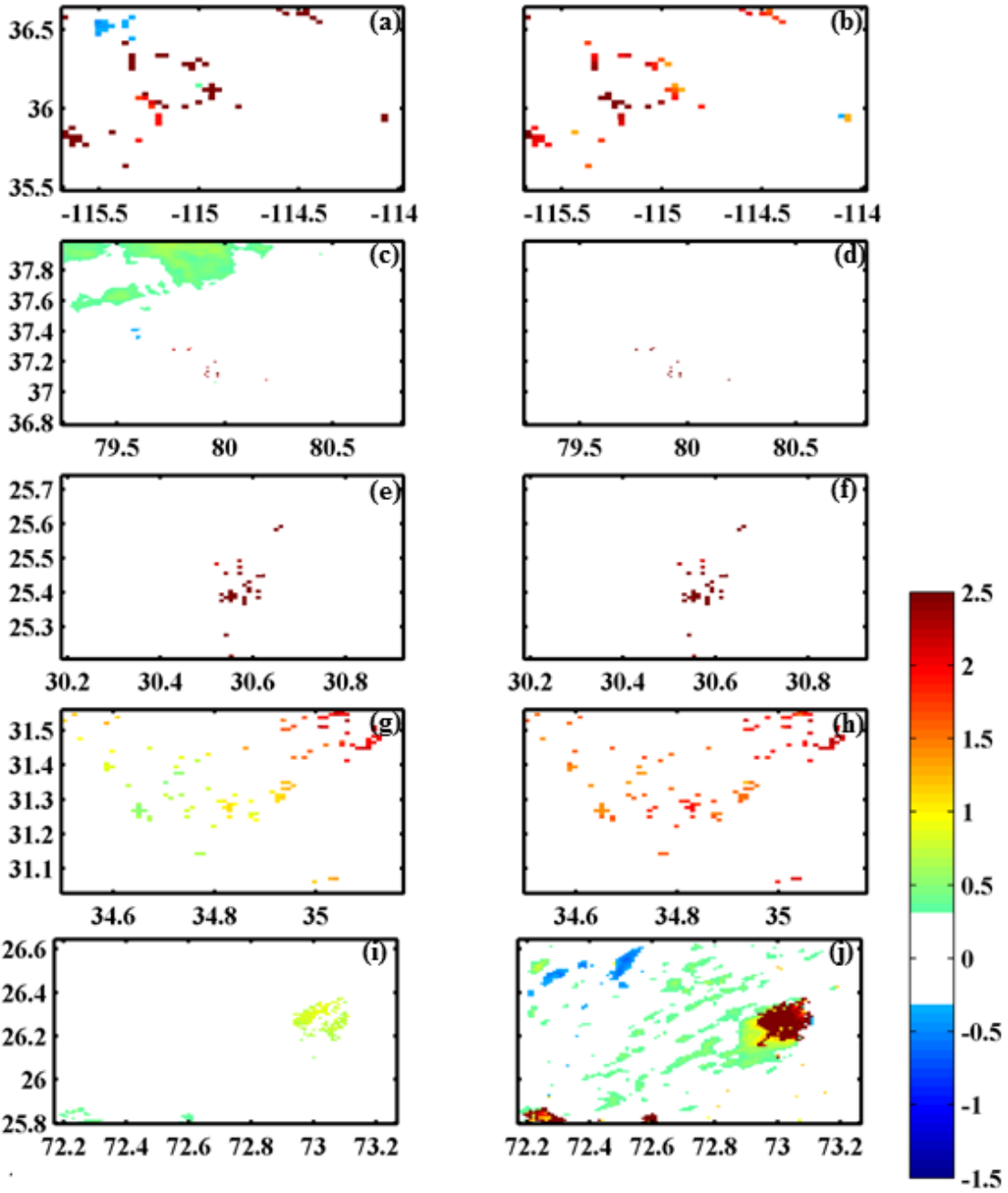

Figure 36 Same as Fig. 35 but for night (2 AM local time)

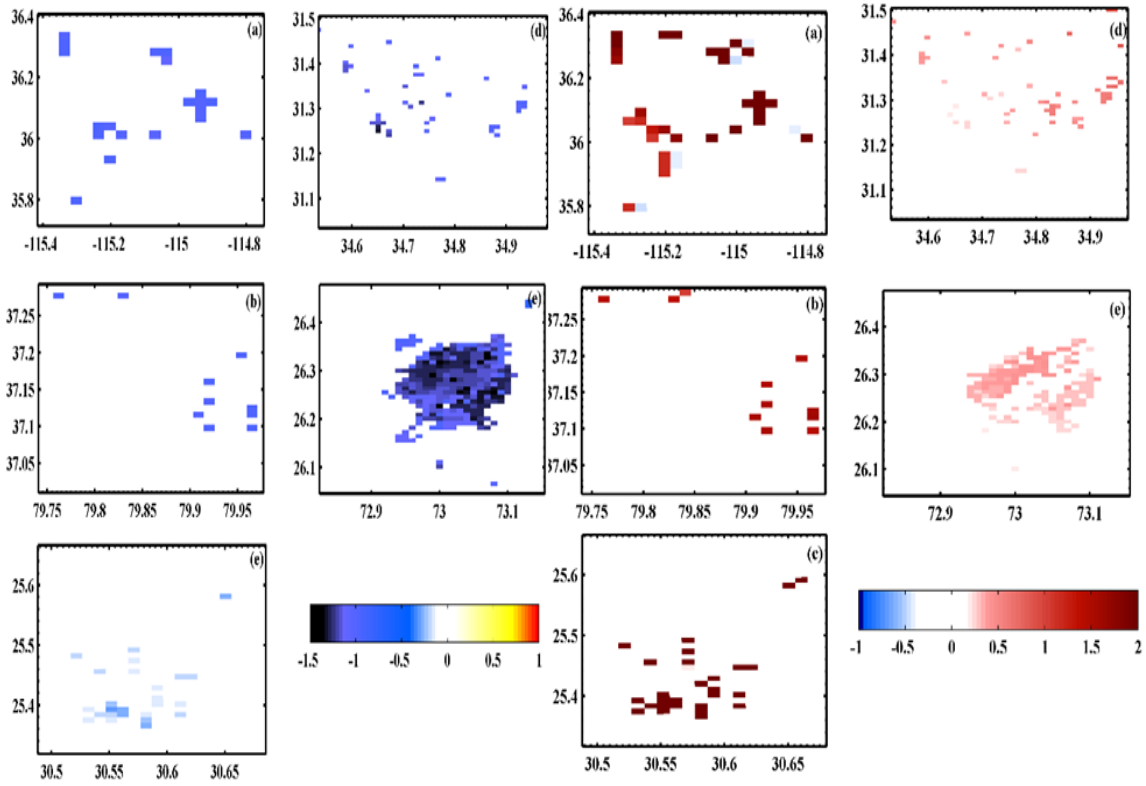

Figure 37. Two meter temperature change maps in the close vicinity of the urban center in Figures 34 and 35.

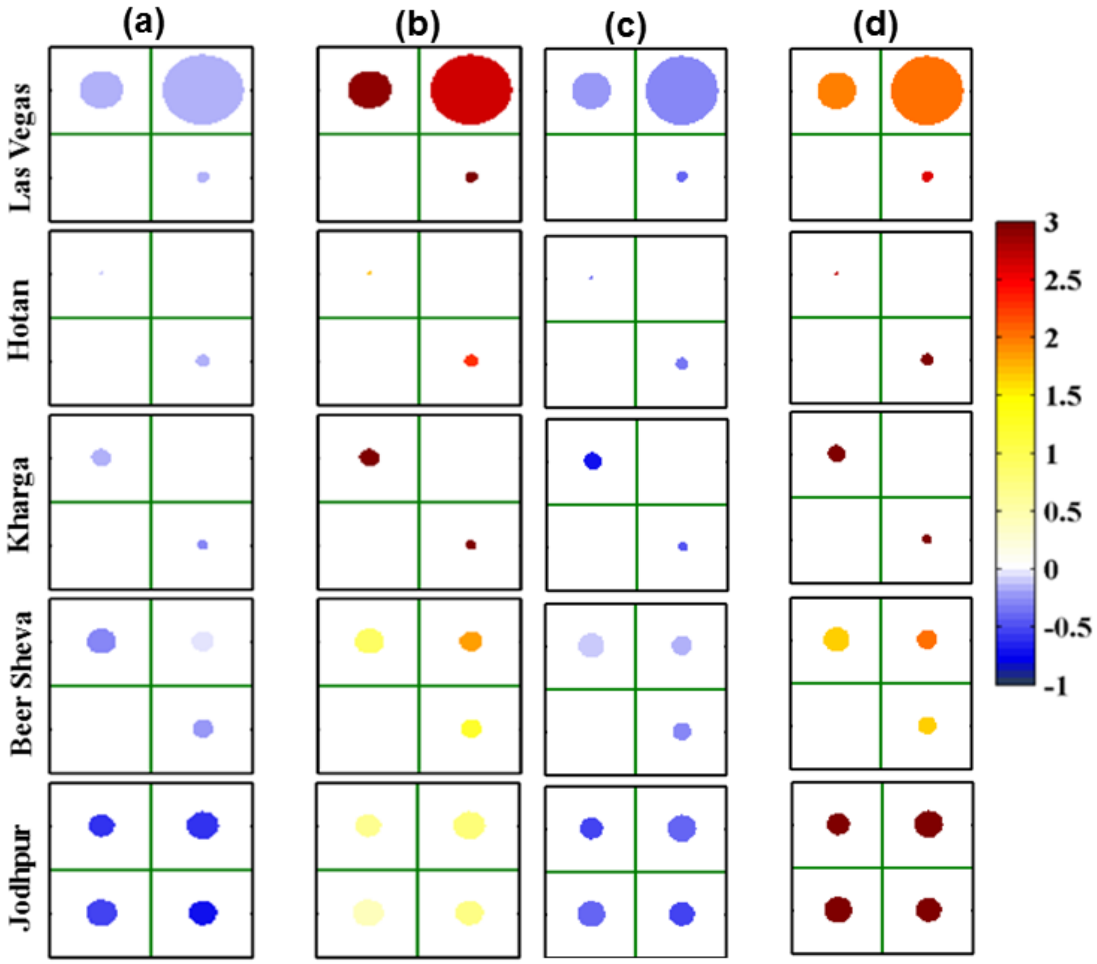

Figure 38. The color of each circle represents the temperature change due to a particular land use change in °C. The area of the filled circle is proportional to the area where the specific type of land-use change occurred for the specific city. Each raw represents a city, columns (a),(b) represent summer day, summer night, respectively. For Las Vegas Hotan, and Beer Sheva, the corners of each corner of the black square represent the following transitions, starting from the top left and going clockwise: Barren or Sparely vegetated to Urban and Build-up land, Shrubland to Urban and Build-up, Irrigated Cropland and Pasture to Urban and Build-up Land, and From Dry Cropland to Urban and Build-up land. For Jodhpur the third square transition from Irrigated cropland and pasture is replaced by mixed forest to urban.

Figure 38 shows a summary of the magnitude of the effect of the 5 main land use changes on the 2 meter temperature and the area effected by such change for summer and

winter. The summary in Figure 38 reaffirms the robust features of nighttime warming and relatively weak daytime cooling due to urbanization over desert cities. Notably, this effect stays the same for the four cities that are significantly smaller than Las Vegas. This generally reflects the localized nature of atmospheric response to small-scale land-use changes, at least in the WRF model. In other words, the local response does not significantly spill over to neighboring areas. As noted by Kamal et al. (2015), in WRF simulations the vertical extent of the atmospheric thermal response to a localized land-use change is generally shallow. The signal diminishes before it reaches the middle of the planetary boundary layer, lest the free atmosphere. This makes it difficult for the signal to disperse horizontally to areas far away from the city. Whether this characteristic is true in observation remains to be investigated.

CHAPTER 7

SUMMARY AND DISCUSSION

7.1 Publications and conferences

In this study we used 18 high resolution land-use maps representing different stages of urbanization for 5 desert cities to investigate the universal effects of urbanization on the climate of desert cities. The maps are used to construct surface BCs in 18 sets of twin numerical experiments for summer and winter total simulation time of 4674 days.

The study results in 3 publication. Results for the Las Vegas experiment are presented in:

Kamal, S., H.-P. Huang, and S. W. Myint, 2015: The influence of urbanization on the climate of Las Vegas metropolitan area: A numerical study, J. Appl. Meteorol. Climatology, doi:10.1175/JAMC-D-15-003.1, in press

Results for the 2010-1986 five city experiment are included in:

Kamal, S., H.-P. Huang, and S. W. Myint, 2015: The universal effect of urbanization on the climate of desert cities Samy Kamal, Huei-Ping Huang, and Soe W. Myint, submitted to Environmental Research Letters.

Results of that experiment are also presented in AGU2014, and AMS2015 conferences.

Results for 2010, 2030 five city projections are included in

Kamal, S., H.-P. Huang, and S. W. Myint, 2015: The expected effect of urbanization on the climate of desert cities under future projection scenarios, in preparation.

7.2 Concluding discussion

Our results for this study are only valid in the scope of using WRF model with the numerical setup descried in chapters 2 and 3. Resolution either of 1 km or 3 km and 4:4:1 or 5:5:1 nesting ratio is used. At these resolution we can resolve the city but not detect small features in the city (like gardens and parks), also all of the surface physics are parametrized. The most of the relevant processes are parameterized through NOAH land surface model and 1D UCM. The lack of more detailed and accurate urban parameters may have hindered our ability to see significant differences between the five cities. Once such data becomes available, they need to be included in the model. Our results might be sensitive to the type of parameterization schemes in the model. More complicated and detailed models of the urban canopy physics exist. Such models have more accurate physics (for example anthropogenic heat sources are included). We haven't studied the sensitivity of our results on the choice of parametrization scheme.

While we compared model results to observation data that was only for 2006 Las Vegas and only for 2 seasons. We didn't validate long term trends, or systematic bias far from a large airport (all of the stations used for model validation are in an airport).

We only used 1 resolution for each city and did not study the sensitivity of the results on the resolution.

CHAPTER 8

CONCLUSION, RECOMMENDATIONS AND FUTURE WORK

8.1 Conclusion.

The goal of this study was to find the universal features of the change in climate associated with urban development of desert cities. We used 18 high resolution land-use maps to study the climate of 5 desert cities for summer and winter (4428 days total simulation time). The maps represent different stages of urbanization from 1985 to future projections (2030). The chosen cities range in size from ~50 km (Las Vegas) to less than 10 km (Kharga) with a diverse baseline climatology ranging from Mediterranean, to continental and Indian monsoon. The climate of Las Vegas is studied in more detail by inspecting the change in heat advection at 80 meter height and surface velocity field.

We validated the model and methodology by comparing model output for Las Vegas with observations from 4 weather stations. The study for Las Vegas showed that urbanization of the city led to nighttime heating and relatively weak daytime cooling. The effect was restricted only to the changed grid points and dies off before reaching the middle of the PBL. The changes in Albedo and effective emissivity were shown to be the main driver of the temperature change. We showed that the emerging urban structure slows down the local wind field which in turn changes the temperature. The signal in 2m temperature is similar for summer and winter.

The study for the other 4 cities a similar pattern: all the grid points changed urban build up witnessed the classical UHI at night and cooling during the day. The pattern was shown to be robust regardless of the initial type of the point, the size or the distribution of

the changed area. Scattered non-urban related land-use changes are also shown but not discussed in this study.

Future projections of land use changes for each city showed a diverse and contrasting pattern of urbanization. In Las Vegas, urbanization is expected to grow steadily as a ring around the current city and at the cost of the surrounding shrubland. Beer Sheva is expected to grow in size and generate satellite communities in the desert surrounding it. Jodhpur, however, is expected grow at the expense of barren land and mixed forest. While the main effect of these changes on the temperature is similar (daytime cooling and nighttime heating) the magnitude of such change is different as the daytime cooling for Jodhpur is a lot stronger than that expected for Las Vegas.

8.2 Recommendations

Our results showed that urbanization, and land use change in general effects the climate by changing the values effective emissivity and Albedo and surface roughness (u*). Change in the first two results in change in skin and subsequently surface air temperatures. The change in surface roughness results in change in the diurnal wind cycle, which in turn further modify the temperature.

In the scope of the results of this study, we learned three ways to minimize the climatological impact of urban expansions.

1-Increase total reflectivity of the urban area.

That can be achieved by

(a) Using more reflective materials in buildings and streets.

(b) Paint existing structure with highly reflective covers (lighter colors)

(c) Add plants or solar cells on top of already existing structures.

2- Decrease the effective emissivity.

That can be achieved by:

(a) Minimize the use of concrete and black asphalt in desert cities, as both have large emissivity (and low albedo).

(b) Decrease total roughness of the urban area which will in turn decreases the total exposed area decreasing the effective emissivity.

(c) Include more open spaces around the urban area.

4- Increase ventilation and decrease the overall drag of the urban area.

(a) Align new roads with the dominant wind direction.

(b) Decrease the overall height of buildings and include more open areas.

5-Increase evaporative cooling. That can be achieved by increasing planted areas.

It is also important to take into account the local circulation to decrease the total drag exerted by emerging urban structures on the local wind field. It is important to decrease the overall drag of the planned urban developments as ventilation is shown to play an important role in alleviating the effects of heat island and removing pollutants. That is especially important for large sources of pollution (like factories and roads). As careful placement of such establishments (using the increase venting during the day) can minimize insertion of these pollutants to the urban area.

In this study we used a simple 1D urban canopy model. While it was validated by observational data of Las Vegas, more detailed urban parameterization schemes now

exist. Such new schemes need to be included in future runs to assess the sensitivity of the results.

Comparison between observations and the model (and included parametrization schemes) are required at higher grid resolutions. For cities near the sea (Kharga, and Beer Sheva), we used the default reanalysis 2.5^o x 2.5^o Surface Temperature (SST) data. More accurate and higher resolution SST data is needed to study the interaction of the sea breeze with urban induced changes.

8.3 Future work

The study of Las Vegas showed that urban structures do modify the local circulation (in this case, valley wind). This is also expected for Beer Sheva, as Mediterranean Sea breeze modifies the temperature diurnal cycle. Jodhpur is effected by the Indian monsoon which also cannot be filtered out in our simulation. To examine the in the interaction of urbanization with Mediterranean sea-breeze, and Indian Monsoon, future work should include numerical study of the velocity field, and energy budget field of Beer Sheva and Jodhpur . We used a simple 1D urban canopy model. While it was validated by observational data of Las Vegas, more detailed urban parameterization schemes now exist. Such new schemes need to be included in future runs to assess the sensitivity of the results. Surface energy budget need to be investigated for Hotan and Jodhpur to explain the change in temperature due to converting irrigated land, and mixed forest to urban build-up.

REFERENCES

Acevedo W., L. Gaydos, J. Tilley, C. Mladinich, J. Buchanan, S. Blauer, K. Kruger, and J Schubert, 2013 : Urban Land Use Change in the Las Vegas Valley, http://geochange.er.usgs.gov/sw/changes/anthropogenic/population/las_vegas/ Averyt, M.Tignor and H.L. Miller (eds.)]. Cambridge University Press, Cambridge, United Kingdom and New York, NY, USA.

Barnett, T. P, and D. W. Pierce, 2008 : When will Lake Mead go dry?, Water Resour. Res., 44, W03201, doi:10.1029/2007WR006704.

Barnett, T. P., D. W. Pierce, H. G. Hidalgo, C. Bonfils, B. D. Santer, T. Das, G. Bala, A. W. Wood, T. Nozawa, A. A. Mirin, D. R. Cayan , and M. D. Dettinger, 2008 : Human-induced changes in the hydrology of the western United States, Science, 319, 1080 – 1083, doi:10.1126/ science.1152538.

Barnett, T. P., R. Malone, W. Pennell, D. Stammer, B. Semtner, and W. Washington (2004), The effects of climate change on water resources in the west, Clim. Change, 62, 1– 11, doi:10.1023/B:CLIM.0000013695. 21726.b8

Brazel, A., N. Selover, R. Vose, and G. Heisler, 2000: The tale of two climates– Baltimore and Phoenix urban LTER sites, Clim. Res., **15**, 123–135. doi:10.3354/cr015123

Brazel, A., P. Gober, L. Seung-Jae, S. Grossman-Clarke, J. Zehnder, B. Hedquist, and E. Comparri , 2007: Determinants of changes in the regional urban heat island in metropolitan Phoenix (Arizona, USA) between 1990 and 2004, Clim. Res., 33, 171–182, doi:10.3354/cr033171.

Brazel, A., P. Gober, S. J. Lee, S. Grossman-Clarke, J. Zehnder, B. Hedquist, and E. Comparri, 2007: Determinants of changes in the regional urban heat island in metropolitan Phoenix (Arizona, USA) between 1990 and 2004, Clim. Res., **33**, 171–182.

Caldwell, P., H.-N. S. Chin, D. C. Bader, and G. Bala, 2008: Evaluation of WRF dynamical downscaling simulation, Climatic Change., **95**, 499-521. doi:10.1007/s10584-009-9583-5

Carnahan, W. H., and R. C. Larson, 1990: An analysis of an urban heat sink, Remote Sensing Environ., **33**, 65-71

Changnon S.A (2001), Assessment of historical thunderstorm data for urban effects: the Chicago case, Climate Change 49:161–169. doi: 10.1023/A:1010797013336 characteristics in Las Vegas from Landsat and ASTER data, Photogramm. Eng. Remote

Chen, F., and J. Dudhia, 2001: Coupling an advanced land surface-hydrology model with the Penn State-NCAR MM5 modeling system, Part I: model implementation and sensitivity, Mon. Weather Rev., **129**, 569-585

Chen, F., H. Kusaka, R. Bornstein, J. Ching, C. S. B. Grimmond, S. Grossman-Clarke, T. Loridan, K. W. Manning, A. Martilli, S. Miao, D. Sailor, F. P. Salamanca, H. Taha, M. Tewari, X. Wang, A. A. Wyszogrodzki, and C. Zhang, 2011: The integrated WRF/urban modelling system: development, evaluation, and applications to urban environmental problems, Int. J. Climatol., **31**, 273-288

Chen, F., M. Tewari, H. Kusaka, and T. T. Warner, 2006: Current status of urban modeling in the community Weather Research and Forecast (WRF) model. Joint Sixth Symposium on the Urban Environment and AMS Forum: Managing our Physical and Natural Resources: Successes and Challenges, Atlanta, GA, USA, Amer. Meteor. Soc. CD-ROM. J1.4. Concept and Addressing Uncertainties, Natl. Acad. Press, Washington, D. C.

Chomitz, K.M., & D. A. Gary, 1998, Roads, land use and deforestation : a spatial model applied to Belize. The world Bank Economic Review, 10(3):487-512.
Diffenbaugh, N. S., 2009: Influence of modern land cover on the climate of the United States. Clim. Dynam., **33**, 945–958. doi:10.1007/s00382-009-0566z

ESRI., 1993: Environmental Systems Research Institute. Digital Chart of the World CD-ROM. Redlands, CA: ESRI.

Fragkias, M. and K.C Seto, 2007, Modeling urban growth in data-sparse enviroments: a new approach, Environment and planning B, 32(5):858-883

Fry, J., G. Xian, S. Jin, J. Dewitz, C. Homer, L. Yang, C. Barnes, N. Herold, and J. Wickham, 2011: Completion of the 2006 National Land Cover Database for the Conterminous United States, Photogramm. Eng. Remote Sensing., **77**, 858-864.

Fry, J., Xian, G., Jin, S., Dewitz, J., Homer, C., Yang, L., Barnes, C., Herold, N., and Wickham, J., 2011: Completion of the 2006 National Land Cover Database for the Conterminous United States, PE&RS, Vol. 77(9):858-864.

Georgescu, M, M. Moustaoui, A. Mahalov, and J. Dudhia, 2011: An alternative explanation of the semiarid urban area "oasis effect", J. Geophys. Res., **116**, doi:10.1029/2011JD016720

Georgescu, M., G. Miguez-Macho, L. T. Steyaert, and C. P. Weaver 2008: Sensitivity of summer climate to anthropogenic land-cover change over the Greater Phoenix, AZ, region, J. Arid Environ., 72, 1358 – 1373, doi:10.1016/j.jaridenv.2008.01.004.

Georgescu, M., G. Miguez-Macho, L. T. Steyaert, and C. P. Weaver, 2009: Climatic effects of 30 years of landscape change over the Greater Phoenix, Arizona, region: 2.

Dynamical and thermodynamical response, J. Geophys. Res., **114**, D05111. doi: 10.1029/2008JD010762

Giorgi, Filippo, 1990: Simulation of Regional Climate Using a Limited Area Model Nested in a General Circulation Model. J. Climate, 3, 941–963.

Heikkila, U., A. Sandvik, and A. Sorteberg, 2011: Dynamical downscaling of ERA-40 in complex terrain using the WRF regional climate model, Clim. Dynam., **37**, 1551–1564. doi:10.1007/s00382-010-0928-6

Hurrell W. J. , 1995: Decadal trends in the North Atlantic Oscillation – Regional temperatures and precipitation. Science, 269: 676–679.

IPCC, (2007), Climate Change 2007, The Physical Science Basis. Contribution of Working Group I to the Fourth Assessment Report of the Intergovernmental Panel on Climate Change [Solomon, S., D. Qin, M. Manning, Z. Chen, M. Marquis, K.B. island of Vancouver. British Columbia, Phys. Geography., **21**, 283-304

Kamal, S., H.-P. Huang, and S. W. Myint, 2015: The influence of urbanization on the climate of Las Vegas metropolitan area: A numerical study, J. Appl. Meteorol. Climatology, doi:10.1175/JAMC-D-15-003.1, in press

Kusaka H., M. Hara, and Y. Takane, 2012: Urban Climate Projection by the WRF Model at 3 km Horizontal Grid Increment: Dynamical Downscaling and Predicting Heat Stress in the 2070's August for Tokyo, Osaka, and Nagoya Metropolises, Journal of the Meteorological Society of Japan, Vol. 90B, pp. 47--63, 2012 47 doi:10.2151/jmsj.2012-B04

Kusaka, H., and F. Kimura, 2004: Coupling a single-layer urban canopy model with a simple atmospheric model: Impact on urban heat island simulation for an idealized case, J. Meteor. Soc. Japan, **82**, 67-80

Kusaka, H., H. Kondo, Y. Kikegawa, and F. Kimura, 2001: A simple single-layer urban canopy model for atmospheric models: Comparison with multi-layer and slab models. Bound.-Layer Meteor., 101, 329–358.

Kusaka, H., M. Hara, and Y. Takane, 2012: Urban climate projection by the WRF Model at 3 km horizontal grid increment: dynamical downscaling and predicting heat stress in the 2070's August for Tokyo, Osaka, and Nagoya Metropolises, J. Meteor. Soc. Japan, **90B**, 47-63, doi:10.2151/jmsj.2012-B04

Lebassi-Habtezion, B., and N. S. Diffenbaugh, 2013: Nonhydrostatic nested climate modeling: A case study of the 2010 summer season over the western United States, J. Geophys. Res. Atmos., 118, 10,944–10,962, doi:10.1002/jgrd.50773.

Lee T.-W., J.Y. Lee, and Z-H Wang, 2012: Scaling of the urban heat island intensity using time-dependent energy balance. Urban Climate 2 (2012) 16–24

Lee, T.-W., H. S. Choi, and J. Lee, 2014: Generalized scaling of urban heat island effect and its applications for energy consumption and renewable energy, Adv. Meteorology, **2014**, Article ID 948306, doi:10.1155/2014/948306

Leung, L. R., L. O. Mearns, F. Giorgi, and R. L. Wilby, 2003: Regional climate research: needs and opportunities, Bull. Am. Meteor. Soc., **84**, 89-95

Liang X- Z., M. Xu Xing, Y. Tiejun Ling, H. Choi, F. Zhang, L. Chen, S. Liu, S. Su, F. Qiao. Yuxianghe, X.L Julian, 2012: Regional research and forecast model. Bull. Am. Meteor. Soc.

Matsui, T., and R. A. Pielke, 2006: Measurement-based estimation of the spatial gradient of aerosol radiative forcing, Geophys. Res. Lett., 33, L11813, doi:10.1029/2006GL025974

Mearns, L. O., R. Arritt, S. Biner, M. S. Bukovsky, S. McGinnis, S. Sain, D. Caya, J. Correia, D. Flory, W. Gutowski, E. S. Takle, R. Jones, R. Leung, W. Moufouma-Okia, L. McDaniel, A. M. B. Nunes, Y. Qian, J. Roads, L. Sloan, and M. Snyder, 2012: The North American Regional Climate Change Assessment Program: overview of Phase I results, Bull. Am. Meteor. Soc., **93**, 1337-1362

Meir, T., P. M. Orton, J. Pullen, T. Holt, W. T. Thompson, and M. F. Arend, 2013: Forecasting the New York City urban heat island and sea breeze during extreme heat events. Wea. Forecasting, **28**, 1460-1477

Miller, J. A., 2011: Urban and regional temperature trends in Las Vegas and southern Nevada, J. Ariz. Nev. Acad. Sci., **43**, 27-39

Morris, C. J. G., I. Simmonds, and N. Plummer, 2001: Quantification of the influences of wind and cloud on the nocturnal urban heat island of a large city, J. Appl. Meteorol., **40**, 169-182

Moser, S., G. Franco, S. Pittiglio, W. Chou, and D. Cayan, 2009: The Future Is Now: An Update on Climate Change Science Impacts and Response Options for California. California Energy Commission, PIER Energy-Related Environmental Research Program. CEC-500-2008 071.

Myint, S. W., E. A. Wentz, A. J. Brazel, and D. A. Quattrochi, 2013: The impact of distinct anthropogenic and vegetation features on urban warming, Landscape Ecology, **28**, 959-978

National Centers for Environmental Prediction/National Weather Service/NOAA/U.S. Department of Commerce, 2000: updated daily. NCEP FNL Operational Model Global Tropospheric Analyses, continuing from July 1999. Research Data Archive at the National Center for Atmospheric Research, Computational and Information Systems Laboratory.

National Research Council, 2005: Radiative Forcing of Climate Change: Expanding the Concept and Addressing Uncertainties, Natl. Acad. Press, Washington, D. C.
National Research Council, 2012: Urban meteorology: forecasting, monitoring, and meeting

Nelson, G.C & D. Hellerstein, 1997. Do roads cause deforestation? Using satellite images in econometric analysis of land use. American Journal of Agricultural Economics

Nelson, G.C and J. Geoghegan., 2002, Deforestation and Land Use Change: Sparse Data Environments, Agricolutural Econonmics, 27:201-216.

Nickerson, Cynthia, R. Ebel, A. Borchers, and F. Carriazo, 2011: Major Uses of Land in the United States, 2007. EIB-89. U.S. Dept. Agr., Econ. Res. Serv. Dec.
Oke, T. R., 1982: The energetic basis of the urban heat island, Q. J. R. Meteorol. Soc., **108**, 1-24

Pan, L., S. Chen, D. Cayan,. M. Hart, Q. Zhang, Y. Liu,and J. Wang, 2011: Influence of climate change on the California and Nevada regions revealed by a high-resolution dynamical downscaling study, Clim. Dynam., 37, 2005-2020, doi:10.1007/s00382-010-0961-5

Pfaff, A.S.P., 1999 What Derives Deforestation in the Brazilian Amazon? Evidence from Satellite and Socioeconomic Data, Journal of Environmental Economics and Management 37(1):26-43

Pielke, R.A. Sr.,, A. Pitman, D. Niyogi, R. Mahmood, C. McAlpine, F. Hossain, K. K. Goldewijk, U. Nair, R. Betts, S. Fall, M. Reichstein, P. Kabat, and N. de Noblet, 2011: Land use/land cover changes and climate: modeling analysis and observational evidence, Wiley Interdisciplinary Rev.: Climate Change, **2**, 828-850

Roth, M., 2007: Review of urban climate research in (sub) tropical regions, International Journal of Climatology, 27, 1859-1873

Rozoff, C. M., W. R. Cotton, J. O. A. Degoke, 2002: Simulation of St. Louis, Missouri, land use impacts on thunderstorms, J. Appl. Meteorol., **42**, 716-738

Runnalls, K. E., and T. R. Oke, 2000: Dynamics and controls of the near-surface heat Sensing, **74**, 473–481

Seto K.C, and B. Guneralp, 2008: Environmental impacts of urban growth from an integrated dynamic perspective: A case study of Shenzhen, South China, Global Environmental Change 18 720–735

Sharma, A., and H.-P. Huang, 2012: Regional climate simulation for Arizona: impact of resolution on precipitation, Adv. Meteorology, Article ID 505726, doi:10.1155/2012/505726

Skamarock, W. C., J. B. Klemp, J. Dudhia, D. O. Gill, D. M. Barker, M. G. Duda, X. Y. Huang, W. Wang, and J. G. Powers, 2008: A description of the advanced research WRF version 3, NCAR Tech. Note NCAR/TN-475+STR. National Center for Atmospheric Research, Boulder, Colorado, 125 pp.

Takahashi, K., T. Mikami, and H. Takahashi, 2011: Influence of the urban heat island phenomenon in Tokyo on the local wind system at nighttime in summer, J. Geography, **120**, 341-358

U.S. Department of Agriculture, Natural Resources Conservation Service and Iowa State University Statistical Laboratory, 2009: Summary Report: 2007 National Resources Inventory, http://www.nrcs.usda.gov/wps/ portal/nrcs/main/national/technical/nra/nri/

UNEP (United Nations Environment Programme), 1997: World atlas of desertification 2ED. UNEP, London.

UNEP/GRID, 1991: United Nations Environment Program/ Global Resource Information Database. Global Digital Datasets for Land Degradation Studies: a GIS Approach. Prepared by U. Diechmann and L. Eklundh. GRID Case Study Series No. 4. UNEP/GEMS and GRID. Nairobi, Kenya.

United Nations, Department of Economic and Social Affairs, Population Division, , 2012: World Urbanization Prospects: The 2011 Revision. CD-ROM Edition – Data in digital form (ST/ESA/SER.A/319). user's needs, The National Academies Press, 176 pp.

Vogelmann, J. E., S. M. Howard, L. Yang, C. R. Larson, B. K. Wylie, and J. N. Van Driel, 2001: Completion of the 1990's National Land Cover Data Set for the conterminous United States, Photogramm. Eng. Remote Sensing, **67**, 650-662

Wicker, L. J and W. C. Skamarock, 2002: Time splitting methods for elastic models using forward time schemes, Mon. Wea. Rev., 130,2088-297.

Xian G., M. Crane, and C. McMahon, 2009: Quantifying Multi-temporal Urban Development Characteristics in Las Vegas from Landsat and ASTER Data, Photogrammetric Engineering & Remote Sensing Vol. 74, No. 4, April 2008, pp. 473–481.

Zheng, B., S. W. Myint, and C. Fan, 2014: Spatial configuration of anthropogenic land cover impacts on urban warming, Landscape and Urban Planning, **130**, 104-111

Zhou, X., and Y-C. Want, (2011), Dynamics of Land Surface Temperature in Response to Land-Use/Cover Change, Geographic Research, 49 (1):23–36

APPENDIX A

WRF NAMELISTFILES AND LAND USE CATEGORIES

Table 8. WRF land use categories

Land Use Category	Land Use Description
1	Urban and Built-up Land
2	Dry Cropland and Pasture
3	Irrigated Cropland and Pasture
4	Mixed Dryland/Irrigated Cropland and Pasture
5	Cropland/Grassland Mosaic
6	Cropland/Woodland Mosaic
7	Grassland
8	Shrubland
9	Mixed Shrubland/Grassland
10	Savanna
11	Deciduous Broadleaf Forest
12	Deciduous Needleleaf Forest
13	Evergreen Broadleaf
14	Evergreen Needleleaf
15	Mixed Forest
16	Water Bodies
17	Herbaceous Wetland
18	Wooden Wetland
19	Barren or Sparsely Vegetated
20	Herbaceous Tundra
21	Wooded Tundra
22	Mixed Tundra
23	Bare Ground Tundra
24	Snow or Ice

Table 9. Cross references between the land use categories in WRF model and the two NLCD datasets used in this study. All other categories not listed in this table together account for less than 1% of the land cover over the greater Las Vegas region.

WRF category	1	14	7	16	19	8
Land surface type	Urban build up	Evergreen needle leaf	Grass land	Water bodies	Barren	Shrub land
NLCD 1992	21,22,23	42	71	11	31	52
NLCD 2006	21,22,23,24	42	71	11	31	52

Namelist.input for Las Vegas future run

```
TIME CONTROL
&time_control
run_days                 = 123,
run_hours                = 0,
run_minutes              = 0,
run_seconds              = 0,
start_year               = 2010,    2010,    2010,
start_month              = 05,      05,      05,
start_day                = 03,      03,      03,
start_hour               = 00,      00,      00,
start_minute             = 00,      00,      00,
start_second             = 00,      00,      00,
end_year                 = 2010,    2010,    2010,
end_month                = 09,      09,      09,
end_day                  = 03,      03,      03,
end_hour                 = 00,      00,      00,
end_minute               = 00,      00,      00,
end_second               = 00,      00,      00,
interval_seconds         = 21600,
input_from_file          = .true.,  .true.,  .true.,
fine_input_stream        = 0,       2,       2,
io_form_auxinput2        = 2,
history_interval         = 129600,  360,     60,
frames_per_outfile       = 1,       1,       1,
restart                  = .false.,
restart_interval         = 43200,
io_form_history          = 2,
io_form_restart          = 2,
io_form_input            = 2,
io_form_boundary         = 2,
debug_level              = 0,
/

COMPUTATIONAL DOMAIN SETUP
&domains
time_step                = 288,
time_step_fract_num      = 0,
time_step_fract_den      = 1,
max_dom                  = 3,
e_we                     = 71,    113,     53,
e_sn                     = 60,    93,      45,
```

```
e_vert                = 28,      28,      28,
 p_top_requested          = 5000,
num_metgrid_levels       = 27,
num_metgrid_soil_levels  = 4,
dx                    = 48000,   12000,    3000,
dy                    = 48000,   12000,    3000,
grid_id                 = 1,       2,       3,
parent_id               = 1,       1,       2,
i_parent_start          = 1,      25,      41,
j_parent_start          = 1,      19,      41,
parent_grid_ratio       = 1,       4,       4,
parent_time_step_ratio  = 1,       4,       4,
feedback                = 1,
smooth_option           = 0,
 /
CONTROLS FOR PHYSICS AND UNRESOLVED PROCESSES
&physics
mp_physics    = 3,       3,       3,
ra_lw_physics = 1,       1,       1,
ra_sw_physics  = 1,      1,       1,
radt     = 30,      30,      30,
sf_sfclay_physics  = 1,       1,       1,
sf_surface_physics = 2,       2,       2,
bl_pbl_physics  = 1,       1,       1,
bldt   = 0,       0,       0,
cu_physics= 1,       1,       0,
sf_urban_physics  = 1,       1,       1,
cudt = 5,       5,       5,
isfflx                  = 1,
ifsnow                  = 0,
icloud                  = 1,
surface_input_source    = 1,
num_soil_layers         = 5,
maxiens                 = 1,
maxens                  = 3,
maxens2                 = 3,
maxens3                 = 16,
ensdim                  = 144,
```

Namelist.wps (WRF Preprocessing System)

```
TIME CONTROL
&share
 wrf_core = 'ARW',
 max_dom = 3,
 start_date = '2010-05-03_00:00:00', '2010-05-03_00:00:00', '2010-05-03_00:00:00',
 end_date   = '2010-09-03_00:00:00', '2010-09-03_00:00:00', '2010-09-03_00:00:00',
 interval_seconds = 21600
 io_form_geogrid = 2,
 /
SURFACE BCs SETUP
&geogrid
  parent_id         = 1,1,2,
 parent_grid_ratio = 1,4,4,
 i_parent_start    = 1,25,41,
 j_parent_start    = 1,19,41,
 e_we          = 71,113,53,
 e_sn          = 60,93,45,
 geog_data_res = '10m','10m','10m',
 dx = 48000,
 dy = 48000,
 map_proj =  'lambert',
 ref_lat   = 36.12,
 ref_lon   = -115.17,
 truelat1  = 36.12,
 truelat2  = 36.12,
 stand_lon = -115.17,
 geog_data_path = '/usr2/kamal/geog',
ref_x = 35.5,
 ref_y = 30.0,
/
LATERAL BCs SET UP
&ungrib
 out_format = 'WPS',
 prefix = 'FILE',
/
COMPINING BOTH BCs INTO ONE FILE PERDOMAIN FOR TIMES DAILY
&metgrid
 fg_name = 'FILE',
 io_form_metgrid = 2,

VERTICAL BCs and PRESSURE LEVELS

&mod_levs
```

```
 press_pa = 201300 , 200100 , 100000 ,
            95000 ,  90000 ,
            85000 ,  80000 ,
            75000 ,  70000 ,
            65000 ,  60000 ,
            55000 ,  50000 ,
            45000 ,  40000 ,
            35000 ,  30000 ,
            25000 ,  20000 ,
            15000 ,  10000 ,
             5000 ,   1000
 /
```

APPENDIX B

CODE

Below is the code to calculate the first term in the RHS of Eq.7 $-\boldsymbol{V} \bullet \nabla\theta$

```
……
……
load('Dm1','long2')
load('Dm1','lat2')
load('Dm1','long2')
load('Dm1','Dam')
%%load names for netcdf files
name6w='wrf2006wintterT.nc';
namenw='wrf2006wnew.nc';
name192w='T1992winter.nc';
name192w='wrf1992winterT.nc';
name92s='wrf1992summerT.nc';
namens='wrf2006snew.nc';
name6s='WRF2006summeru.nc';
namenwnew='newvegasno.nc';
namenew2006='wrf2006newlong.nc';
%% Only do the calculation near downtown
i_1=27;
i_2=47;
j_1=22;
j_2=44;
longn(1:21,1:23)=long2(i_1:i_2,j_1:j_2);
latn(1:21,1:23)=lat2(i_1:i_2,j_1:j_2);
Nx=21;
Ny=23;
Nz=27;
Nt=3120;
P_eta=GetVarpiece(name1,'P',27,47,22,44,Nt,27)+GetVarpiece(name1,'PB',27,47,22,44,
Nt,27);
Pe1(1:Nx,1:Ny,1:Nt)=squeeze(P_eta(:,:,1,:));
%%Pressure level for the calculation
P_000=920;
P_00=P_000*100;
Nz=27;
P_top=20*100;
N_levels=30;
Pcor=linspace(P_00,P_top,N_levels);
[Nx,Ny,Nz,Nt]=size(P_eta);
n=20;
Nt2=Nt-1;
Nx=21;
Ny=23;
Nz=27;
```

```
Nt=3120;
%%Get and interpolate Y component of the horizontal velocity
V_ps=inteb_4D(GetVarpiece(name1,'V',27,47,22,44,Nt,27),P_eta,Pcor,Nx,Ny,Nz,Nt,n);
%%Get and interpolate X component of the horizontal velocity
U_ps=inteb_4D(GetVarpiece(name1,'U',27,47,22,44,Nt,27),P_eta,Pcor,Nx,Ny,Nz,Nt,n);
T_p=inteb_4D((GetVarpiece(name1,'T',27,47,22,44,Nt,27)+300),P_eta,Pcor,Nx,Ny,Nz,N
t,n);
T=((GetVarpiece(name1,'T',27,47,22,44,Nt,27)+300));
%% Horizontal grid in km from downtown
load('Dm1','X');
load('Dm1','Y');
 [Nx,Ny,Nz,Nt2]=size(T_p);
Nt=2952;
XXX(1:21,1:23)=X(i_1:i_2,j_1:j_2);
YYY(1:21,1:23)=Y(i_1:i_2,j_1:j_2);
Damn(1:21,1:23)=Dam(i_1:i_2,j_1:j_2);
fprintf('gothere 1 \n')
%% Turn 2D variable into 3D and turn km to meter
for i=1:Nx
for j=1:Ny
   for k=1:Nz
          XX(i,j,k)=XXX(i,j)*(1000);
          YY(i,j,k)=YYY(i,j)*(1000);
   end
end
end
Nt=2952;
UGthet(1:Nx,1:Ny,1:Nz,1:2952)=0;
Gthetax(1:Nx,1:Ny,1:Nz,1:2952)=0;
Gthetay(1:Nx,1:Ny,1:Nz,1:2952)=0;
U_p(1:Nx,1:Ny,1:Nz,1:3120)=0;
V_p(1:Nx,1:Ny,1:Nz,1:3120)=0;
Dn(1:Nx,1:Ny,1:2952)=0;
Ng(1:2952)=0;
a=0;
Nt=3120;
%% Get U and V in theta coordinates
for t=1:Nt
for i=1:Nx-1
for j=1:Ny-1
for k=1:Nz-1
U_p(i,j,k,t)= (U_ps(i+1,j,k,t)+U_ps(i,j,k,t))/2;
V_p(i,j,k,t)= (V_ps(i,j+1,k,t)+V_ps(i,j,k,t))/2;
end
end
```

```
end
end
t=0;
%% Calculate the gradient using Central difference
clear Ng UGthetDtt Dn
t=0;
ts=169;
tf=3120;
for tt=ts:tf
      t=t+1;
      t_t(t)=t;
      t_tt(t)=tt;
for i=2:Nx-1
for j=2:Ny-1
          if ((Pe1(i,j,tt) > P_00)&& (Damn(i,j)==1) && (Pe1(i+1,j,tt) > P_00)&&
(Pe1(i,j+1,tt) > P_00)&& (Pe1(i-1,j,tt) > P_00)&& (Pe1(i,j-1,tt) > P_00))
   a=a+1 ;
Dxt(a)=i;
Dyt(a)=j;
Dn(i,j,t)=1;
for k=1:Nz-1
     Gthetax(i,j,k,t)=((T_p(i+1,j,k,tt)-T_p(i-1,j,k,tt))/(XX(i+1,j,k)-XX(i-1,j,k)));
     Gthetay(i,j,k,t)=((T_p(i,j+1,k,tt)-T_p(i,j-1,k,tt))/(YY(i,j+1,k)-YY(i,j-1,k)));
     UGthet(i,j,k,t)=-1*(U_p(i,j,k,tt)*Gthetax(i,j,k,t)+ V_p(i,j,k,tt)*Gthetay(i,j,k,t));
end
end
end
end
Ng(t)=a;
UGthetDtt(t)=(sum(sum(squeeze(UGthet(:,:,1,t)))))/Ng(t);
clear Dxt Dyt
a=0;
end
NgDt=(reshape(Ng,24,123));
Ngda=mean(NgDt,2);
UgthetDtttime=mean(reshape(UGthetDtt,24,123),2);
```

……

……

Below is the code used to calculate the second term of Eq.7 ($\frac{\partial}{\partial p}(\overline{\omega'\theta'})$)

……

```
%NETCDF files
name6w='wrf2006wintterT.nc';
```

```
namenw='wrf2006wnew.nc';
name192w='T1992winter.nc';
name92s='wrf1992summerT.nc';
namens='wrf2006snew.nc';
name6s='WRF2006summeru.nc';
namenwnew='newvegasno.nc';
name1='wrf2006newlong.nc';
%%domain coordinates
load('Dm1','long2')
load('Dm1','lat2')
load('Dm1','long2')
load('Dm1','Dam')
%% To save computational time we do the calculation only around the city
i_1=27;
i_2=47;
j_1=22;
j_2=44;
longn(1:21,1:23)=long2(i_1:i_2,j_1:j_2);
latn(1:21,1:23)=lat2(i_1:i_2,j_1:j_2);
Nx=21;
Ny=23;
Nz=27;
Nt=3120;
%%pressure in eta coordinates
P_eta=GetVarpiece(name1,'P',27,47,22,44,Nt,27)+GetVarpiece(name1,'PB',27,47,22,44,
Nt,27);
Pe1(1:Nx,1:Ny,1:Nt)=squeeze(P_eta(:,:,1,:));
%% Pressure level chosen for the calculation
P_000=920;
P_00=P_000*100;
Nz=27;
P_top=20*100;
N_levels=30;
%% New pressure coordinates
Pcor=linspace(P_00,P_top,N_levels);
[Nx,Ny,Nz,Nt]=size(P_eta);
n=20;
Nt2=Nt-1;
Nx=21;
Ny=23;
Nz=27;
Nt=3120;
g=9.81;
%%interpolation of the physical height into the new pressure coordinates,
```

```
Z_p=inteb_4D((GetVarpiece(name1,'PHP',27,47,22,44,Nt,27)/g),P_eta,Pcor,Nx,Ny,Nz,N
t,n);
%% Vertical velocity in eta coordinates interpolated to pressure coordinates
W_pp=inteb_4D(GetVarpiece(name1,'W',27,47,22,44,Nt,27),P_eta,Pcor,Nx,Ny,Nz,Nt,n)
;
%% Potential temperature in eta coordinates interpolated to pressure coordinates
T_p=inteb_4D((GetVarpiece(name1,'T',27,47,22,44,Nt,27)+300),P_eta,Pcor,Nx,Ny,Nz,N
t,n);
%% Horizontal grid in km from downtown (Calculated separately by another subroutine)
load('Dm1','X');
load('Dm1','Y');
 [Nx,Ny,Nz,Nt]=size(T_p);
XX(1:21,1:23)=X(i_1:i_2,j_1:j_2);
YY(1:21,1:23)=Y(i_1:i_2,j_1:j_2);
Damn(1:21,1:23)=Dam(i_1:i_2,j_1:j_2);
for i=1:Nx
for j=1:Ny
   for k=1:Nz
          Pc(i,j,k)=Pcor(k);
   end
end
end
wpdtht(1:Nx,1:Ny,1:Nz,1:Nt)=0;
Dn(1:Nx,1:Ny,1:Nt)=0;
clear a
a=0;
Nt=2952;
%%Change W_p from staggered grid to theta grid
for t=1:3120
for i=1:Nx
for j=1:Ny
for k=1:Nz-1
    W_p(i,j,k,t)=(W_pp(i,j,k+1,t)+W_pp(i,j,k,t))/2;
end
end
end
end
t=0;
ts=169;
te=3120;
%% Go over the grid and only get the gradient at points where the 920 pressure level is
above the surface
for tt=ts:te
      t=t+1;
      t_t(t)=t;
```

```
      t_tt(t)=tt;
for i=1:Nx
for j=1:Ny
            if ((Damn(i,j)==1) && (Pe1(i,j,tt) > P_00))
      a=a+1 ;
Dxt(a)=i;
Dyt(a)=j;
Dn(i,j,t)=1;
for k=1:Nz-1
    dpdz(i,j,k,t)=(Pc(i,j,k+1)-Pc(i,j,k))/(Z_p(i,j,k+1,tt)-Z_p(i,j,k,tt));
    dthtadp(i,j,k,t)=((T_p(i,j,k+1,tt)-T_p(i,j,k,tt))/(Pc(i,j,k+1)-Pc(i,j,k)));
    wpdtht(i,j,k,t)=-1*(W_p(i,j,k,tt)*dpdz(i,j,k,t)*dthtadp(i,j,k,t));
end
end
end
end
Ng(t)=a;
wpdthtDtt(t)=(sum(sum(squeeze(wpdtht(:,:,1,t)))))/Ng(t);
clear Dxt Dyt
a=0;
end
NgDt=(reshape(Ng,24,123));
Ngda=mean(NgDt,2);
wpdthtDtttime=mean(reshape(wpdthtDtt,24,123),2);
```

……

……

The Code for the subroutine inteb-4D and GetVarPiece

……

```
function[Fp]=inteb_4D(Fetaa,P_etaa,P,Nx,Ny,Nz,Nt,n)
%the function take a 4D Feta (x,y,eta,t) and interpolate it to 4D
%Fp(x,y,p,t); P is 1D P_eta is 4D(x,y,).
% load('Dm1','longn');
% load('Dm1','latn');
ZZ=size(P,2);
Fpp(1:Nx,1:Ny,1:ZZ,1:Nt)=0;
Feta=Fetaa(1:Nx,1:Ny,1:Nz,1:Nt);
for i=1:Nx
   for j=1:Ny
      for t=1:Nt
a_p = interp1(squeeze(P_etaa(i,j,1:27,t)),squeeze(Feta(i,j,1:27,t)),P);
Fpp(i,j,:,t)=a_p;
   end
   end
   end
```

```
Fp(1:Nx,1:Ny,1:n,1:Nt)=Fpp(1:Nx,1:Ny,1:n,1:Nt);
.....
.....
function[T2]=GetVarpiece(name,varwanted,i_1,i_2,j_1,j_2,Nt,Nz)
%get the var varwanted from netcdf file varwanted
Nxx=(i_2-i_1)+1;
Nyy=(j_2-j_1)+1;
ne=nargin;
if nargin==2
nn= netcdf.open(name,'NC_NOWRITE');
varid = netcdf.inqVarID(nn,varwanted);
T2=netcdf.getVar(nn,varid);
netcdf.close(nn)
else
   %% it gets a slice of vertical data at i j and t
nn= netcdf.open(name,'NC_NOWRITE');
varid = netcdf.inqVarID(nn,varwanted);
T2=squeeze(netcdf.getVar(nn,varid,[i_1 j_1 0 0],[Nxx Nyy Nz Nt]));
netcdf.close(nn)
end
```

BIOGRAPHICAL SKETCH

Samy Kamal was born and raised in Cairo. Graduated from the physics department, Cairo University. Soon after moved to United States and joined the physics department, San Francisco State University, where he got MS in physics. Masters research was in the field of Computational Fluid Dynamics (CFD). Results were presented in the American Physical Society (APS) division of fluid dynamics 63rd conference. Later Samy joined the School for Engineering of Matter, Transport, and Energy, Arizona State University, Tempe. Research interests are in the field of environmental fluid dynamics.